UNIVERSITÀ DEGLI STUDI DI MILANO

DEPARTMENT OF PHYSICS

PHD SCHOOL IN
PHYSICS, ASTROPHYSICS AND APPLIED PHYSICS

Ciclo XXXII°

Amplituhedra for ϕ^3 theory at tree and loop level

Disciplinary Scientific Sector FIS/02

Director of the School: Prof. Matteo Paris

Supervisor of the Thesis: Prof. Silke Klemm

Ph.D. Thesis of:
Giulio Salvatori

A. Y. 2019-2020

Commission of the final examination:

External Member: Prof. Nima Arkani-Hamed

External Member: Prof. Pierpaolo Mastrolia

Internal Member: Prof. Silke Klemm

Final examination:

Date 25 October 2019
Università degli Studi di Milano, Dipartimento di Fisica, Milano, Italy

To My Family

Acknowledgements

Although my collaboration with Nima Arkani-Hamed spanned a minor part of my Ph.D., interacting with him had a dramatic influence on me. Nima has shown me a different, courageous, unrelenting and optimistic way to do Physics. For this, his support and the great time spent working together I am deeply grateful.

I would also like to thank Song He for inviting me to visit him in Beijing for a very stimulating month during which we could discuss and collaborate on some of the topics of this thesis, Hugh Thomas for many explanations about generalized ABHY associahedra, Hadleigh Frost for a stimulating cooperation which, I hope, will continue in the coming years, Federico Faedo for constant logistical support, Giulio Ruzza for years of stimulating conversations and tentative collaborations, Sergio Cacciatori for important lessons on topics in Physics and Mathematics as well as a useful collaboration and Gilberto Bini for a number of good hints that have always put me on the right track.

Another special thank is due to Vittorio Del Duca, Francesco Moriello, Leila Maestri, Martijn Hidding and the particle physics group of ETH. Vittorio gave me a great opportunity to work with them in a fascinating project, the computation of master integrals relevant for Higgs+Jet production. From Francesco I learned more about differential equations and Feynman integrals in just a few months than I did in the rest of my Ph.D. Moreover, working hand-in-hand on such a big project with him, Leila and Martijn proved to be one of the most enjoyable time of my Ph.D. My only regret is that in the end we could not apply the Amplituhedron to it...

Last but not least, I must thank my family and friends for the constant support during the most difficult moments of my Ph.D, they had confidence in me when I could not.

Contents

Introduction

Recent years have witnessed a tremendous progress in the computation of scattering amplitudes, which has been characterized by a recurrent theme. Using cutting edge computational technology - and at times by heroic efforts - some new amplitude is computed. Then one stares at the answer and, sometimes, learns that it possesses unexpected properties which were completely obscured in the intermediate steps of the computation. This newly acquired knowledge usually inspires new computational techniques to get directly the final answer, which then allow to obtain new "theoretical data" - i.e. previously intractable amplitudes - where even more new features might be discovered.

A prime example of this virtuous loop is the celebrated scattering amplitude for n gluons, computed by Parke and Taylor in 1985. The textbook Feynman diagram technique leads to a proliferation of terms which however collapse to the surprisingly simple result

$$\mathrm{A_{MHV}}(1^+, 2^+, \ldots, \mathrm{i}^-, \ldots, \mathrm{j}^-, \ldots, \mathrm{n}^+) = \frac{\langle \mathrm{ij} \rangle^4}{\langle 12 \rangle \langle 23 \rangle \ldots \langle \mathrm{n1} \rangle},$$

when expressed using spinor helicity variables. The attempt of explaining the origin of this compact result lead to new hindsights such as Witten's Twistor String Theory or Berends-Giele, Cachazo-Svrcek-Witten and Britto-Cachazo-Feng-Witten recursion relations. Using these new techniques deriving the Parke-Taylor amplitude is now a matter of undergraduate homework.

Another example of an unexpected structure unearthed in the study of scattering amplitudes is the *Amplituhedron* [11], a generalization of a polytope which was found out to be intimately connected with amplitudes and integrands in planar $\mathcal{N} = 4$ SYM theory. In this picture the computation of amplitudes is translated in the geometrical problem of finding a decomposition of the Amplituhedron into smaller pieces, sometimes simplifying dramatically the computation. An intriguing aspect of

this formulation of the S-matrix is that the notion of *Locality* and *Unitarity*, pillars of Relativity and Quantum Mechanics, are emergent from a deeper - if somewhat still mysterious - concept, that of *Positivity*.

More precisely, in perturbative Quantum Field Theory locality and unitarity are made manifest by the Lagrangian and Feynman diagrams, since they represent amplitudes as a sum over local histories of particles which interact at space-time points, the vertices of the graph, and propagate freely along the propagators. The quantitative consequences of this representation for the amplitudes are encoded in the famous formula

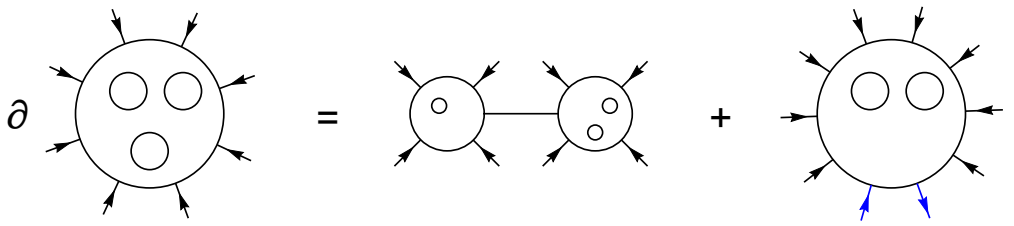

(1)

which is a precise statement on the analytical properties of the S-matrix: scattering amplitudes have singularities when a subset of the external particles go on-shell and factorize into lower point amplitudes there. In addition, scattering *integrands* have poles when a virtual particle goes on-shell and there reduce to a lower-loop integrand with two extra particles in the forward limit. On the other hand, the Amplituhedron is defined by a certain positivity requirement which has nothing to do with (1): very roughly speaking it is the convex hull of the external kinematical data. As a consequence of this definition the Amplituhedron develops an important *boundary structure*, in a sense the Amplituhedron solves (1) by replacing "singularities" with "boundaries". In turn this implies the correct singularity structure for the scattering amplitudes.

In the past couple of years, the idea that the Amplituhedron could provide a new theoretical framework for the S-matrix has been put on a more firm basis in [10] by introducing the concept of *Positive Geometry*, of which the Amplituhedron represents a special instance. A positive geometry is defined by a pair (X, Ω), X is a semi-algebraic variety - that is a space defined by equalities and inequalities - and Ω a differential form, called *canonical form*, defined by the requirement of having logarithmic singularities at the boundaries of X. Furthermore, the residue of Ω along a boundary ∂X of must be the canonical form of that boundary, so that the pair $(\partial X, \mathrm{Res}\ \Omega)$ forms another positive geometry. It is worth men-

tioning that this concept proved to be useful also beyond the world of amplitudes: example of "Positive Physics" have been discovered in Conformal Field Theory, Effective Field Theory as well as Cosmology [4; 5; 6]. Going back to amplitudes, an important step forward made in [8] is that also tree level amplitudes in the much simpler ϕ^3 bi-adjoint scalar theory admit the same description. Indeed, it was discovered that a positive geometry - called Associahedron - lives in the kinematical space of these amplitudes and allows their computation translating almost word-per-word the original picture of $\mathcal{N} = 4$ SYM and the Amplituhedron. In a beautiful parallel between the two stories, the newly discovered Amplituhedron made manifest previously unknown properties of amplitudes in ϕ^3 and also inspired new methods to compute them.

It is becoming more and more evident that Amplituhedra exists hidden in plain sight even in the simplest quantum field theories, and it is then a fascinating and pressing problem to understand whether this increasingly applicable theory of the S-matrix has a deeper physical meaning. In order to do so, and in light of the general wisdom of Amplitudeology, it is desirable to gather more "theoretical data": examples of positive geometries with physically meaningful boundary structures and examples of amplitudes computed from them. This investigation is the main topic of the present thesis.

As a start this exploration can be formulated as a purely geometrical problem: are there positive geometries compatible with (1) and where can they be found? When faced with this question, a mathematician comes up immediately with an answer [1]: the compactified moduli space of punctured Riemann surfaces $\overline{\mathcal{M}}_{g,n}$. The space $\overline{\mathcal{M}}_{g,n}$ is a rather fundamental mathematical object: in its simplest incarnation, when the surface is a sphere, $\overline{\mathcal{M}}_{0,n}$ can be thought of as the space of n complex variables up to projective transformations. Furthermore, $\overline{\mathcal{M}}_{g,n}$ plays an important role in many fields of physics precisely because of its peculiar boundary structure, for example it is a natural space to describe CFT correlators - famously computed by prescribing appropriate factorizing and scaling behaviours - and therefore worldsheet formulations of perturbative string amplitudes. For similar reasons it is important in worldsheet-like formulations of field amplitudes, such as the CHY formalism or ambi-twistor theory. Perhaps it is not too surprising, then, that $\overline{\mathcal{M}}_{g,n}$ turns out to be also an important example of positive geometry, as was first pointed out in [8].

Despite its importance, the boundary structure of $\overline{\mathcal{M}}_{g,n}$ is not made

[1] At least this was the case for the mathematician to whom I asked this question, Prof. Gilberto Bini.

manifest in the usual way physicists think about it. In the simplest case, the bulk of $\overline{\mathcal{M}}_{0,n}$ is a $(n-3)$-dimensional simplex and the boundary $\partial\overline{\mathcal{M}}_{0,n}$ it is hidden at the vertices[2] of this simplex: to probe it one has to "zoom-in" at the vertices by performing a blow-up. This picture is a consequence of the choice of coordinates used to chart $\overline{\mathcal{M}}_{0,n}$, the locations of the punctures on the sphere, which is well defined only when the punctures are distinct. At the boundaries of $\overline{\mathcal{M}}_{0,n}$, however, the punctures collide and thus the patch of coordinate breaks down[3]. Since boundaries play such a central role in our story, it would be desirable to have better coordinates when thinking of $\overline{\mathcal{M}}_{g,n}$ in connection with positive geometries. A natural solution comes from hyperbolic geometry, using which one obtains coordinates over $\overline{\mathcal{M}}_{g,n}$ that make completely manifest they way its boundaries factorizes. We will offer a review of these ideas in Chapter 1, which is partly based on [2] and successive investigations in collaboration with Nima Arkani-Hamed and Song He. In particular, we will illustrate simple examples of moduli spaces and their interpretation as positive geometries whose boundary structures "solve" (1) as it would be written in the case a cubic scalar theory.

The study of the positive geometries living in moduli spaces is an interesting problem on its own, however scattering amplitudes depend on kinematical variables which are unrelated to $\overline{\mathcal{M}}_{g,n}$. Therefore it is not immediately clear how to make a connection between the two objects. This was clarified in the seminal paper [8], where it was shown how the scattering equations provide the missing link between the two worlds. In the language of [10], the scattering equations are an isomorphism of positive geometries connecting the moduli space to a copy of it living directly in kinematical space. Although it is very likely that this picture can be generalized - perhaps even providing new inspiration for higher genera scattering equations - we will not develop this idea much further here. Instead, in Chapter 2 we will show how avatars of the new positive geometries found in $\overline{\mathcal{M}}_{g,n}$ can also be found in kinematical space in the form of convex polytopes. As we will discuss, this fact is deeply connected with the existence of a certain differential form called *Scattering Form* and with the fact that this form enjoys a novel symmetry: it is projectively invariant. This fact is very reminiscent of the familiar hidden dual conformal invariance (DCI) of $\mathcal{N} = 4$ SYM: amplitudes of this theory are DCI because a certain "infinity twistor", representing an arbitrary choice of a line at infinity in kinematical space, appears in intermediate computation

[2]More precisely, this happens at every boundary, of any dimension, of the simplex.

[3]In order to fix this problem one must rescale the coordinates by using the relative velocities of the colliding punctures, which is in practice the meaning of the blow-up

but ultimately drops out of the final result. Similarly, the projectivity of the scattering form is equivalent to the absence of a pole at infinity which appears term by term in the form.

Finally, in Chapter 3 we will discuss how the positive geometries previously discussed can be used to compute scattering amplitudes, even more efficiently than one could expect from such a simple theory as ϕ^3. The general idea is that amplitudes are extracted from the scattering form, which can be computed by triangulating the relevant Amplituhedron. This yields recursive formulae with spurious poles which are reminiscent of BCFW. We will study the case of tree level amplitudes in ϕ^3, where a novel triangulation of the relevant Amplituhedron led us to a formula which is even more efficient than the famous Berends-Giele recursive formula. We will also present a number of interesting triangulations of the Amplituhedra for the 1-loop integrand, which include a forward-limit formula generalizing one discussed in [23].

To summarize, this thesis is organized as follows.

Chapter 1: Positive Geometries in the Moduli space A review of the hyperbolic approach to the study of positive geometries living in moduli spaces of Riemann surfaces. Using *Fenchel-Nielsen* coordinates one is lead to the Associahedron, the Cyclohedron and the Halohedron. Using *Penner*'s coordinates one is lead to cluster algebras of finite type.

Chapter 2: Positive Geometries in Kinematical space Introduction to projective Scattering Forms and their relation to polytopes. In particular, description of the 1-loop scattering form and its generalizations. Realization of the positive geometries previously found in the moduli space as convex polytopes in the kinematical space of amplitudes and integrands.

Chapter 3: Amplitudes from Geometry How to extract scattering amplitudes from the Scattering Form, even in the presence of double poles. Triangulations and recursive formulae: *soft-limit* formula for tree level amplitudes, *forward-limit* formula for 1-loop integrands and others.

CHAPTER 1

The Positive Geometry of $\overline{\mathcal{M}}_{g,n}$

1.1 Review of hyperbolic geometry

Here we review some elementary facts of plane hyperbolic geometry, Riemann surfaces and their moduli. Further details can be found in [31; 32].

1.1.1 Hyperbolic Plane

The simplest and most fundamental Riemann surface is the hyperbolic plane, which can be thought of in many ways. The first model of the hyperbolic plane is the *Poincaré disk*, which is defined as the open disk $\mathbf{D} \subset \mathbb{C}$ of radius 1 centered at the origin. Its automorphism group $\mathrm{Aut}_{\mathbf{D}}$ is formed by the bi-holomorphic maps $\psi : \mathbf{D} \to \mathbf{D}$ of the form

$$\psi : z \mapsto \psi(z) = \frac{az + b}{\bar{b}z + \bar{a}},$$

where $a, b \in \mathbb{C}$ and $|a|^2 > |b|^2$. Among all the conformally equivalent metrics which we can consider on $\mathbf{D}$ there is a privileged one which is given by the infinitesimal distance

$$\rho_{\mathbf{D}} = \frac{2|dz|}{1 - |z|^2}.$$

The Poincaré disk equipped with $\rho_{\mathbf{D}}$ is a Riemannian manifold called *Hyperbolic plane*. By definition, $\rho_{\mathbf{D}}$ is left invariant by all the elements of $\mathrm{Aut}_{\mathbf{D}}$, and any other Riemannian metric of $\mathbf{D}$ compatible with this requirement is obtained by a global scaling of $\rho_{\mathbf{D}}$[1]. In terms of this privileged metric we can define objects invariant under $\mathrm{Aut}_{\mathbf{D}}$, such as lengths, areas, geodesics, circles and so on. Furthermore, we can use $\rho_{\mathbf{D}}$ to partition the

[1]The factor 2 in the numerator of $\rho_{\mathbf{D}}$ is chosen to normalize the curvature of $\mathbf{D}$ to -1.

elements of $\mathrm{Aut}_{\mathbf{D}}$ into parabolic, elliptic and hyperbolic transformations as follows. For each $\psi \in \mathrm{Aut}_{\mathbf{D}}$ define $m(\psi) := \inf_{z\in\mathbf{D}} \mathrm{d}(z, \psi(z))$, where d is the geodesic distance. Then we have the following table.

Parabolic	One fixed point in $\partial\mathbf{D}$	$m(\psi) = 0$, Infimum not in $\mathbf{D}$
Elliptic	One fixed point in $\mathbf{D}$	$m(\psi) = 0$, Infimum in $\mathbf{D}$
Hyperbolic	Two fixed points in $\partial\mathbf{D}$	$m(\psi) > 0$

There are many other models of the Hyperbolic plane, one with an immediate connection with the scattering amplitudes is the upper half plane model. The upper half plane is the set $\mathbb{H} \subset \mathbb{C}$ with $\mathrm{Im}(z) > 0$. Since it is simply connected, it must be bi-holomorphic to $\mathbf{D}$, and, indeed, there is a very well known map,

$$\begin{aligned} \mathcal{C} : \mathbf{D} &\to \mathbb{H} \\ z &\to \sigma = \frac{i(z+1)}{1-z}, \end{aligned}$$

called the (inverse) Cayley transform. $\mathcal{C}$ is a Moebius map which sends the boundary of $\mathbf{D}$ to the real axis. The automorphism group $\mathrm{Aut}_{\mathbb{H}}$ is given by

$$\phi : z \mapsto \phi(z) = \frac{az+b}{cz+d},$$

with $a, b, c, d \in \mathbb{R}$ and with $ac-bd > 0$. We can identify $\mathrm{Aut}_{\mathbb{H}} \approx \mathrm{PSL}(2,\mathbb{R}) = \mathrm{SL}(2,\mathbb{R})/\{\pm \mathrm{I}\}$. The reader familiar with the scattering equations literature will notice that the real section of the moduli space used in [8] to define a positive geometry is very close to $\mathbb{H}$. Indeed, there one considers punctures on the real axis, up to the full $\mathrm{SL}(2,\mathbb{R})$ (see also [18; 12]).

A third model of the hyperbolic plane is the so called *Hyperboloid model*. In a Minkowski space-time $\mathbb{R}^{1,2}$ of signature $(-,+,+)$ and with coordinates $x = (x^0, x^1, x^2)$, consider the upper branch of the hyperboloid H of equation $x^2 = 1$. We can induce a positive definite metric on it, which turns it into a Riemannian manifold isometric to $(\mathbf{D}, \rho_{\mathbf{D}})$. We can construct such isometry as follows. Put a disk of euclidean radius 1 at the origin of the spatial plane $x^0 = 0$, and map every point of H to the disk by a projection through the point $(-1, 0, 0)$, see Fig. 1.1.

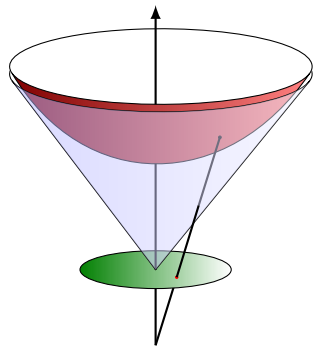

Figure 1.1: The projection sends a point on the hyperboloid to a point on the disk.

Under this isometry, an element of $SO^{\uparrow}(1,2)$ is conjugated to an element of $\mathrm{Aut}_{\mathbf{D}}$. Using the hyperboloid model, we can compute explicitly the distance between two points P and Q corresponding to time-like vectors l_P and l_Q, using the formula

$$\cosh(d(P,Q)) = l_P \cdot l_Q.$$

Moreover, many geometrical objects on the hyperbolic plane can be represented by planes in the hyperboloid model: if k, l and v are respectively null, time, and space like momenta, define the planes $w \cdot k = 1$, $w \cdot v = 1$ and $w \cdot l = 0$, $w \in \mathbb{R}^{1,2}$. The intersection of these planes with H yields respectively a horocycle, a circle and a geodesic. Later, we will use this fact to construct meaningful maps from the set of kinematical data of a scattering process to the moduli space of Riemann surfaces.

1.1.2 Hyperbolic Riemann surfaces and their moduli

Recall that a *Riemann surface* is a topological surface X locally charted by open sets homeomorphic to $\mathbb{C}$ and such that the transition functions are holomorphic maps. Equivalently, one can define a Riemann surface to be an equivalence class of Riemannian metrics on a differentiable manifold X of real dimension 2, two such metrics are equivalent if related by a local rescaling. The equivalence between the two definitions is a well known classical fact.

The Riemann uniformization theorem establishes that, up to isomorphisms, there are only three simply connected Riemann surfaces: the Riemann sphere $\mathbb{CP}^1$, the complex plane $\mathbb{C}$ and the Poincaré disk $\mathbf{D}$.

A powerful tool in studying Riemann surfaces is the concept of a covering space: every Riemann surface X admits a universal covering sur-

face $\tilde{X}$ which is simply connected and, therefore, must be one among the three above. It turns out that almost every surface is covered by $\mathbf{D}$, the only exceptions being $\mathbb{C}$, $\mathbb{CP}^1$ and a torus without punctures. The crucial property of the universal covering space is that it allows to lift any continuous map $f : X \to X'$ to a map of covering spaces $\tilde{f} : \tilde{X} \to \tilde{X}'$. In particular, we can lift a loop on X by thinking of it as a map $\gamma : [0, 1] \to X$ with $\gamma(0) = \gamma(1)$. The lift $\tilde{\gamma}$ is a path that connects preimages of the base point $\gamma(0)$, however $\tilde{\gamma}$ does not have to be a loop itself, and indeed it is not unless γ is contractible to a point. Therefore if γ is not a trivial loop, $\tilde{\gamma}$ defines an element of $\mathrm{Aut}_{\mathbf{D}}$. This produces a representation of the fundamental group $\pi(X)$ with values in $\mathrm{Aut}_{\mathbf{D}}$, the image of which is a torsion-free discrete subgroup of $\mathrm{Aut}_{\mathbf{D}}$, such groups are called *Fuchsian groups*. The knowledge of the covering map $\mathbf{D} \to X$ yields a Fuchsian group, but we can go in the opposite direction: given any Fuchsian group Γ the quotient $\mathbf{D}/\Gamma$ yields a Riemann surface.

Using the above construction we can equip every Riemann surface[2] with an hyperbolic metric: any open set $U \subset X$ is bi-holomorphic to a subset of $\mathbf{D}$, thus we can induce the metric $\rho_{\mathbf{D}}$ on U, one then shows that these locally defined metrics agree with each other. The resulting metric on X is called its *intrinsic hyperbolic metric* and provides a characterisation of the complex structure of X: X and X' equipped with their intrinsic metrics are isomorphic as Riemannian surfaces if and only if they are bi-holomorphic, i.e. isomorphic as Riemann surfaces[3]. Because of this, each equivalence class of Riemann surfaces (a point in the moduli space) has a canonical representative in the intrinsic hyperbolic metric. One can use this metric to measure "topological landmarks" in the surface, which provide invariants of that class. In other words, the intrinsic metric provides coordinates on the moduli space. There are two famous choices of landmarks: arcs of a pants decomposition and arcs of a triangulations. The first choice lead to the so called *Fenchel-Nielsen coordinates*, the second to *Penner's coordinates* (or λ-lengths). We will describe in some detail both cases in the rest of this chapter.

There is one last subtlety: actually the coordinates obtained from the intrinsic metric parametrize what is called Teichmüller space. The moduli space is then obtained from Teichmüller by modding out the action of the Mapping Class Group (MCG) of the surface [28], which is the group of isotopy classes of orientation-preserving homeomorphisms of the surface.

[2]More precisely, this can be done for all the surfaces covered by $\mathbf{D}$, which are also called *hyperbolic surfaces*

[3]Picturing Riemann surfaces as equivalence classes of metrics, we can think of the intrinsic metric as a canonical gauge fixing procedure.

However, in the cases of the surfaces we will consider the MCG is trivial and so we can neglect this fact.

1.2 Pants Decomposition

A classical result in the theory of borderless Riemann surfaces is that they can be decomposed in smaller pieces called *pairs of pants*. This is done by considering a system of closed loops in the surface such that by cutting along these loops produces a collection of surfaces homeomorphic to a thrice puncture sphere, see Fig. 1.2. Furthermore, one can deform each of the loops without changing its homotopy class so that it is a geodesic in the intrinsic hyperbolic metric of the surface. By construction, the lengths of these geodesics are invariants of the surface and thus can be used to parametrize the moduli space. Indeed, one can unambiguously reconstruct the surface by specifying the gluings patterns of the pairs of pants (a purely combinatorial data), the lengths of their loops and the relative angles by which we attach them. Therefore, for each loop we have to specify two real numbers, a length $0 \leq \ell \leq \infty$ and an angle $0 \leq \theta \leq 2\pi$, which together are called *Fenchel-Nielsen* coordinates. The angle is a priori defined to be in the range $0 \leq \theta \leq \infty$ as well, it is another classical result that to each loop is associated a generator of the mapping class group, called *Dehn Twist*, whose action is to twist the surface by increasing this angle by 2π. Because we are ultimately interested in modding out the mapping class group, the angle can be safely restricted in the range $0 \leq \theta \leq 2\pi$.

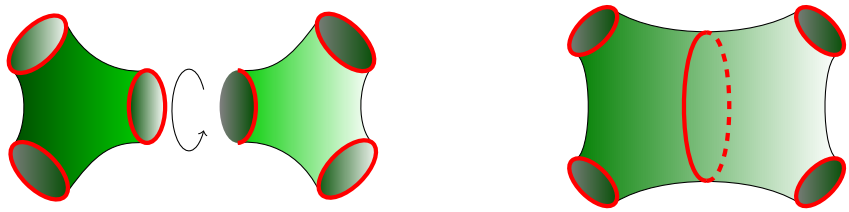

Figure 1.2: Two pairs of pants are glued to form a sphere with four boundary components. The length of the geodesic and the relative angle by which the pants are glued are parameters over the moduli space.

Fenchel-Nielsen coordinates are particularly useful to study the boundary structure of the moduli space. A boundary is obtained by setting some length ℓ_α to zero, which corresponds to pinching the geodesic α to a point. We obtain a nodal surface whose moduli space can be stud-

ied again in terms of pants decompositions. Precisely those loops which did not cross the pinched geodesic α can appear in a pants decomposition of the new surface. One can iterate the procedure and probe lower dimensional boundaries of the moduli space by pinching several compatible geodesics. Finally, when a geodesic is pinched the twisting angle there loses meaning therefore we do not have to specify it anymore.

As an example, consider a sphere with four punctures σ_i, $i = 1, \dots, 4$. A pants decomposition is obtained by choosing a loop α that separates the punctures in the two sets $\{\sigma_1, \sigma_2\}$ and $\{\sigma_3, \sigma_4\}$, and loops of length zero around each puncture. Since we only have to specifiy the length ℓ_α and the angle θ_α, the moduli space has real dimension two as expected. Setting $\ell_\alpha = 0$ we go on a boundary of the moduli space, which is now zero dimensional since the twisting angle is lost in the process. Clearly there are other two pants decompositions, corresponding to the separation of the punctures in the sets $\{\sigma_1, \sigma_3\}$,$\{\sigma_2, \sigma_4\}$ or in the sets $\{\sigma_1, \sigma_4\}$,$\{\sigma_2, \sigma_3\}$. The corresponding Fenchel-Nielsen coordinates allow to access two other boundary components, and putting everything together one recovers the familiar moduli space $\mathcal{M}_{0,4} = \mathbb{P}^1 - \{0, 1, \infty\}$.

From this simple example we see that a single pants decomposition is not enough to study the entire moduli space. We can think of a pants decomposition as giving a patch of coordinates that allows to see some of its boundaries, but then one has to consider the full sets of pants decompositions, known as *pants complex*, to see the remaining ones. To change coordinates, we can perform a series of local elementary moves on a pants decomposition to produce new pants decompositions. The simplest one is to consider a pair of pants attached by a loop α, which form a sphere with four boundary components similar to the example above, and replace α with another loop β picked from the two remaining choices. Unfortunately, the effect of this move on the Fenchel-Nielsen coordinates is quite untractable. Let us introduce $L_i := \cosh(\ell_i/2)$, where ℓ_i is the length of the i-th boundary component, and similarly $L_\alpha = \cosh(l_\alpha/2)$ and $L_\beta = \cosh(l_\beta/2)$. We also replace twisting angles θ with distances τ measured on the geodesical loop, so that τ_α increases by ℓ_α when θ_α increases by 2π. Then we have [35]

$$\begin{aligned} L_\beta(L_\alpha^2 - 1) &= L_1L_2 + L_3L_4 + L_\alpha(L_1L_3 + L_2L_4) \\ &+ \cosh(\tau_\alpha)\sqrt{L_\alpha^2 + 2L_1L_4L_\alpha + L_1^2 + L_4^2 - 1}\sqrt{L_\alpha^2 + 2L_2L_3L_\alpha + L_2^2 + L_3^2 - 1}, \end{aligned} \tag{1.1}$$

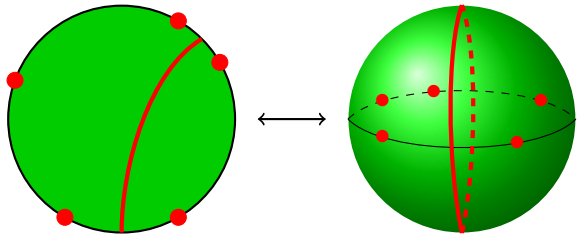

Figure 1.3: The double of a disk with marked points on its boundary is a sphere with punctures aligned on a single circle. The pants decomposition of the latter descends to a system of arcs on the former. Note that the twisting angles must always be zero in order to guarantee the alignment of the punctures on the sphere.

and

$$\cosh(\tau_\beta) = \frac{(L_\beta^2-1)L_\alpha - L_1L_4 - L_2L_3 - L_\beta(L_1L_3+L_2L_4)}{\sqrt{\left[L_1^2+L_2^2+2L_1L_2L_\beta+(L_\beta^2-1)\right]\left[L_3^2+L_4^2+2L_3L_4L_\beta+(L_\beta^2-1)\right]}}. \tag{1.2}$$

The pants decomposition of a surface X is well defined when X is compact, or it is obtained from a compact surface by removing a finite number of points and disks. In order to extend the approach to other surfaces, such as a disk with punctures or an annulus with punctures, one considers the *complex double* $X^{\mathbb{C}}$ of the surface. Roughly speaking, this is obtained by considering another copy of the topological surface underlying X and endowing it with an atlas obtained from the original one by replacing its complex coordinate z with $\overline{z}$. Then $X^{\mathbb{C}}$ is obtaining by gluing X and its mirror image along the corresponding boundary components. For example, the mirror copy of the upper half-plane $\mathbb{H} = \{z \in \mathbb{C} | \mathrm{Im(z)} \geq 0\}$ is the lower half plane $\mathbb{H} = \{z \in \mathbb{C} | \mathrm{Im(z)} \leq 0\}$ and its double is the full complex plane $\mathbb{C} = \mathbb{H}^{\mathbb{C}}$. The double of a disk is a sphere as shown in Fig. 1.3, the double of an annulus is a torus and so on. Further details of this construction can be found in [31; 29]. By construction, the double $X^{\mathbb{C}}$ is always a borderless surface, possibly with punctures, and then one can apply the pants decomposition method to it to construct coordinates for the moduli space of X. The system of loops of pants decomposition of $X^{\mathbb{C}}$ descends to a system of loops and arcs on X, where by arc we mean a non-closed geodesic joining different points on boundary components of X. In practice, we can understand the boundary structure of the moduli space of X without really picturing its double simply by pinching loops and arcs. In the remaining part of this section we will study the simplest

cases of moduli spaces using pants decompositions, the disk with n punctures on its boundary, the disk with n punctures on its boundary and one in the interior and the annulus with n punctures on its boundary.

1.2.1 The Disk and the Associahedron

We now unwind the pants decomposition method applied to the moduli space of disks with n markings on the boundary, which we denote as $\mathcal{M}_{\mathbf{D},n}$. Notice that the complex double of such a disk is a punctured Riemann sphere, with punctures on a single circle. Therefore, it is natural to expect a connection with the real section of the moduli space of genus zero Riemann surfaces, where the Associahedron studied in [8] belongs.

Let X be a disk with markings and $X^{\mathbb{C}}$ the sphere resulting from the doubling procedure. Any pants decomposition of $X^{\mathbb{C}}$ consists of geodesics that suitably partition the punctures: on the original copy of X these are geodesic arcs that touch non adjacent boundary components. We can consider an n-gon obtained substituting punctures and geodesic boundaries with edges and vertices. Using this picture it is then obvious that the geodesic arcs are in bijection with the diagonals of the n-gon: this establishes the combinatorial equivalence of $\mathcal{M}_{\mathbf{D},n}$ with the Associahedron $\mathcal{A}_{n-3}$. As shown in Fig. 1.4, by contracting a diagonal we get two nodal disks and therefore we recover the usual factorisation $\mathcal{A}_{n-3} \approx \mathcal{A}_m \times \mathcal{A}_{n-m-3}$.

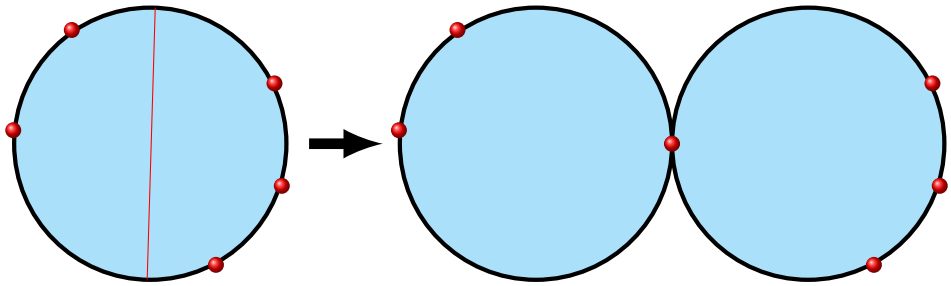

Figure 1.4: The contraction of a geodesic arc produces two nodal disks.

In principle, we should compute the intrinsic metric of $X^{\mathbb{C}}$ by the Fuchsian group Γ such that $X^{\mathbb{C}} \sim \mathbf{D}/\Gamma$. However, to write the group Γ as a function of the punctures is a notoriously difficult problem in mathematics. Instead we consider the *geodesic convex hull* Y of the points themselves, i.e. the region delimited by the geodesics joining consecutive points shown in Fig. 1.5. By construction the intrinsic metric of Y is the restriction of the metric $\rho_{\mathbf{D}}$ of the Poincaré disk, therefore we can immediately compute

the Fenchel-Nielsen coordinates of Y. Let α be a diagonal separating the punctures in two sets $z_L = \{z_j, z_{j+1}, \ldots, z_i\}$ and $z_R = \{z_{i+1}, z_{i+2}, \ldots, z_{j-1}\}$, as in Fig. 1.5.

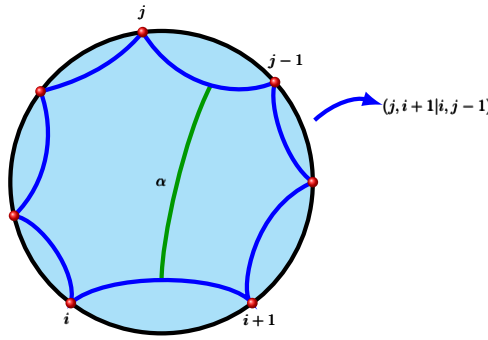

Figure 1.5: The convex hull of several points is shown, the blue lines are its geodesic boundaries and the green line is a geodesic arc.

We have to find the shortest geodesic in the homotopy class of α. In order to do so we first perform a Moebius map to send $(z_{i+1}, z_{j-1}, z_j, z_i)$ to $(-b, -a, a, b)$ on the real axis, then the geodesic in question (which we still call α) is the line $\mathrm{Re}(\sigma) = 0$, and the geodesic arc length is $\mathrm{arcosh}(1+\frac{(b-a)^2}{2ab})$. We can write this result as

$$\cosh(l_\alpha) = 1 - 2\,(j\; i+1|i\; j-1), \tag{1.3}$$

where

$$(ij|kl) = \frac{(z_k - z_i)(z_l - z_j)}{(z_k - z_j)(z_l - z_i)},$$

is a cross ratio. It is evident that we can trade the geodesic lengths for the cross ratios as moduli for Y. Geodesic lengths are obviously positive and as a consequence of (1.1) they also satisfy non-trivial inequalities. Through (1.3) these constraints translate in imposing the cross ratios to be negative and bounded by inequalities which guarantee that the cyclic order of the particles is preserved. Notice that the cross ratios x appearing in (1.3) are not the same as the cross ratios u considered in [8], and on which we will elaborate more in Section 1.3. The two set of cross ratios are related by

$$x = \frac{u}{u-1},$$

as one can easily see recalling that cross ratios satisfy the following rela-

tions

$$\begin{aligned}(ab|cd) &= 1 - (ac|bd),\\ (ab|cd) &= \frac{1}{(ba|cd)},\\ (ab|cd) &= (ab|ce)(ab|ed) \quad \text{(cocycle condition)}.\end{aligned} \tag{1.4}$$

Keeping in mind that the lengths of the arcs drawn on the disk are half of the lengths of the pants decomposition of its double, it is possible to recover (1.1) and (1.2) from (1.3) and the above cross ratios relations. One should also keep in mind that the twist parameters τ are always 1, since the punctures must always be aligned on a single circle.

Parametrizing the Fenchel-Nielsen coordinates in terms of cross ratios, one recover the usual picture of the boundary of the moduli space in terms of colliding punctures. Suppose that α is being contracted, then either the punctures σ_j, σ_i or the punctures $\sigma_{i+1}, \sigma_{j-1}$ are collapsing and, because of the cyclic order, this forces the punctures between them to collapse as well. However this does not mean that the lengths of the remaining diagonals have to vanish, neither on the left nor on the right side of α, only that if we want to compute them in terms of puncture variables then we have to introduce a new set of puncture variables for the nodal disks. In contrast with this, the Fenchel-Nielsen coordinates directly factorize into two sets of coordinates for each of the nodal disks.

1.2.2 The Annulus and the Halohedron

Consider an annulus with n marked points on one of his boundary components, e.g. the outer one, and denote by $\mathcal{M}_{\mathbf{D},1;n}$ its moduli space. As described in [29] it turns out that $\mathcal{M}_{\mathbf{D},1;n}$ is a polytope, called *Halohedron* and denoted $\mathrm{H_n}$, which is a close kin of the Associahedron. Indeed, both the Halohedron and the Associahedron fit in a very general combinatorial description in terms of marked tubings on a graph. This picture also includes the Cyclohedron $\mathcal{B}_{n-1}$ whose face lattice represents the possible ways to associate particles on a circle rather than on a segment like in the case of the Associahedron.

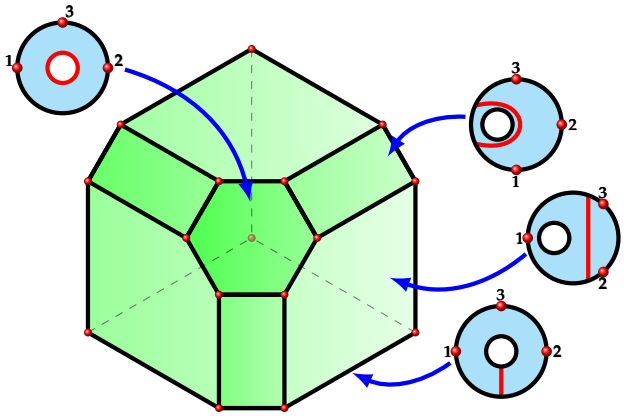

Figure 1.6: The three dimensional Halohedron. There are three *tadpole factorisation* square facets, three *factorisation* pentagons, three *cut* pentagons and a Cyclohedron.

The description of $\mathrm{H_n}$ relevant to scattering amplitudes is in terms of arcs on a marked annulus. The arcs are obtained by the pants decomposition of the torus and unlike in the previous section can now be of different types. Arcs carry an associated modulus, the length of the geodesic they represent, if the modulus is zero then the arc is contracted and we obtain nodal disks. As for $\mathcal{M}_{\mathbf{D},n}$, only those arcs that upon contraction produce stable nodal components are admissible, but now we have a new kind of stable lowest dimensional component: a disk with a marked point in the interior and a marked point on the boundary, see Fig.1.7.

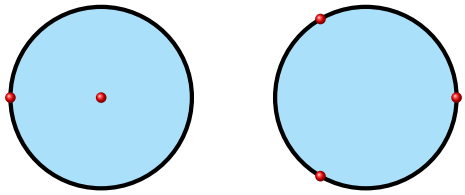

Figure 1.7: The smallest possible stable components that appear when contracting arcs.

Facets of the Halohedron correspond to contracted arcs. As proved in [29], the facets of $\mathrm{H_n}$ are exactly one *Cyclohedron* $\mathcal{B}_{n-1}$, n Associahedra $\mathcal{A}_{n-1}$ and $n^2 - n$ facets of the form $\mathcal{A}_m \times \mathrm{H_{n-m}}$ for $n \geq m \geq 0$. In Table 1.1 are shown the possible arcs of the Halohedron and the corresponding contractions, in Fig.1.6 the three dimensional Halohedron $\mathrm{H_3}$ is shown with some of its facets labelled. The cyclohedral facet arises by the contraction

Geodesical Arc	Facet type	Planar Variable
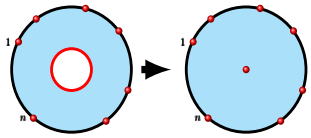	Cyclohedron $\mathcal{B}_{n-1}$	X_0
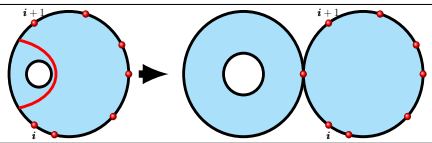	Tadpole Factorisation $\mathcal{A}_{n-1} \times \mathrm{H}_1$	$X_{(i+1,i+2,\ldots,i)}$
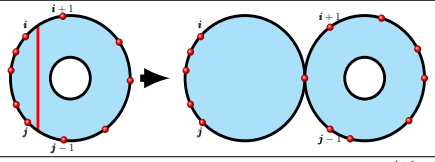	Factorisation $\mathcal{A}_m \times \mathrm{H}_{\mathrm{n-m}}$	$X_{(j,j+1,\ldots,i)}$
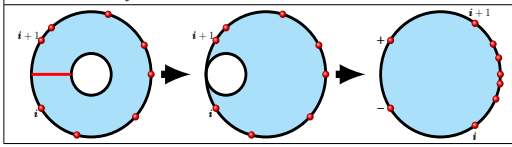	Cut Associahedron $\mathcal{A}_{n-1}$	X_i

Table 1.1: List of the arcs contraction and corresponding facet of the Halohedron. For future convenience, they are also labelled by dual planar variables.

of the loop geodetical arc, the effect of which is to shrink the internal circle to a puncture. Therefore this facet represents the moduli space of a disk with one internal puncture.

By comparison with (1) we see that some of the facets of $\mathrm{H_n}$ have an immediate physical interpretation. Factorisation facets with $m < n$ are in 1-1 correspondence with the possible factorisations of a 1-loop planar integrand, and their factorisation into $\mathcal{A}_m \times \mathrm{H}_{\mathrm{n-m}}$ mirrors the factorisation of the integrand in a tree level amplitude and a lower point integrand. Similarly, we have an associahedral facet for each possible cut of the integrand, and since Associahedra compute tree level amplitudes, we can interpret these facets as reflecting the forward limit of a cutted integrand. For this reason we will refer to these as the *cut facets* of the Halohedron.

On the other hand, there is no obvious interpretation for the cyclohedral facet and the tadpole factorisation facets (those with $m = n$). However, we can find one by looking at the vertices of $\mathrm{H_n}$. A vertex corresponds to a maximal choice of arcs. It is easy to see that we can pick a maximum of n non intersecting admissible arcs. To a maximal choice of arcs we can associate a cubic Feynman diagram, essentially in the same way as was done in [8]: the arcs partition the annulus in zones, to each zone we associate a cubic vertex and then we contract the vertices with propagators intersecting the arcs. As shown in Fig. 1.8, the result is a

cubic 1-loop planar diagram.

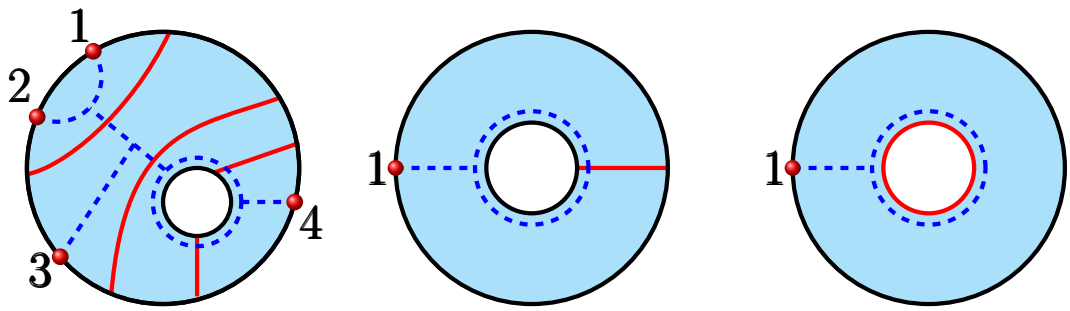

Figure 1.8: Examples of Feynman diagrams (blue, dashed) dual to choices of arcs (red). The middle and right figures show how tadpoles are created, we call these "IR" and "UV" tadpole respectively.

Using this rule we can label all the vertices of $\mathrm{H_n}$ with Feynman diagrams, this is done explicitly for H_2 in Fig.1.9. We would like to stress that in general one obtains diagrams with external bubbles and tadpoles. In particular, tadpoles are due to the cyclohedral facet and to tadpole factorisation facets[4]. As it is clear from Fig.1.8, tadpoles always appear in pairs that we called *IR-UV* for reasons that will be explained later in Section 2.4

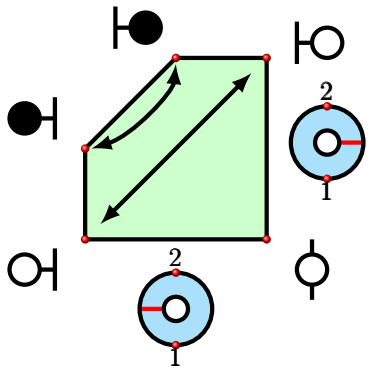

Figure 1.9: H_2 is shown with all of its vertices labelled by Feynman diagrams. Note that tadpoles appear in IR-UV pairs (white-black), but also in pairs dictated by the Cyclohedron (black arrows). The associahedral facets correspond to the cyclic order $\alpha = (-, 1, 2, +)$ and $\alpha = (-, 2, 1, +)$ in the formula (1.5), but they do not intersect at their tadpole vertices.

Before ending this section we would like to make some observations on the combinatorics of tadpole vertices. To begin with, note that the

[4]Which explains their name.

cyclohedral facet has only tadpole vertices. Moreover, when constructing a maximal set of arcs for one of its vertices we are esentially building a maximal set of arcs as we did in the case of the tree level Associahedra with $n+1$ particles, $\mathcal{M}_{\mathbf{D},n+1}$. The tadpole is inserted in a cubic vertex at which we can unambiguously perform the move depicted in Fig.1.10. As shown in Fig. 1.9, the result is a pairing on adjacent vertices of $\mathcal{B}_{n-1}$.

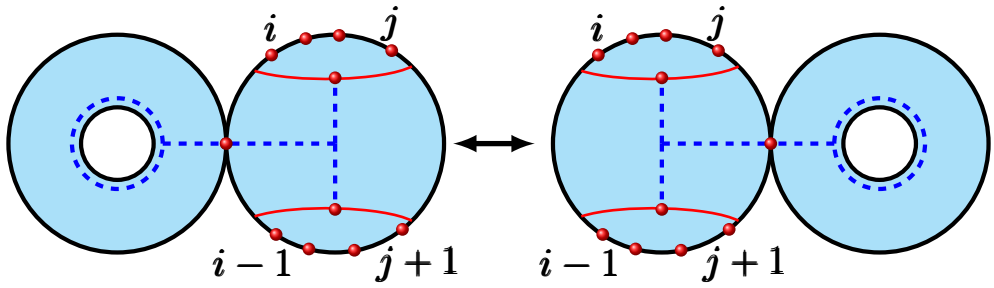

Figure 1.10: A vertex of the Cyclohedron is represented by a nodal disk as in the left figure. We can pair it with the vertex represented by the nodal disk in the right.

Because of the IR-UV pairing, we can extend this cyclohedral pairing to all the tadpole vertices of $\mathrm{H_n}$. The emerging combinatorics is reminiscent of a formula proposed by He et al [23] that builds the 1-loop integrands of the bi-adjoint theory from the forward limit of tree level amplitudes. We report this formula here

$$m_n^{1-\text{loop}}(\pi|\rho) = \int \frac{d^D\ell}{(2\pi)^D}\frac{1}{\ell^2}\lim_{k_\pm\to\pm\ell}\sum_{\substack{\alpha\in\text{cyc}(\pi)\\ \beta\in\text{cyc}(\rho)}} m_{n+2}^{\text{tree}}(-,\alpha,+|-,\beta,+), \qquad (1.5)$$

the inner sum is done over all cyclic permutations of the order π and ρ and $m_{n+2}^{\text{tree}}(-\alpha+|-\beta+)$ is the tree level double-partial amplitude for $n+2$ particles, the two extra particles are labelled by $\pm$ and carry momenta $k_\pm = \pm\ell$ in the forward limit. Computing these tree level amplitudes as a sum over Feynman diagrams one gets cutted tadpole diagrams, but these come in pairs with opposite signs and cancel. In particular, in our case with $\rho = \pi = (1,\ldots,n)$, for fixed α the sum over β produces the amplitude $m_{n+2}^{\text{tree}}(-,\alpha,+|-,\alpha,+)$ plus the off diagonal elements that happen to cancel the tadpoles of $m_{n+2}^{\text{tree}}(-,\alpha,+|-,\alpha,+)$. Thanks to the recent interpretation [12] of tree level scattering amplitudes as intersection numbers of associahedra in $\mathcal{M}_n(\mathbb{R})$, we can give a beautiful geometrical description of this cancellation. Recall that for each of the ordering $(-,\alpha,+)$ there is an As-

sociahedron living in $\mathcal{M}_{n-1}(\mathbb{R})$. Associahedra corresponding to different orderings touch precisely at those vertices whose dual Feynman diagrams appear in the partial amplitude $m^{\text{tree}}_{n+2}(-,\alpha,+|-,\beta,+)$. If we interpret the particles $-$ and $+$ as coming from a cutted propagators, these diagrams are tadpole diagrams. The cancellation explained above is then due to the fact that any given tadpole appears both in the Associahedron for the ordering $(-,\alpha,+)$ and for some other ordering $(-,\beta,+)$. This means that the cutted tadpole diagram, thought of as a tree level diagram, can be drawn in such a way that is planar with respect to either ordering. If we sew back the cutted propagator in both case, we obtain two different 1-loop tadpole diagrams precisely related by the flip of Fig. 1.10. It is tempting to speculate that the tadpole facets of the Halohedron should play a role in the cancellation of tadpoles for the 1-loop bi-adjoint integrand in a CHY approach that does not use the nodal sphere, but is rather formulated directly on the torus.

To summarise, in this section we saw that the moduli space $\mathcal{M}_{\mathbf{D},1;n}$ is naturally identified with the Halohedron $\mathrm{H_n}$. We discovered that its geometry encodes the factorisation and cut properties of a 1-loop double-partial integrand $m^{1-\text{loop}}(1,\ldots,n|1,\ldots,n)$. However, it also possesses boundaries which are clearly connected to one loop tadpoles of which we should get rid of somehow. Interestingly, the combinatorics of these facets seem to be related to the cancellation of tadpoles in the forward limit representation of the 1-loop integrand.

1.2.3 Higher genera and non polytopality

It is natural to expect that the boundary structure of the moduli space of a bi-annulus, i.e. with two internal circles, should be connected to higher loop integrands. Similarly, the moduli space of an annulus with punctures on both boundary component should be relevant for non planar 1-loop integrands. However, it was shown in [29] that beyond the cases studied discussed here, moduli spaces cease to be *polytopal*, i.e. cannot be realised as convex polytopes in some space. The root of the problem can be understood in the simplest case of a disk with two internal punctures. Among the legal loops, there is one circling both punctures and carrying *two* coordinates (ℓ,θ) [5]. As mentioned earlier, sending $\ell\to 0$ has the effect that θ ceases to be a meaningful coordinate, therefore we reach a codimension two boundary. It is impossible then, that the system of

[5] We recall that twisting angles did not make an appearance in the cases studied so far because if punctures live on the boundary of the surface we cannot make a twist in the double surface, or we would move them away from the boundary

pants decomposition on this surface can be mimicked by the face poset of a convex polytope. By pinching, any other type of surface will eventually produce a nodal disk with two internal punctures so the problem propagates to all surfaces but those described here. We also wish to emphasize that the problem is intimately connected to having a non-trivial mapping class group.

1.3 Triangulations and Cluster Algebras

We now illustrate a different approach to the studi of moduli spaces, ideated by Robert Penner [28]. Instead of using a decomposition of the surface into pair of pants and measuring the lengths and twisting angles, Penner proposed to choose an *ideal triangulation* and measure the length of the edges of the triangles. By ideal triangulation it is meant one whose edges start and end at the punctures of the surface. However, in the intrinsic hyperbolic metric these punctures looks infinitely far away, so the geodesical distance between them is infinite. To solve this problem, one considers horocycles at the punctures and measure the distance between them. If γ is a geodesic connecting a pair of punctures σ_i and σ_j, and $\ell(\gamma)$ is the signed hyperbolic distance between two horocycles at these punctures[6], one defines the λ-length:

$$\lambda_{i,j} = \exp(\ell(\gamma)/2).$$

Clearly, λ-lengths depend not only on the surface and its punctures, but also on the choices of horocycles decorating each puncture, thus λ-lengths carry an extra redundancy that has to be modded away. Changing an horocycle centered at σ_i has the effect of rescaling all the λ-lengths with an index i, therefore we can make horocycle-independent quantities out of ratios of λ-lengths. The situation is similar to what happens with projective spaces, and in this sense λ-lengths are homogeneous coordinates for the moduli space. Also, note that λ-lengths are positive real numbers by construction.

To any triangulation of a surface we can now associate a patch of homogeneous coordinates for the moduli space. The great advantage of Penner's approach is that, unlike changing pair of pants, changing triangulation is easy. The basic move we have to consider is the so called Whitehead move, also called "flip": for a pair of triangles sharing an edge, we remove that edge and replace it with the other diagonal of the square formed by the two triangles. Crucially, under such transforma-

[6] positive if the horocycles intersect, negative otherwise

tion λ-lengths transform in a simple way. If we denote the vertices of the square as $(1,2,3,4)$ we have

$$\lambda_{1,3}\lambda_{2,4} = \lambda_{1,2}\lambda_{3,4} + \lambda_{1,4}\lambda_{2,3}, \tag{1.6}$$

note that both sides are indeed homogeneous with respect to each index. The rule (1.6) is called *Ptolemy relation* or, in more modern language, *mutation relation* and is at the core of the connection with cluster algebras [27].

In a series of seminal works [27], Fomin, Zelevinsky and Thurston defined a rich world of cluster algebras associated to (almost) every type of Riemann surface. In order to do so, they had to enrich Penner's construction introducing the concept of *tagged* triangulations. For the sake of brevity, it suffices for us to know that this means to add λ-lengths which have inverse scaling weight with respect to some of its indices. Each (tagged) triangulation is then associated to a cluster, i.e. a set of generators of the cluster algebra, and triangulation flips correspond to mutation of clusters. The whole set of clusters form a connected complex known as cluster complex, which in general is infinite. Perhaps not too surprisingly, the simplest surfaces are related to the simplest finite type cluster algebras: $\mathcal{A}, \mathcal{B}, \mathcal{C}$ and $\mathcal{D}$. We will study these first cases in details in the next sections and see how the factorizing boundary structure of the moduli space is made manifest by the λ-lengths.

1.3.1 The moduli space of the disk and $\mathcal{A}$

Consider a disk with n punctures on its boundary, we can think of it as an n-gon with vertices corresponding to the punctures. Any triangulation of this n-gon is composed by short arcs with associated λ-lengths $\lambda_{i,i+1}$, i.e. the edges of the n-gon itself, plus $n-3$ internal edges. Together, this set of λ-lengths forms a patch of homogeneous coordinates on the moduli space. Any two triangulations are related to each other by a sequence of flips performed on the internal edges, by solving the associated cluster mutations (1.6) we can express the λ-lengths of one triangulation in terms of those of the other triangulation. Since the short arcs $\lambda_{i,i+1}$ are never flipped, the corresponding λ-lengths are called *frozen* in the cluster algebra literature, while the internal edges are called *unfrozen*. In this case the cluster algebra defined by the λ-lengths is a finite algebra, i.e. with a finite set of clusters, of type $\mathcal{A}$. It is well known that its cluster complex is an Associahedron, also called cluster polytope of type $\mathcal{A}$. As an example, when $n = 5$ there are 5 clusters, 5 frozen variables and 5 unfrozen variables. The clusters, labelled by triangulation of the 5-gon, correspond to

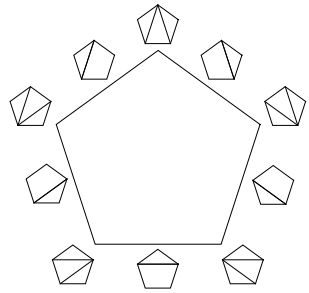

Figure 1.11: The cluster polytope $\mathcal{A}_2$, formed by the triangulations of a pentagon, turns out to be a pentagon

the vertices of the pentagon in Fig. 1.11. If we start from the triangulation with variables $x \coloneqq \lambda_{1,3}$ and $y \coloneqq \lambda_{1,4}$, the remaining variables are given by $\{\lambda_{2,4}, \lambda_{2,5}, \lambda_{3,5}\} = \{\frac{1+x}{y}, \frac{1+x+y}{xy}, \frac{1+y}{x}\}$.

In order to build horocycle-independent quantities associated to the disk we have to consider ratios of λ-lengths with zero weight in each of the punctures indices. Although we can build several of such ratios, a particularly convenient choice is

$$u_{i,j} = \frac{\lambda_{i,j+1}\lambda_{i+1,j}}{\lambda_{i,j}\lambda_{i+1,j+1}}, \tag{1.7}$$

for non-adjacent indices i and j. Note that indeed the RHS of (1.7) is independent under rescaling of any horocycle, since the same indices appear in the numerator and denominator. The advantage of the variables u is that they make the boundary structure of the moduli space manifest, as pointed out in [8], because they satisfy the equation

$$u_I + \prod_{J \not\asymp I} u_J = 1, \tag{1.8}$$

where the product is taken over all edges J of the n-gon crossing the edge I. Note that the u variables are positive and therefore (1.8) implies $0 \leq u_{i,j} \leq 1$. A boundary of the moduli space is attained saturating these constraints, but if $u_{i,j}$ vanishes then (1.8) forces the crossing variables to become 1. Therefore the full set of u-variables factorizes into two sets, associated to the internal edges of the two polygons in which the original n-gon is cutted into by the edge (i, j). Furthermore, the surviving variables now satisfy two independent set of equations (1.8) built directly by looking at these two polygons, because the crossing variables have disappeared from the product in (1.8).

Equation (1.8) naturally gives a notion of compatibility for the u variables, since not all of them can be set to zero simultaneously to probe lower dimensional boundaries of the moduli space. Similarly as done for the λ-lengths, we can then arrange the u variables in a complex where each facet corresponds to a variable, and vertices to a maximal set of $n-3$ compatible variables. It is not difficult to see that the resulting complex is combinatorially equivalent to the one of λ-lengths, i.e. is again an Associahedron.

Equation (1.8) is a consequence of the mutation relations satisfied by the λ-lengths, as one can easily seen by plugging the definition (1.7) in (1.8). Thus we can think of the map $\lambda \to u$ as a useful parametrisation to solve the constraints (1.8). However, this can be done in a different way [8] by writing

$$u_{i,j} = \frac{(\sigma_i - \sigma_{j+1})(\sigma_{i+1} - \sigma_j)}{(\sigma_i - \sigma_j)(\sigma_{i+1} - \sigma_{j+1})}, \tag{1.9}$$

for ordered punctures σ_i on the boundary of the disk, or on the real line. Then the variables $u_{i,j}$ are identified as particular cross ratios known as *dihedral coordinates* first introduced by Francis Brown. As we argued in Section 1.2, the approach based on pants decomposition also leads to cross ratios, albeit a different one. We see that in the particularly simple case of the disk, many approaches to the study of the moduli space (puncture coordinates, Fenchel-Nielsen coordinates, Penner coordinates) are easily seen to be equivalent. Already in the next case we will study this will not be the case anymore.

1.3.2 The moduli space of the punctured disk, $\mathcal{D}$ and $\mathcal{B}$.

We now consider the moduli space of a disk with n punctures on its boundary and an extra puncture in its interior. A triangulation of this surface is composed by arcs joining pair of punctures on the boundary or the internal puncture with a puncture on the boundary. In the first case, it is no longer sufficient to specify the pair of punctures to label the arc, because we can draw two inequivalent arcs separated by the internal puncture. We distinguish the two possibilities by using the labels $\lambda_{i,j}$ or $\lambda_{j,i}$ based on the orientation of the arc with respect to the internal puncture. In the second case we simply use the label λ_i, keeping in mind though that this variable carry a weight with respect to the internal puncture σ_0. As mentioned earlier, in order to obtain a proper cluster algebra one has to introduce the notion of tagged arcs and tagged triangulations. In this simple case the extra tagged arcs join an external puncture to the internal

one, but are distinguished from the previous ones so we denote them as λ'_i. The difference is that to such arcs we associate a λ-lengths which measure the distance from the horocycle at σ_i and the *conjugated* horocycle at σ_0, i.e. one with inverse length. For this reason, λ'_i scales with inverse weight with respect to λ_i upon rescaling of the horocycle at σ_0.

The usual notion of compatibility of λ-lengths coming from the crossing of arcs is extended to tagged triangulations. The tagged variables λ'_i are compatible with variables $\lambda_{i,j}$ if the associated arcs do not cross and are compatible with all the other tagged variables λ'_j, but are compatible with λ_j if and only if $j = i$[7].

Finally, the original Ptolemy relations are extended to take into account tagged variables. Inside of a punctured bi-gon with vertices σ_i, σ_j and edges $\lambda_{i,j}$ and $\lambda_{j,i}$ we can have a triangulation formed by the arcs λ_i and λ_j. We can then mutate λ_i to λ'_j, obtaining the relation

$$\lambda_i \lambda'_j = \lambda_{i,j} + \lambda_{j,i}, \tag{1.10}$$

note how both sides of the equation have the same weight with respect to each of the punctures σ_i, σ_j, and σ_0.

The cluster complex associated to the tagged triangulations of the punctured disk and their mutations is again finite, and it is called generalised Associahedron of type $\mathcal{D}_n$. Furthermore, it is combinatorially equivalent to the face lattice of a convex polytope.

As in the case of the disk, we can build moduli for the punctured disk by building ratios of λ-lengths, with the novelty that we have to take into account the different scaling of the variables λ'_i. A judicious choice is the following

$$u_{i,j} = \frac{\lambda_{i,j+1}\lambda_{i+1,j}}{\lambda_{i,j}\lambda_{i+1,j+1}} \quad \mathrm{j} \neq \mathrm{i}+1 \tag{1.11}$$

$$u_{i+1,i} = \frac{\lambda_{i+1}\lambda'_{i+1}\lambda_{i+2,i}}{\lambda_{i+1,i}\lambda_{i+2,i+1}} \tag{1.12}$$

$$u_i = \frac{\lambda_{i+1,i}}{\lambda'_i \lambda_{i+1}} \quad u'_i = \frac{\lambda_{i+1,i}}{\lambda'_{i+1}\lambda_i}. \tag{1.13}$$

Note that we have an u variable for each of the unfrozen cluster variables of $\mathcal{D}_n$. However, implicit in their definition is the fact that $u_i = u'_i$, since

[7] To some extent, one can understand these compatibility relations by imagining that the arc associated to λ'_i starts and ends at σ_i, looping around σ_0 and creating a self-folded triangle with λ_i. However, this picture fails to capture that different λ'_i are compatible.

(1.10) implies

$$\lambda_i \lambda'_{i+1} = \lambda_{i+1,i} + \lambda_{i,i+1} = \lambda'_i \lambda_{i+1}.$$

Due to mutation relations, u variables satisfy equation that make manifest the boundary structure of the moduli space:

$$u_I + \prod_{J \not\prec I} u_J^{\mathrm{d(I,J)}} = 1, \tag{1.14}$$

the product runs over all variables u_J associated to tagged and non-tagged arcs J crossing the arc I, the novelty with respect to the previous case are the exponents $\mathrm{d(I,J)}$ which are the number of intersections between arcs I and J. In counting them we consider tagged and non-tagged arcs as intersecting once, unless they are compatible. The boundaries are attained when some variable u goes to zero, which forces non compatible variables to go to 1 due to (1.14). The arc corresponding to a variable $u_{i,j}$ separates the punctured disk into a smaller punctured disk and an unpunctured n-gon, if $u_{i,j} \to 0$ the remaining variables factorize accordingly into a set of variables for the two surfaces. Consider now a variable $u_i = u'_i$. Its vanishing forces all the remaining variables u_j to go to 1. On the other hand, both variables $u_{i,j}$ and $u_{j,i}$ survive the limit. We can interpret the leftover set of variables and their new constraints as those satisfied by the moduli of an unpunctured $n+1$-gon with a new puncture σ_0 between σ_i and σ_{i+1}. Arranging the u variables in a complex according to their compatibility, as dictated by (1.14), we obtain a polytope combinatorially equivalent to the Cyclohedron $\mathcal{B}_{n-1}$. This is what we should expect, since we already know from Section 1.2 that the moduli space of the punctured disk is a cyclohedron.

It is interesting to remark that for the n-gon the map $\lambda \to u$ did not change the combinatorics of the compatibility cluster, while in the case of the punctured disk it changes from being $\mathcal{D}_n$ to being $\mathcal{B}_{n-1}$.

1.3.3 Feynman diagrams and Triangulations

We have seen how to understand the boundary structure of simple moduli spaces in terms of triangulations and cluster algebras. To make a connection with scattering amplitudes we wish to understand this boundary structure in terms of Feynman diagrams as well. This can be done using a well known duality between triangulations of surfaces and cubic diagrams. In the case of a disk with no internal puncture this involve only tree level *planar* diagrams, see Fig. 1.12, and is at the core of the relation between $\mathcal{A}_{n-3}$ and tree level amplitudes discovered in [8]. Note that flips

Figure 1.12: Examples of triangulations of punctured surfaces and the dual Feynman diagrams

of triangulation are dual to *s/t-channel swaps*. The duality extends to triangulations of disks with an arbitrary number of punctures in the interior and loop diagrams, however we now have a departure from the combinatorics of cluster algebras, which requires *tagged* triangulations. The situation is less dramatic for $\mathcal{B}_{n-1}$, because we can unambiguously interpret a pair of plain and tagged arcs as a single self-folded triangle, which is dual to a tadpole, see Fig. 1.13. In this picture not all the vertex adjacencies of $\mathcal{B}_{n-1}$ can be understood as s/t-channel swaps, there is an extra flip rule given by exchanging the two choices of pairs of tagged and plain arcs inside of a bi-gon. Dually this rule translates to the same *tadpole flip* pictured in Fig. 1.10. In any case, let us emphasize again that there is a mismatch between the full set of 1-loop planar cubic diagrams and vertices of $\mathcal{D}_n$. This fact will later guide us to the definition of a new convex polytope whose combinatorics will be in complete agreement with that of 1-loop diagrams, see Section 2.3.

Figure 1.13: A pair of tagged and un-tagged arcs can unambiguously replaced with a self-folded triangle, which in the dual picture yields a tadpole.

1.3.4 Other surfaces and cluster infinity

The combinatorics of the cluster algebra associated to a once punctured n-gon is naturally tied to 1-loop diagrams, via the duality between triangulations and cubic diagrams. The source of the loop is due to the internal

puncture, therefore the picture begs to be extended at higher loop by simply adding extra punctures. However there is a formidable obstruction to do so in a naive way. If we consider a twice punctured n-gon the associated cluster algebra becomes infinite, i.e. the process of mutating a cluster never ends, but rather produces more and more cluster variables. The origin of this phenomenon is that we can draw an arc joining an external puncture σ_i to an internal puncture σ_A in infinitely many inequivalent ways, by winding around the other internal puncture σ_B. Indeed, it is possible to apply a sequence of mutations that given a triangulation produces a new triangulation where all arcs start and end in the same punctures but the winding numbers of the ones going to the internal punctures are changed.

Combinatorially, this annoying fact can be forgotten by either considering the quiver associated to the triangulation or by drawing the dual Feynman diagram[8], which are left invariate. The case of Feynman diagrams is particularly interesting. Let us label the momenta flowing in the propagators using dual variables, and suppose to follow the path of mutations that increase the winding number. It turns out that after the sequence of mutations the net effect is to swap the variables associated to the internal zones. Clearly this operation is physically meaningless, and therefore the infinity associated to winding numbers should be modded out.

As was the case for the non-polytopality of higher genera moduli spaces in the Fenchel-Nielsen coordinates approach, the origin of the infinity in the cluster algebra can be traced back to the presence of a non-trivial mapping class group. To a pair of punctures in the interior of the disk we can associate a Dehn twist whose action on λ-lengths is precisely to change winding numbers. It is a pressing question if the positive geometry of the space obtained from the infinite cluster algebra after modding out the mapping class group has the correct boundary structure to capture the singularities of higher loop integrands.

[8]Obviously there is a finite number of cubic Feynman diagrams at a given order and number of external legs

CHAPTER 2

Positive Geometries in Kinematical space

2.1 Projective Scattering Forms and Polytopes

2.1.1 The Scattering Form and Feynman Polytopes

In the previous chapter we discussed several examples of geometries with meaningful boundary structures, in the sense that they reproduce the singular properties of amplitudes described by (1). However, all these geometries live in the auxiliary space $\overline{\mathcal{M}}_{g,n}$ and at first glance it is not obvious how to relate them to scattering amplitudes. A more natural approach would then be to look for avatars of these objects directly in the space of kinematical variables on which amplitudes and integrands depend on. More precisely, in most of this Chapter the kinematical space will be taken to be the space of all propagators appearing in some set of Feynman diagrams. In this space, following [8], we will seek to rediscover the geometries we already found in the previous chapter in the form of *convex polytopes*, which are the simplest examples of positive geometries.

A priori the existence of such polytopes is not guaranteed, since it is not obvious from the Feynman diagrammatic representation of amplitudes whether their singularities satisfy the appropriate combinatorical and topological requirements to be compatible with a polytopal structure. A first clue of their existence, however, is provided by one of the central element of our story: the *Scattering Form*.

The scattering form is a differential form on the kinematical space which is constructed as follows: first, label any Feynman diagram with its dual variables [1], assign an arbitrary ordering to the propagators and

[1] This choice of labelling foreshadows that we will mainly be interested in planar diagrams, which are dual to the pants decomposition and triangulations we discussed in Chapter 1. However, it is possible to build scattering forms for non-planar diagrams in the same way.

then sum over all diagrams the dlog forms built with these variables:

$$\Omega = \sum_{g \in \text{diagrams}} \text{sgn}(g) \bigwedge_{a \in \text{propagators}} \frac{dX_a}{X_a}, \tag{2.1}$$

where we have not said yet how to fix the relative signs of the dlogs. These signs are uniquely fixed by requiring the scattering form to be *projective*, i.e. invariant under *local* $\mathrm{GL}(1)$ rescaling of all the planar variables: $X \to \alpha(X)X$. A priori, there is no guarantee that one can fix coherently the signs in order to ensure projectivity of the scattering form. However, the existence of a convex polytope whose face lattice reproduces the singularity structure of the corresponding amplitude implies that this can be done. More precisely, there must be a one to one correspondence between the various faces of the polytope and iterated residues of the amplitude, so that codimension one facets correspond to propagators, codimension two faces to pairs of compatible propagators and so on down to vertices which must correspond to Feynman diagrams. Then one can recognize (2.1) as a particular representation of the *canonical form* of such polytope, obtained by a triangulation of its dual. Moreover, the projectivity of Ω becomes equivalent to the cancellation of a spurious pole at infinity, introduced term by term in the triangulation.

On the other hand, even if a convex realisation of the putatively associated polytope is not known, one can still try and build a projective scattering form. Let us show by some examples how this works in practice, starting from the simplest case of a 4-point planar amplitude at tree level. Suppose we start with an s-channel diagram; in planar variables this means we have a contribution $d\log(X_{1,3})$ to the scattering form. Under local rescaling this is not invariant since it transforms as $d\log(X_{1,3}) \to d\log(X_{1,3}) + d\log(\alpha)$, but the extra term can be cancelled by adding a t-channel with opposite sign:

$$\begin{aligned} \Omega &= d\log(X_{1,3}) - d\log(X_{2,4}) \\ &\to d\log(X_{1,3}) - d\log(X_{2,4}) + d\log(\alpha) - d\log(\alpha) = \Omega. \end{aligned} \tag{2.2}$$

Geometrically we can interpret Ω as the canonical form of the segment depicted in Fig. 2.1. We could try to build a scattering form for the full non-planar amplitude by adding an extra term $d\log(u)$ to the scattering form. However, it is now impossible to choose relative signs between the three contributions so that the complete scattering form is projectively invariant. This is a reflection of the fact that it is impossible to find a one dimensional polytope with three vertices. We see then that the existence

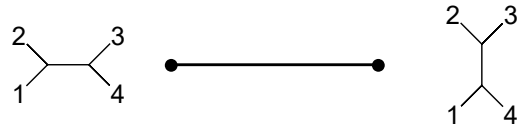

Figure 2.1: The simplest polytope is a segment, its boundary structure reproduces that of a planar four point scalar amplitude.

of a projective scattering form is a first check on the polytopal structure of the singularities of a scattering amplitude.

A lesson to be learned from this simple example is that we can try to build a scattering form by starting from a diagram of our choice and then adding diagrams to compensate for the terms in its variation. The new diagrams are obtained by doing a simple transformation on the original one: in the example above it was the s/t-channel swap, but in general one can expect different transformations and indeed this will be the case at 1-loop. Of course the variation of the newly added diagrams will have to be compensated as well, which will require to add more and more diagrams, and it is highly non-trivial that the procedure will eventually stop.

We now turn to loop level, the simplest 1-loop diagram is the two point bubble which is dual to a triangulation of the punctured bi-gon with arcs X_1 and X_2. For reasons that will become clear immediately, we choose to give a common internal mass to all propagators so that $X_i = \ell_i^2 - m^2$. The bubble contributes to a putative 1-loop 2-point scattering form with $d\log(X_1) \wedge d\log(X_2)$, whose variation under rescaling is $d\log(\alpha)[d\log(X_2) - d\log(X_1)]$. In order to build a projective form, we are thus forced to add two diagrams that compensate for the variation of the two propagators X_1 and X_2. The simplest thing to do is to use again the s/t-channel swap on the propagators of the bubble, its effect is to produce two tadpole diagrams which we add to the scattering form. Let us call $X_0 = -m^2$ the tadpole propagator, then the total scattering form is

$$\Omega = d\log(X_1) \wedge d\log(X_2) - d\log(X_0) \wedge d\log(X_2) - d\log(X_1) \wedge d\log(X_0),$$

the reader is invited to check the projectivity of the above form, which is guaranteed by the fact that we can arrange the bubble and tadpole diagrams on the vertices of a triangle (2.2). Note that not only tadpoles compensate for the bubble variation because they are related to it by an s/t-channel swap, they also compensate for each other's variation of the propagator X_0 because they are related by a *tadpole flip*.

We now move to a three-point example. We can start building our scattering form from the *ring diagram*, the s/t-channel swaps now create external bubbles, if we consider the external legs on-shell then the bubble

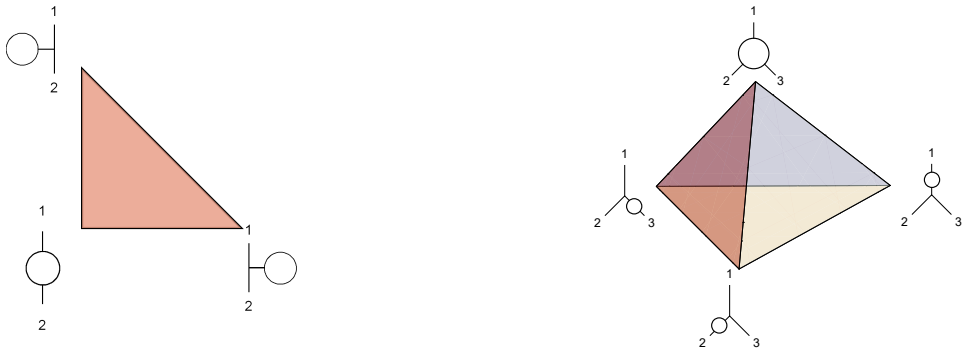

Figure 2.2: Examples of Feynman polytopes at 1-loop.

propagators are again $X_{i,i+1} = k_i^2 - m^2 = -m^2 = X_0$. By adding the four diagrams we get a projective scattering form (we omit the wedge signs for compactness)

$$\begin{aligned}\Omega = &d\log(X_1)d\log(X_2)d\log(X_3) - d\log(X_0)d\log(X_2)d\log(X_3)\\ &- d\log(X_1)d\log(X_0)d\log(X_3) - d\log(X_1)d\log(X_2)d\log(X_0).\end{aligned} \tag{2.3}$$

Once again the projectivity can be explicitly checked, and it is guaranteed by the fact that the four diagrams can be arranged on the vertices of a 3-simplex as in Fig. 2.2. Note that tadpoles are not necessary, since the bubbles compensate for each other.

Let us continue our exploration with some four point examples. Once again we start from the ring diagram and perform s/t-channel swaps, but now something new happens. The sequence of swaps bring us to a diagram with an internal bubble and by momentum conservation the propagators at both sides of the bubble are equal. Then the dlog associated to the bubble is zero due to the wedge product. This is not a problem however: the diagrams connected by swaps to the internal bubble compensate for each other even without the internal bubble! Summing all together and performing a bit of algebra we find the following projective scattering form (we further suppress the $d\log$ symbol)

$$\begin{aligned}\Omega = &(X_1)(X_2)(X_3)(X_4) - (X_{2,4})(X_2)(X_3)(X_4) - (X_1)(X_{1,3})(X_3)(X_4)\\ &- (X_1)(X_2)(X_{2,4})(X_4) - (X_1)(X_2)(X_3)(X_{1,3})\\ &+ [(X_{2,4}) - (X_{1,3})]\,(X_1)(X_2)(X_0) + [(X_{2,4}) - (X_{1,3})]\,(X_2)(X_3)(X_0)\\ &+ [(X_{2,4}) - (X_{1,3})]\,(X_3)(X_4)(X_0) + [(X_{2,4}) - (X_{1,3})]\,(X_4)(X_1)(X_0).\end{aligned} \tag{2.4}$$

This is the simplest example of a projective scattering form for which it is

not known a convex realisation of the putatively associated polytope. [2]

Higher loop cases can be treated in the same fashion. One starts with a specific diagram, labelled using planar variables or loop momenta, and then adds diagrams obtained from it by s/t-channel swaps in order to guarantee projectivity. At any given mutation, the variable labelling the new diagram can be obtained simply by imposing momentum conservation. Diagrams with internal bubbles, eventually reached by such transformations, do not contribute to the total scattering form due to the wedge products combined with momentum conservation. Unfortunately, even the simplest examples are quite cumbersome so we will not report them here. After all, this approach to loop scattering forms encounters an obstacle already at 1-loop since it is not clear how to realize the associated polytopes.

There is another way to deal with internal bubbles and build a larger 1-loop scattering form, which was first proposed in [1]. We can simply state that the two propagators at the side of the internal bubble are labelled by two *different* variables, say $X_{i,j}$ and $X_{j,i}$. It is also convenient to consider external particle to be off-shell so that the bubble propagators $X_{i,i+1} = k_i^2 - m^2$ are all different. By doing so, summing over *all* 1-loop diagrams we find a projective scattering form. For example, for $n = 3$ we find the one associated to the polytope in Fig. 2.3

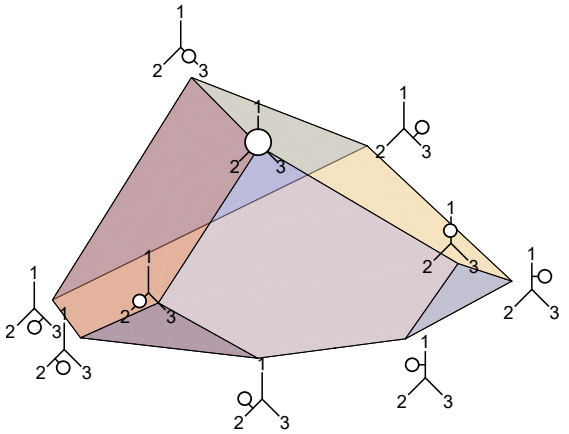

Figure 2.3: The polytope $\overline{\mathcal{D}}_3$, whose vertices are labelled by all 1-loop 3-point Feynman diagrams.

From a physical viewpoint introducing two different variables for the propagators at the side of the internal bubble is tantamount to breaking momentum conservation in the vertices of the graph, which is somewhat

[2]During the writing of this manuscript a convex realisation for the polytope was found by Thomas and Karp, although higher points generalisation are still missing

unsettling. Nevertheless, this deformation is necessary only to discover the convex polytope associated to the form and will eventually be undone in Chapter 3, where we will restore momentum conservation and recover the physical integrand in full glory, double poles included. The projective scattering form built this way is very close to the one associated to the Halohedron, with the difference than the combinatorics of the Halohedron introduce a doubling in the number of tadpole vertices (the IR/UV pairing) and extra tadpole facets. In conclusion, the form introduced here is the most natural to consider at 1-loop and we will devote Section 2.3.1 to the study of the positive geometry underlying it.

2.1.2 Projectivity and Polytopality

As we mentioned earlier, the projectivity of the scattering form is an important check on the existence of a polytope of which it should be the canonical form: if such a polytope exists, then the form can be made projective. This is so because projectivity guarantees that Ω does not have any other poles other than those made manifest by writing it as a sum of dlogs. Let us give a simple example, consider the form

$$\Omega' = \frac{dX_1}{X_1} + \frac{dX_2}{X_2}, \tag{2.5}$$

which is not projective due to the relative plus sign. Naively Ω could be the canonical form of a 1-dimensional polytope with vertices in $X_1 = 0$ and $X_2 = 0$, which could be realised in some 1-dimensional subspace obtained by setting $X_2 = a + bX_1$. However, if we pullback Ω to this subspace we obtain

$$\Omega' = dX_1 \left(\frac{1}{X_1} + \frac{b}{a + bX_1} \right) = dX_1 \frac{a + 2bX_1}{X_1(a + bX_1)},$$

which develops a pole at infinity, regardless of the choice of a and b [3]. Instead the projective form

$$\Omega = \frac{dX_1}{X_1} - \frac{dX_2}{X_2}, \tag{2.6}$$

[3]Unless we chose $b = 0$ but in that case we do not have a convex realisation of the polytope

pulls back to

$$\Omega = dX_1 \left(\frac{1}{X_1} - \frac{b}{a + bX_1} \right) = dX_1 \frac{a}{X_1(a + bX_1)}, \tag{2.7}$$

which is the correct canonical form of the interval with vertices in $X_1 = 0$ and $X_1 = -a/b$. More generally, consider a differential form Ω written as in (2.1)

$$\Omega = \sum_{v \in \mathrm{V}} \mathrm{sgn(v)} \bigwedge_{\mathrm{i}=1}^{\mathrm{m}} \frac{\mathrm{dX_{a_i}}}{\mathrm{X_{a_i}}}, \tag{2.8}$$

for some set of "vertices" V, X_{a_i} represent a subset of m "facets" intersecting at the vertex v. If Ω is projective then it can be thought as a differential form on a projective space $\mathbb{P}^{F+1}$ with homogeneous coordinates $\mathcal{Y} = [M, X_1, \ldots, X_F]$, where X_a are all the variables on which it explicitly depends and M an auxiliary variable. In order to give a convex realisation of a m-dimensional polytope, we consider an m-dimensional projective subspace given by equalities $X_a = MW_a^0 + \sum_{i=1}^m X_i W_a^i =: Y \cdot W_a$, with homogeneous coordinates $Y = [M, X_1, \ldots, X_m]$ and pullback Ω there. We can further use the global rescaling to fix $M = 1$ thus we obtain a form defined on the affine space $\mathbb{R}^m$ with poles along the hyperplanes $X_a = 0$ and no pole along the hyperplane at infinity $Y \cdot W^* = M = 0$. The absence of this pole is clear from the fact that M never appeared in (2.8) in the first place.

Another interpretation of this fact, following [8], is that we can compute the canonical form of a polytope by triangulating its dual using simplices with vertices $\{W_{a_1}, \ldots, W_{a_m}, W^*\}$. In homogeneous coordinates we obtain

$$\Omega = \langle Y d^m Y \rangle \sum_{v \in \mathrm{vertices}} \mathrm{sgn'(v)} \frac{\langle \mathrm{W^* W_{a_1} \ldots W_{a_m}} \rangle}{\mathrm{Y \cdot W^* \prod_{i=1}^{m} Y \cdot W_{a_i}}}, \tag{2.9}$$

where the signs $\mathrm{sgn'(v)}$, dictated by the relative orientations of the simplices of the triangulation, are a priori different from the signs $\mathrm{sgn(v)}$ dictated by the projectivity of Ω. However, they are actually the same and they make so that the pole at infinity, present term by term in (2.9), cancels in the sum. In conclusion, the projectivity of Ω is mandatory if it is to be the canonical form of a polytope and is equivalent to the absence of a pole at infinity.

We now wish to present a geometrical interpretation of the projectivity of a differential form written as in (2.8). The following is based on an on-

going collaboration with Hadleigh Frost. Let us begin with a single dlog term,

$$\omega = \frac{dX_1}{X_1} \wedge ... \wedge \frac{dX_m}{X_m},$$

and compute its transformation under local rescaling $X_i \to \alpha X_i$

$$\omega \to \omega + \sum_{i=1}^{m} (-1)^{i+1} \frac{d\alpha}{\alpha} \wedge \frac{dX_1}{X_1} \wedge ... \wedge \widehat{\frac{dX_i}{X_i}} \wedge \cdots \wedge \frac{dX_m}{X_m},$$

we can write it more succinctly by stripping the factor $\frac{d\alpha}{\alpha}$ and define the *projective variation* operator δ by

$$\delta(\omega) = \sum_{i=1}^{m} (-1)^{i+1} \frac{dX_1}{X_1} \wedge ... \wedge \widehat{\frac{dX_i}{X_i}} \wedge \cdots \wedge \frac{dX_m}{X_m}. \tag{2.10}$$

This expression should be familiar from the usual boundary operator defined in simplicial topology, one can define a simplex as an ordered collection of vertices, $\Delta = \{X_1, \ldots, X_m\}$, and an operator ∂ that acting on Δ produces a linear combination of lower dimensional simplices,

$$\partial\Delta = \sum_{i=1}^{m} (-1)^{i+1} \{X_1, \ldots, \hat{X}_i, \ldots, X_m\},$$

which are its facets. It is very natural to establish a correspondence between simplices and dlog forms,

$$\Delta \leftrightarrow \omega, \tag{2.11}$$

under which the boundary operator ∂ and the projective variation operator δ are mapped into each other. In particular, we automatically obtain that $\delta^2 = 0$. We caution the reader that this correspondence is not the usual one between a polytope and its canonical form, and indeed ω is not the canonical form of Δ. Nevertheless the two concepts are related, since the canonical form of the dual simplex Δ^* is given by $\Omega = \delta(\omega)$, note that the projectivity of Ω is guaranteed by the fact that $\delta^2 = 0$. When dealing with an operator that squares to zero, the first meaningful thing to do is to study its homology. In our case we ask ourselves whether any projective scattering form Ω is the projective variation of some form η. It turns out

that this is always the case, we just have to introduce a new variable M:

$$\delta\left(\frac{dM}{M}\wedge\Omega\right)=\Omega-\frac{dM}{M}\wedge\delta(\Omega)=\Omega. \tag{2.12}$$

Now suppose that Ω is given by a sum of dlog terms as in (2.8). We can consider the simplicial chain c [4] defined by the purely combinatorical data of the simplices corresponding to the dlog terms and their relative orientations encoded in Ω. The projectivity of the latter translates, via the correspondence (2.11), to the statement that this chain is actually a cycle, that is $\partial c = 0$. Furthermore, because of (2.12) we know that c is actually the boundary of another simplicial chain b which is given by a sum of simplices sharing a common vertex M. By analogy with the example of the simplex, we would like to claim that Ω is the canonical form associated to the polytope of which b is the dual. However, we do not know yet if b has the appropriate topological properties to be realisable as a convex polytope. Since b is tautologically triangulated by the simplices $\{M, X_{a_1}, \dots, X_{a_m}\}$ appearing in $M \wedge \Omega$ we can at least compute its homological groups $H_i(b)$ by explicitly looking for cycles which are not boundaries. In top dimension there is no trivial cycle, since every chain is written as [5]

$$c_m = \frac{dM}{M}\wedge\left(\sum_{v\in \mathrm{U}\subset \mathrm{V}}\frac{dX_{a_1}}{X_{a_1}}\wedge\cdots\wedge\frac{dX_{a_m}}{X_{a_m}}\right),$$

but then $\partial c_m = 0$ implies

$$\sum_{v\in \mathrm{U}\subset \mathrm{V}}\frac{dX_{a_1}}{X_{a_1}}\wedge\cdots\wedge\frac{dX_{a_m}}{X_{a_m}}=0$$

which implies that $c_m = 0$. Therefore $H_m(b)$ is trivially zero. Next consider a generic k-dimensional chain, which we can write separating the dependence on M as

$$c_k = M\wedge\eta_{k-1}+\eta_k,$$

where η_k are k-forms independent on the variable M. The boundary of this chain is given by

$$\delta(c_k)=\eta_{k-1}+\delta(\eta_k)-M\wedge\delta(\eta_{k-1}),$$

[4] By simplicial chain is meant a linear combination of simplices. They define a topological space obtained by gluing the simplices at the shared faces and the topological properties of this space can be computed by the knowledge of the gluing patterns

[5] we make free use of the correspondence between simplices and dlog forms

which can only be zero if $\eta_{k-1} = -\delta(\eta_k)$, but then we can write c_k as a boundary

$$c_k = -\delta(M \wedge \eta_k).$$

Then we conclude that $H_k(b) = 0$ for all $k > 0$. Finally $H_0(b) = \mathbb{Z}$ since b is connected: all the simplices share the vertex M and then any two points can be joined by a path through it. We conclude that b has the homology groups of a ball.

To summarize, in this section we discussed how the projectivity of the scattering form is a necessary requirement for the polytopality of the corresponding positive geometry. This is a promising result, in light of the plethora of projective scattering forms that have been found here and elsewhere [36; 37; 38], going well beyond ϕ^3 theory. Particularly exciting is the fact that projective scattering forms associated to higher loop integrands have already been discovered, which is then the first step in completing the Amplituhedral picture for ϕ^3 at all loop order. Unfortunately, the knowledge of the projective scattering form by itself gives no useful indication on how to find an actual convex realisation of the polytope, in order to do so we have to lean on some other ideas. In section 2.3.1, this will be achieved for the scattering form of ϕ^3 theory up to 1-loop exploiting the fact that the factorisation properties encoded by (1) are easily seen to be reproduced by the (1+1)-dimensional *wave equation*.

2.2 The Halohedron in Abstract space

In this section we define a convex realisation of the Halohedron in an affine space X with coordinates $(X_1, \ldots, X_n)$. We are going to do so by defining a set of linear functions X_I such that the region where they are all positive cuts an Halohedron. These functions will be in 1-1 correspondence with the facets of the Halohedron, and thus with propagators of 1-loop planar diagrams, and will be labelled as the planar variables listed in Tab. 1.1. The Halohedron is then realised as the intersection of the region where all loop propagators are positive with the space X. We can think of the space X as an abstraction of the natural kinematical space of all planar variables, it is a subspace where the planar variables satisfy relations that guarantee the realisation of the Halohedron, while they do not satisfy other usual relations. For example, momentum conservation is not enforced since the planar variables $X_{(i,\ldots,j)}$ and $X_{(j+1,\ldots,i-1)}$ - which are dual to the propagators at the side of an internal bubble - will not be equal on X. Indeed, this would not be possible since they correspond to different facets of the Halohedron.

In order to find the correct form of the functions X_I, we implement the

convex realisation of the Halohedron described in [29], which is obtained by iterated truncations of an n-dimensional cube. We center one of the corners of the cube at the origin of the space X, so that the coordinates X_i become the face variables of n of the facets of the cube. Next, we introduce functions $X_{(i,i+1)} = \epsilon_i - X_i$, for some positive constant ϵ_i. The positive regions $X_i \geq 0$ and $X_{(i,i+1)} \geq 0$ define the initial cube, which is to be truncated at the intersection of the faces $X_{(i,i+1)}$ in order of increasing dimensions. The first truncation happens at the vertex where all the facets $X_{(i,i+1)}$ meet and it is implemented by considering the function

$$X_0 = \sum_{a=1}^{n} X_{(a,a+1)} - \epsilon_0, \tag{2.13}$$

where ϵ_0 is a new positive constant. Requiring $X_0 \geq 0$ shaves off the vertex where all the $X_{i,i+1}$ are zero, creating a new facet - which is a $(n-1)$-simplex - at the end of all the truncations such facet will be cutted into the cyclohedral facet of the Halohedron. Similarly one truncates all the one dimensional faces given by the intersection of the faces $X_{a,a+1}$ for $a \in (i, i+1, \ldots, i-1)$, by introducing functions

$$X_{(i,i+1,\ldots,i-1)} := \sum_{a=i}^{i-1} X_{(a,a+1)} - \epsilon_{(i,i+1,\ldots,i-1)}, \tag{2.14}$$

and demanding them to be positive. The truncations easily generalize to every dimension, for every subset $I \subset (1, 2, \ldots, n)$ of cyclically consecutive indices we consider a function

$$X_I = \sum_{a \in I'} X_{a,a+1} - \epsilon_I, \tag{2.15}$$

where I' is obtained from I by dropping the last element and ϵ_I is a positive constant. The variables X_i, $X_{i,i+1}$,X_0 and X_I together span the whole set of facets of the Halohedron $\mathrm{H_n}$, and the region where they are simultaneously positive gives a convex realisation of it, an example is shown in Fig. 2.4. Finally, we remark the constants ϵ_I cannot be chosen arbitrarily. The reason is that they modulate the depth of the truncations which must not be too deep, for example ϵ_0 must be smaller than $\epsilon_{(i,i+1)}$ or the facet X_0 created by the truncation will touch the facet X_i.

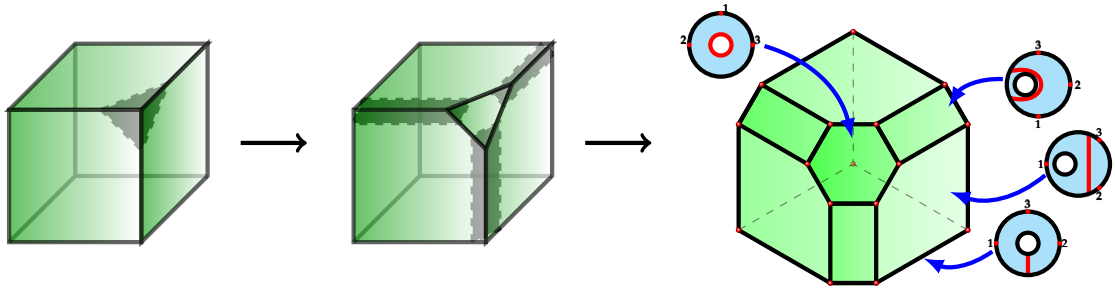

Figure 2.4: The sequence of truncations that produces the 3-dimensional Halohedron.

2.3 ABCD from the Wave Equation

In [8] it was discussed how the cluster polytope $\mathcal{A}_{n-3}$, also known as Associahedron, is related to tree level amplitudes of bi-adjoint scalar theory. In particular, a convex realisation in the kinematical space of Mandelstam variables was found for $\mathcal{A}_{n-3}$. This so-called ABHY realisation, which was previously unknown to mathematicians, was inspired by the simple physical requirement of absence of spurious non planar poles. Later the ABHY construction was extended to $\mathcal{B}_{n-1}/\mathcal{C}_{n-1}$ and $\mathcal{D}_n$ in [34], relying on the connection with the cluster algebras. In this section we propose a new way to rediscover the ABHY construction, building on a phenomenon which is familiar to physicists: the factorisation properties of causal diamonds. Although the final result is equivalent to the one of [34], the new framework has the advantage of making manifest certain properties of ABHY polytopes which have gone unnoticed so far, as well as suggesting natural ways of further generalisation.

2.3.1 From associahedra to the wave equation and back

Let us first review the ABHY construction of the Associahedron in kinematical space, as presented in [8]. The kinematic space is spanned by all *planar variables* $X_{i,j}$ which correspond to the $\frac{n(n-3)}{2}$ diagonals of an n-gon. On the other hand the Associahedron is a $(n-3)$-dimensional polytope, whose codimension-k faces are in one-to-one correspondence with collections of k non-crossing diagonals of an n-gon, or equivalently k compatible planar variables, $X_{i,j}$. To obtain an Associahedron, we intersect the positive region $X_{i,j} \geq 0$ with a subspace [6] defined by the following $\frac{n(n-3)}{2} - (n-3)$ conditions: for non adjacent i, j with $1 \leq i < j \leq n-1$, we

[6] It is a well known results in the theory of convex polytopes, that any convex polytope $\mathcal{P}$ can be obtained by intersecting a simplex with an affine space

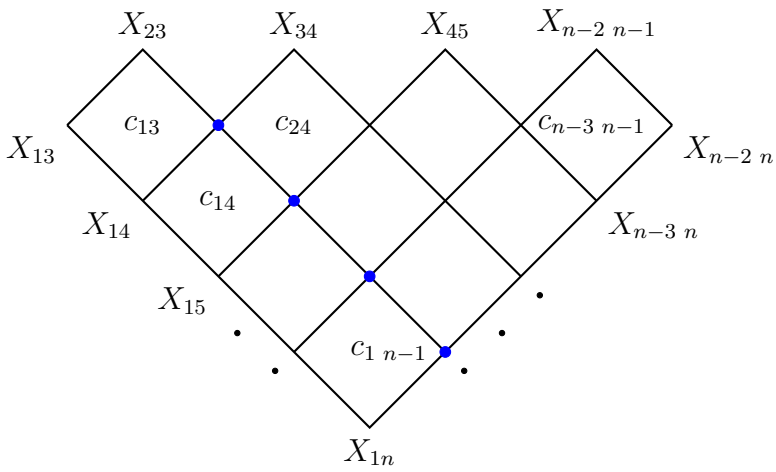

Figure 2.5: A mesh diagram for ABHY realization of associahedra

impose

$$X_{i+1,j+1} - X_{i+1,j} - X_{i,j+1} + X_{i,j} = c_{i,j}. \tag{2.16}$$

where $c_{i,j}$ are arbitrary positive numbers. The key feature of the Associahedron $\mathcal{A}_{n-3}$ is the factorization of its faces into lower dimensional associahedra, for the ABHY realisation this means that

$$\partial_{X_{i,j}}\mathcal{A}_{n-3}(1,2,\cdots,n) = \mathcal{A}^{(L)}_{n_L-3}(i,i{+}1,\cdots,j) \times \mathcal{A}^{(R)}_{n_R-3}(j,j{+}1,\cdots,i{-}1,i)\,, \tag{2.17}$$

where $\partial_{X_{i,j}}$ denotes the facet corresponding to the vanishing of the planar variable $X_{i,j}$, $\mathcal{A}^{(L)}$ (resp. $\mathcal{A}^{(R)}$) is an ABHY polytope built using an n_L-gon (resp. an n_R-gon) with vertices indicated in (2.17).

It is convenient to arrange the set of relations (2.16) in the *mesh diagram* shown in Fig. 2.5. Each condition (2.16) is represented by a diamond, with the planar variables $X_{i,j}$, $X_{i+1,j+1}$, $X_{i,j+1}$ and $X_{i+1,j}$ at its left, right, top and bottom corners and the constant $c_{i,j}$ inside. The entire set of conditions can be drawn simultaneously as a right triangle made of such diamonds, with 45-degree lines representing the i and j axes. We will refer to these as *mesh relations*, and for future convenience we also include the frozen variables $X_{i,i+1}$ for $i = 1, 2, \cdots, n$, which we define to be zero. In the mesh diagram they are located at the bottom point $(1, n)$, and points above the top edge of the triangle, $(1,2),(2,3),\cdots,(n{-}1,n)$. A useful fact which is completely manifest in the mesh picture is that, for any rectangle bounded

by $a \leq i \leq a'$ and $b \leq j \leq b'$, the mesh relations (2.16) associated to the diamonds contained in the rectangle telescopically sum to

$$X_{a,b} + X_{a',b'} - X_{a,b'} - X_{a',b} = \sum_{a \leq i < a'} \sum_{b \leq j < b'} c_{i,j} \,. \tag{2.18}$$

We now turn to the new picture for ABHY polytopes. The basic observation is that the ABHY conditions can be viewed as a discretized version of the $(1+1)$-dimensional wave equation. Indeed, imagine that the points forming the mesh diagram of Fig. 2.5 become infinitely close, or equivalently that the mesh becomes more and more dense. Then we can replace the relation (2.16) with its infinitesimal version, obtained by interpreting differences as derivatives along the two directions (u, v) of the mesh. We obtain

$$\partial_u \partial_v X(u, v) = c(u, v) \,, \tag{2.19}$$

which is the $(1 + 1)$-dimensional wave equation written in light-cone coordinates $u = t - x$, $v = t + x$[7], note that now c has the interpretation of a source for the equation. It is clear that (2.18) is replaced by an integral version: given any rectangular region $a \leq u \leq a'$, $b \leq v \leq b'$ contained in the right triangle, the integral wave equation reads

$$X(a, b) + X(a', b') - X(a, b') - X(a', b) = \int_a^{a'} du \int_b^{b'} dv \, c(u, v) \,, \tag{2.20}$$

where the integral of the source gives the *total charge* inside the rectangle.

At this stage the analogy between the ABHY conditions and the wave equation might appear as a simple coincidence, but in fact it is the first clue of a deeper connection. Perhaps not surprisingly the missing concept we have to call into play is that of positivity. We will therefore focus on the space of *positive* solutions of the wave equation, i.e. with $X(u, v) \geq 0$, which turns out to be a continuum version, or equivalently an infinite n limit, of an ABHY Associahedron $\mathcal{A}_{n-3}$. Before illustrating more precisely this statement, let us point out at some obvious facts about solutions $X(u, v)$ of the wave equation. To begin with, we should specify a domain and choose boundary conditions for $X(u, v)$. With the benefit of hindsight, we choose the right triangle of Fig. 2.6. As boundary conditions we impose $X(u, v) = 0$ at the origin $(u, v) = (0, 0)$ and on the spatial slice $u + v = 2$. Applying the integral equation (2.20) to the rectangle shown in Fig. 2.6, we can express the value of $X(u, v)$ in the bulk of the

[7] In (x, t) variables it would read $(\partial_t^2 - \partial_x^2) X(x, t) = c(x, t)$ instead.

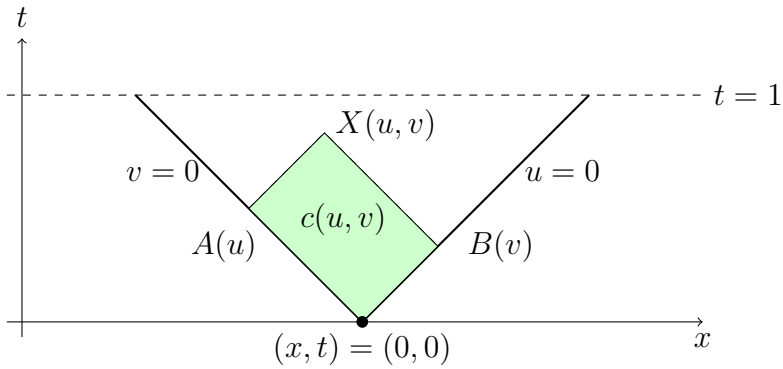

Figure 2.6: The wave equation and general solution inside a right triangle.

domain in terms of the values at its boundaries

$$X(u,v) = X(u,0) + X(0,v) - \int_0^u du' \int_0^v dv'\, c(u',v')\,. \tag{2.21}$$

The boundary condition at the origin implies that $X(u,0) = X(0,v) = 0$, while the vanishing boundary condition on the spacial slice $u+v=2$, i.e. $X(u,2-u)=0$, implies

$$X(0,2-u) = \int_0^u du' \int_0^{2-u} dv'\, c(u',v') - X(u,0)\,, \tag{2.22}$$

so that the entire solution $X(u,v)$ is uniquely fixed by its values at the boundary $v=0$.

The above analysis makes manifest that the space of solutions $\mathcal{S}$ of the wave equation is infinite dimensional and, furthermore, is parametrised by the values $X(u,0)$ which can be chosen arbitrarily. However, because of the signs in (2.21),(2.22), the same is not true for the space of *positive* solutions $\mathcal{S}^+$. To study the latter, it is convenient to first reduce to an $(n-3)$-dimensional subspace obtained by setting to zero $X(u,0)$ in all but $n-3$ points. The positive values $X(u_i,0)$ at these points cannot be chosen arbitrarily, because we might break the positivity of $X(u,v)$ in some of the points related to $X(u_i,0)$ by (2.21) and (2.22). These points are precisely the vertices of the mesh obtained by casting light rays from $(u_i,0)$ and reflecting them at the slice $u+v=2$, see Fig. 2.7. By comparison with Fig. 2.5 it should be clear that then the $(n-3)$-dimensional subspace of $\mathcal{S}^+$ of the wave equation is nothing but an ABHY polytope $\mathcal{A}_{n-3}$. The full space of positive solutions is obtained by allowing more and more non

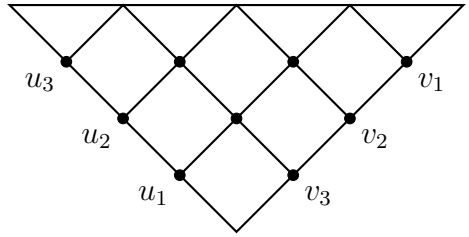

Figure 2.7: The mesh of light rays cast from u_1, u_2, u_3 and reflected at the top boundary of the domain

zero values on the edge $(u, 0)$. Interestingly, each time we add a new non vanishing point $X(u_j, 0)$ this does not affect the values (and in particular the positivity) of $X(u, v)$ at the points of the original mesh. Instead, the values of $X(u_j, 0)$ are only restrained by the positivity requirement on the light ray cast from (u_j). This simple fact will have important geometrical and physical consequences later and thus will be explained in more details.

2.3.2 Causal diamonds and factorization

We have seen how ABHY associahedra arise as a discrete version of the space of positive solutions of the wave equation. As mentioned earlier, the key feature of these associahedra is the factorization of their faces into lower dimensional associahedra. It is natural to ask how this fact is encoded in the new language of the wave equation. Quite pleasantly, it turns out to be a consequence of the casual structure of $(1+1)$-dimensional space time, i.e. of the factorization of casual diamonds.

Let us study the structure of the boundary $\partial\mathcal{S}^+$ of the space of positive solutions[8]. The values of $X(u, v) \geq 0$ themselves are parameters over this space thus the boundaries of $\mathcal{S}^+$ are reached when $X(u, v)$ vanishes at at some point, e.g. $X(u_1, v_1) = 0$. Imposing the vanishing at a single point does not break positivity anywhere else, so it is always allowed and gives a component of $\partial\mathcal{S}^+$. Next we study how these boundaries intersect each other. Because of the integral mesh relation (2.20), $X(u, v)$ cannot vanish simultaneously at points (u_1, v_1) and (u_2, v_2) sitting at the left and right

[8]We are using a somewhat ill defined terminology here, since $\mathcal{S}^+$ is infinite dimensional. Hopefully this should not cause much confusion in the reader.

corners of a casual diamond, since we have

$$X(u_1, v_1) + X(u_2, v_2) = X(u_1, v_2) + X(u_2, v_1) + \int du'dv'\, c(u', v') > 0. \tag{2.23}$$

Such incompatible points lie in the two shaded diamonds shown in Fig. 2.8, they are regions that are space-like separated but causally connected to (u_1, v_1). In other words, $X(u_1, v_1)$ and $X(u_2, v_2)$ can be set to zero simultaneously if and only if (u_2, v_2) is in the light cones of (u_1, v_1) or causally disconnected from it. Let us continue and study how the boundary $X(u_1, v_1) = 0$ looks like. Since the value of $X(u, v)$ at the points in the shaded diamonds can be reconstructed from the knowledge of $X(u, v)$ at the boundaries of the diamonds and since they cannot be used to reach a boundary of $\partial_{X(u_1,v_1)}\mathcal{S}^+$, we can simply forget about them using the "cut and paste" move depicted in Fig. 2.8. On the other hand, we cannot for-

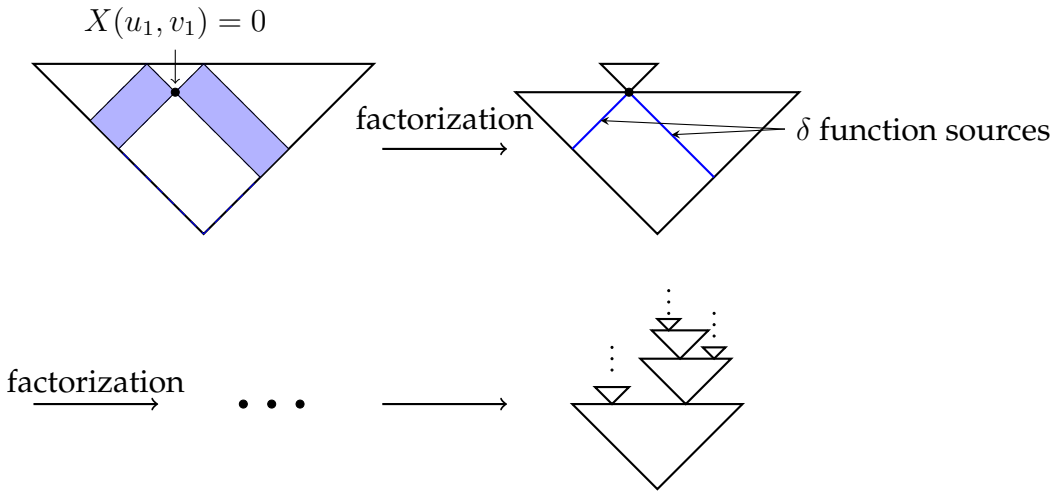

Figure 2.8: Causal diamonds and factorizations in the continuum

get about the charge $c(u, v)$ contained there since it enters in the integral mesh relation of the surviving variables. We can keep track of it by adding a delta function source on the line of gluing. We now have two independent right triangles, where the original boundary solution of the wave equation gives two solutions to the wave equation in each triangle. This means that the boundary $X(u, v) = 0$ is a product of positive solutions spaces in two smaller triangles,

$$\partial_{X(u,v)}\mathcal{S}^+ = \mathcal{S}^+_{\text{top}} \times \mathcal{S}^+_{\text{bottom}}, \tag{2.24}$$

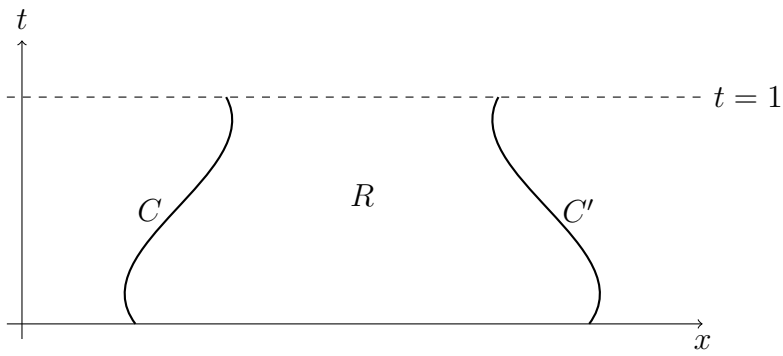

Figure 2.9: A general legal region is bounded by curves C and C'.

which is the continuum limit analogue of (2.17).

So far we have considered as domain for the wave equation a right triangle, which was suggested by the mesh diagram of Fig. 2.5. However, it is natural to expect that other choices of domains will give rise to spaces of positive solutions satisfying factorization properties, by the same mechanism we just studied. It turns out that we can choose any region in the rectangle $\mathcal{R} = \{0 \leq t \leq 1, 0 \leq x \leq 1\}$ and bounded by two non intersecting time like curves C and C' from $t = 0$ to $t = 1$, related to each other by the transformation $(x, t) \to (x + 1, 1 - t)$, see figure Fig. 2.9. We still assume zero boundary conditions at $t = 0$ and $t = 1$, and arbitrary conditions on C and C'. The space $\mathcal{S}^+$ again factorises whenever $X(u, v) = 0$ at some point. Extremal cases occur for C being a single light ray, so that $\mathcal{R}$ becomes the right triangle studied earlier, or when C is vertical, giving the square of Fig. 2.10.

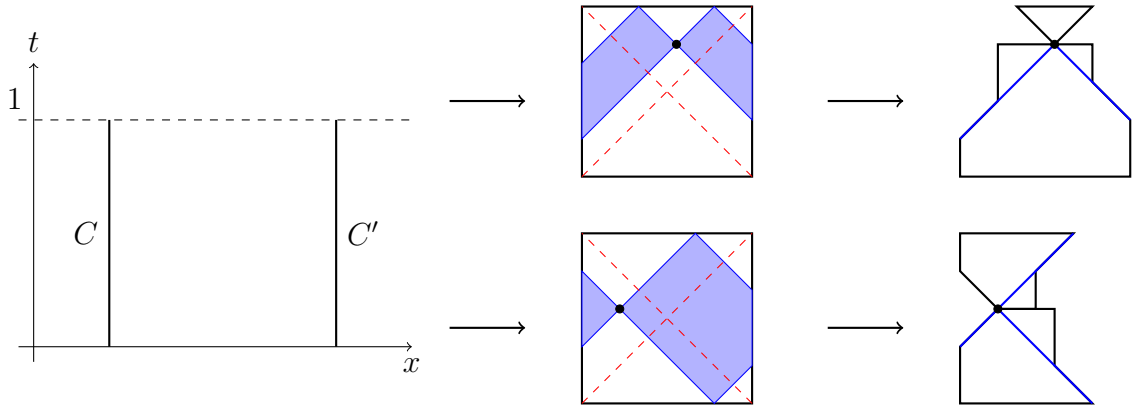

Figure 2.10: Factorisation properties for the square region.

There is another region which will play an important role later. Choose a point (a, b) and consider the light cone emitted from here. Take for C the points (u, v) which lies on the edge of this light cone and further satisfy $u \leq a$. The corresponding *arrow-tail* region is shown in Fig. 2.11. In the case where $(a, b) = (1, 0)$ we get back to the usual right triangle. By constructing the relevant diamonds we see that the region factorizes either into a right triangle times another arrow-tail region, or into two arrow-tail regions. This is interesting because we do not create arbitrarily different shapes upon factorisation or in other words the space $\mathcal{S}^+$ on arrow-tail regions is closed upon taking boundaries. Because of this it is tempting to conjecture that this space must be connected with the Associahedron and thus with tree level amplitudes. Indeed this is the case, as we will discuss in Section 2.3.4.

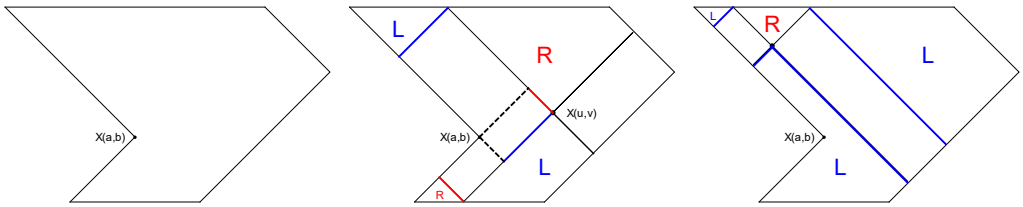

Figure 2.11: The *arrow-tail* region is a generalization of the usual right triangle region. The boundary corresponding to $X(u, v) = 0$ factorizes in either a Left arrow-tail times a Right arrow-tail, or a Left arrow-tail region times a Right triangle, obtained after the gluing along the colored lines.

2.3.3 Projections and the *Soft-limit* Triangulation

We now describe a remarkable feature of the ABHY realisation of the Associahedron $\mathcal{A}_{n-3}$, namely that there exists a *projection* of any n-point Associahedron onto an $(n-1)$-point one. Furthermore, this projection allows us to build a new triangulation of the Associahedron which we will use in Section 3.3.3 to obtain a surprisingly compact new recursion relation for tree level amplitudes.

We begin by choosing a basis of $n-3$ planar variables in terms of which we express the others by solving the ABHY conditions. Although there are many choices, the most natural basis is given (for the standard ABHY realization of $\mathcal{A}_{n-3}$) by the variables $X_{1,i}$, with $i = 3, \ldots, n-1$, i.e. those living in the leftmost edge of right triangle. The reason is that they trivializes the problem of solving the ABHY conditions, which can be done by casting light rays as described in Section 2.3.1 and in more detail in Appendix B.

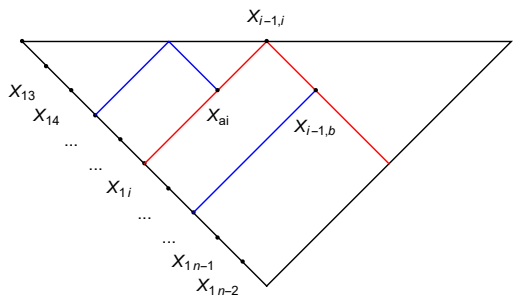

Figure 2.12: Only the variables in the red light rays depend on $X_{1,i}$, because we can cast the blue light rays to find a causal diamond relating them to it.

There is a pattern which immediately strikes the eye in the way the basis element appears in the solutions of the other variables. As it is shown in Fig. 2.12, after solving the ABHY conditions the variable $X_{1,i}$ appears only in a subset of all the variables, those for which it is possible to draw a causal diamond containing both.

As a consequence, we can project from the big space of all the planar variables to a small space obtained by *forgetting* the variables on the red light ray. The remaining variables still satisfy ABHY relations among them, because we can still draw causal diamonds involving them and not the forgotten ones. Therefore the image of the projection of the original Associahedron is another Associahedron and a rapid counting shows that this Associahedron is of codimension one. In another words, we obtain a projection of an n-point Associahedron onto an $(n-1)$-point one.

Such a projection exists for any of the variable $X_{1,i}$, but we will now focus on the particularly simple choice of $X_{1,3}$ and study the corresponding projection in more detail. Constructing the necessary causal diamonds, one finds that the to-be-forgotten variables are given by

$$X_{2,a} = X_{1,a} - X_{1,3} + \sum_{i=3}^{a-1} c_{1,i}, \tag{2.25}$$

in order to forget about $X_{1,3}$ we simply set it to 0. This defines a projection π which sends any point Y of our kinematic space to a point $\pi(Y)$ in the subspace where the facet $X_{1,3}$ of the original Associahedron lives. Now suppose that Y was inside of the original Associahedron $\mathcal{A}_{n-3}$, which by definition means that all the planar variables were positive when evaluated at Y. As it is clear from the minus sign of $X_{1,3}$ in (2.25), the forgotten variables are even more positive on $\pi(Y)$. Furthermore, the remaining variables are positive as well on $\pi(Y)$ since they do not depend on $X_{1,3}$ which is the only basis element changed by π. We conclude that $\pi(Y)$ is

inside the facet $X_{1,3}$ and not merely on the plane $X_{1,3} = 0$. We conclude that π projects $\mathcal{A}_n$ into its facet $X_{1,3}$, which we recall is an $(n-1)$-point Associahedron.

Now imagine to go the other way around, *i.e.* take a point $\bar{Y}$ in the facet $X_{1,3} = 0$ and imagine turning $X_{1,3}$ back on. As $X_{1,3}$ increases, we find a fiber of points which live in the original $\mathcal{A}_{n-3}$ and above $\hat{Y}$. We can not increase $X_{1,3}$ arbitrarily because some of the variables $X_{2,a}$ will eventually turn negative. Therefore, over each point in the facet $X_{1,3}$ there is a maximum height we can reach elevating in the $X_{1,3} \geq 0$ direction, which is dictated by the *smallest* of the forgotten variables at $\hat{Y}$. The facet $X_{1,3}$ is then divided into polytopes given by the minimization problem of the forgotten variables. Said in other words, the cells of the triangulation of the facet $X_{1,3}$ induced by the minimization problem of the forgotten variables $X_{2,a}$ are nothing but the shadows cast by the facets $X_{2,a}$ over the facet $X_{1,3}$ under π. Furthermore, each of these polytopes, together with the fibers of points projecting onto them, gives a triangulation[9] of the larger Associahedron $\mathcal{A}_{n-3}$.

We will refer to this decomposition as the *soft-limit* triangulation of $\mathcal{A}_{n-3}$, the choice of name is motivated by the analogy between the projection into a lower point Associahedron and the notion of forgetting a particle by taking its momentum to be vanishing. We caution the reader, however, that the projection itself is not equivalent to a soft-limit, unless we further send the mesh constant $c_{1,i} \to 0$ for $i = 3, \ldots, n-1$. As was argued in [8], this has the effect of squashing the Associahedron onto its facet $X_{1,3} = 0$ and it is completely equivalent to the soft-limit $k_1^\mu \to 0$.

Unlike previously known triangulations of $\mathcal{A}_{n-3}$, the structure of the soft-limit triangulation is very simple: each of the polytopes into which $\mathcal{A}_{n-3}$ is divided is a prism, i.e. a polytope with two distinguished "top" and "bottom" facets and such that the remaining "side" facets meet at a common point. This point can be used to define a projection which acts as a diffeomorphism of positive geometries, as defined in [10], between the top and bottom facets. In particular, this mean that the top and bottom facets have the same combinatorical structure and their canonical forms can be push-forwarded into each other by means of the projection.

Let us consider an explicit example. For $n = 6$ points the three facets $X_{2,4} = 0$, $X_{2,5} = 0$, $X_{2,6} = 0$ of $\mathcal{A}_3$ project to the facet $X_{1,3} = 0$, their image under the projection are combinatorially equivalent to, respectively, $\mathcal{A}_2$, $\mathcal{A}_1 \times \mathcal{A}_1$ and $\mathcal{A}_2$ and triangulate the facet $X_{1,3}$. Furthermore, the prism built on each of them decompose $\mathcal{A}_3$ as shown in Fig. 2.13. A quick count-

[9] More precisely, it is a decomposition of the polytope into smaller polytopes of known shapes.

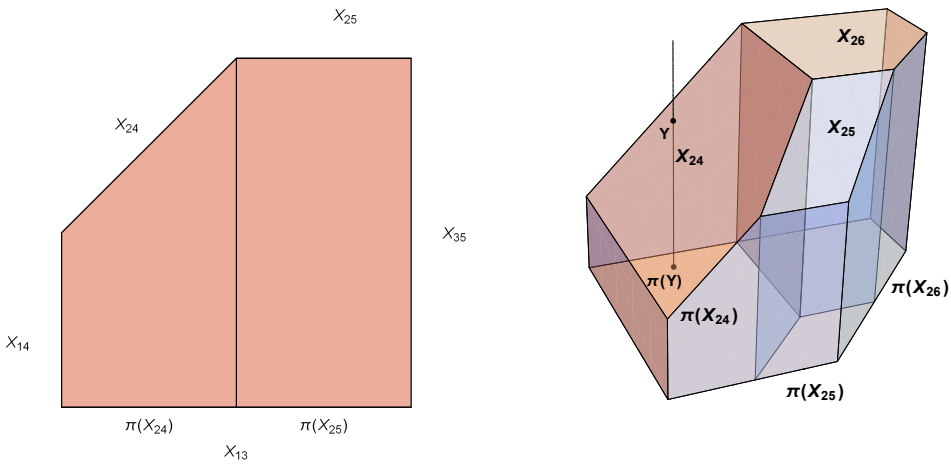

Figure 2.13: The soft-limit triangulation for $n = 5$ (left) and $n = 6$ (right).

ing shows that the soft limit triangulation is extremely efficient: it only requires $n - 3$ pieces, as opposed to the standard triangulation considered in [8], which consists in convex hulls based at a specific vertex and thus require $\mathcal{O}(n^2)$ pieces. Furthermore, due to the simple combinatorical structure of prisms, the soft-limit triangulation allows to derive a particularly clearn recursive formula for tree amplitudes, as we will explain in in Section 3.3.

Before ending this section, let us give a more projective description of the projection. Using the coordinates $Y = (1, X_{1,3}, X_{1,4}, \ldots, X_{1,n-1})$ the factorization facets which do not cast a shadow are given by $Y \cdot W_{i,j} = 0$, with

$$W_{i,j} = \pm(*, 0, *, *, \cdots, *)^{\mathrm{T}},$$

and they all meet at a point at infinity

$$Z = (0, 1, 0, 0 \cdots, 0)^{\mathrm{T}},$$

since clearly $Z \cdot W_{i,j} = 0$. We can use this point to define a projection on the facet $X_{1,3} = 0$, each forgotten facet $X_{2,i} = 0$ together with its image under this projection on the facet $X_{1,3} = 0$ define the upper and bottom facet of the prisms appearing in the triangulation.

2.3.4 New realizations of associahedra

In Section 2.3.2 we argued that there are different possible choices of region $\mathcal{R}$ for which the space $\mathcal{S}^+$ of positive solutions of the wave equation satisfy the crucial factorisation property. In particular, we described in

some detail the arrow-tail region which factorizes into products of other arrow-tail regions. We now wish to study the discrete version of this region and we will do so by exploiting again the projection property of $\mathcal{S}^+$, i.e. that we can consider subspaces of $\mathcal{S}^+$ obtained by forgetting the values of $X(u,v)$ on all but a finite number of points on the left edge C.

We pick a set of points on C, including also the special point (a,b) where C has a cusp, and construct a mesh out of the light rays emitted from this points, reflecting them if we hit the top and bottom edges of $\mathcal{R}$. To make connection with the usual notation, we name the points up to the cusp $X_{1,i}$ with $i = 3,\dots,m$, and the remaining ones $X_{n,m}, X_{n-1,m},\dots,X_{m+2,n}$. In doing this we are following the convention that in the u direction we increase the first index and in the v direction the second. By the same rule we can label the remaining vertices of the mesh with planar variable labels $X_{i,j}$, note that we produce labels $X_{j,i}$ with $j > i$, in which case we interpret them as $X_{i,j}$ instead.

With these labellings, we can look again at the factorisation implied by the wave equation and recognise again the formula (2.17). We conclude that this subspace of $\mathcal{S}^+$ is an Associahedron. On the other hand, the mesh relations read off the causal diamonds only partly match those of (2.16): all those contained in the future cone of $(a+1,1-b)$ have been replaced by those contained in the past cone of (a,b). Therefore, we see that the arrow-tail region provides a new convex realisation of $\mathcal{A}_{n-3}$. Indeed, using the language of [34], this corresponds to the *initial quiver* shown in Fig. 2.14. It turns out that all the realisations described in [34] can be

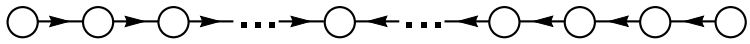

Figure 2.14: The initial quiver corresponding to the ABHY realisation obtained from the arrow-tail region, the node at which the orientation of the quiver changes is in correspondence with the cusp of the curve C.

obtained by choosing the appropriate curve C and then considering the discretised version of $\mathcal{S}^+$, a flip in the orientation of the quivers translates in an inversion point for C. For example, the square region of Fig. 2.10 upon discretisation give rise to the realisation with the maximum number of flips.

2.3.5 ABHY realizations for polytopes of type $\mathcal{B}/\mathcal{C}$ and $\mathcal{D}$

The ABHY convex realisation of the cluster polytope $\mathcal{A}$ was first generalized in [34] for the remaining types. For the sake of self-containedness, we will describe here the realisation in a minimalistic way, omitting in

particular the proof of its correctness, for which we refer the reader to the original paper [34]. We begin with $\mathcal{D}$, whose cluster variables are labelled by the variables $X_{i,j}$, $X_{j,i}$, X_i and X'_i, which represents (tagged) arcs of an once punctured n-gon, see Fig. 2.15.

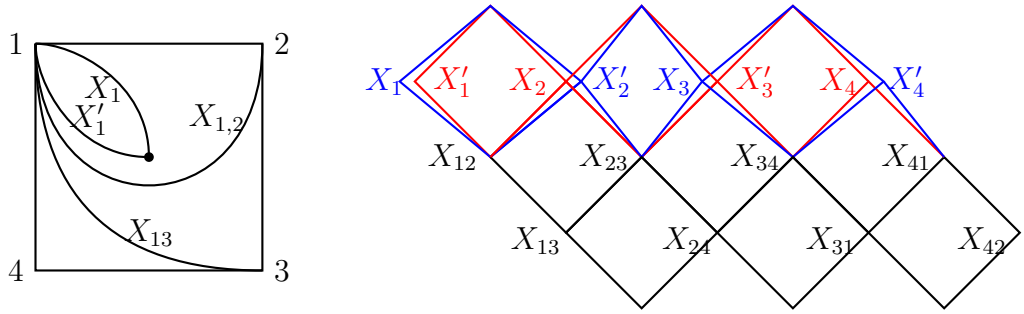

Figure 2.15: The correspondence between some variables of $\mathcal{D}_4$ and (tagged) arcs of the punctured n-gon is shown on the left. The variables can be arranged in the mesh diagram shown on the right.

As usual, we arrange these variables in a mesh diagram as in Fig. 2.15 each diamond of which correspond to an ABHY condition. There are two novelties, firstly we have blue and red diamonds in the top of the diagram which correspond to the conditions $X_i + X'_{i+1} - X_{i,i+1} = c_i$ and $X'_i + X_{i+1} - X_{i,i+1} = c'_i$ and secondly we have five-terms conditions

$$X_{i,i+1} + X_{i+1,i+2} - X_{i,i+2} - X_{i+1} - X'_{i+1} = c_{i,i+1} \quad i = 1, \ldots, n-1,$$

which do not correspond precisely to a diamond. For example, the mesh diagram of Fig. 2.15 implies 12 conditions, the one coming from the left-most part of the diagram are

$$\begin{aligned} &X_{13} + X_{24} - X_{23} = c_{13}, \quad X_{12} + X_{23} - X_{13} - X_2 - X'_2 = c_{12}, \\ &X_1 + X'_2 - X_{12} = c_1, \quad X'_1 + X_2 - X_{12} = c'_1\,, \end{aligned}$$

the others are obtained by cyclic shift. For general n the relations are given by (we use the convention that $X_{i+1,i} = 0$)

$$\begin{aligned} &X_{i,j} + X_{i+1,j+1} - X_{i,j+1} - X_{i+1,j} = c_{i,j}\,, && \text{for } |j-i| > 1, i \neq n \\ &X_{i,i+1} + X_{i+1,i+2} - X_{i,i+2} - X_{i+1} - X'_{i+1} = c_{i,i+1}\,, && \text{for } 1 \leq i < n \\ &X_i + X'_{i+1} - X_{i,i+1} = c_i\,, \quad X'_i + X_{i+1} - X_{i,i+1} = c'_i\,, && \text{for } 1 \leq i \leq n. \end{aligned} \tag{2.26}$$

The ABHY conditions define a subspace in the space of all the variables X. As in the case of $\mathcal{A}$, the intersection of this subspace with the positive

region $X \geq 0$ is a polytope combinatorially equivalent to the cluster polytope $\mathcal{D}_n$, see Fig. 2.16 for an example with $n = 3$. The ABHY realisation

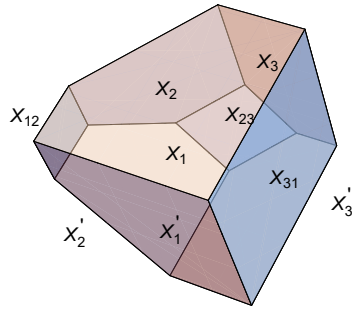

Figure 2.16: The ABHY $\mathcal{D}_3$ polytope. Its facets contains 3+3 ABHY $\mathcal{A}_2$ polytopes (pentagons) associated with X_i and X'_i, plus three copies of $\mathcal{D}_2$ associated with $X_{i,i+1}$.

of $\mathcal{B}$ comes for free with the ABHY realisation of $\mathcal{D}$: it is obtained simply by fusing the variables X'_i and X_i into a single variable $X^+_i = X_i + X'_i$ for every i, and reading relations out of (2.26). We obtain

$$\begin{aligned} &X_{i,j} + X_{i+1,j+1} - X_{i,j+1} - X_{i+1,j} = c_{i,j}\,, && \text{for } |j-i| > 1, i \neq n \\ &X_{i,i+1} + X_{i+1,i+2} - X_{i,i+2} - X^+_{i+1} = c_{i,i+1}\,, && \text{for } 1 \leq i < n \\ &\frac{1}{2}X^+_i + \frac{1}{2}X^+_{i+1} - X_{i,i+1} = \frac{1}{2}(c_i + c'_i), && \text{for } 1 \leq i \leq n\,. \end{aligned} \quad (2.27)$$

Next, we turn to the continuum limit. Between the relations (2.26) and (2.27), the latter are a better starting point to find an infinitesimal version. The only problem is the last of (2.27) because it involves only three terms and moreover has strange factors $1/2$ all over the place, but this begs to be interpreted as half of an ordinary mesh relation, which can be done in an obvious way. First we consider a symmetric arrow-tail region, i.e. one symmetric with respect to the transformation $(x,t) \to (1+x, 1-t)$ as in Fig. 2.17, we also assume that the charge density has the same symmetry, $c(u,v) = c(1+v, u-1)$. Finally, we now consider the space of positive solutions subjected to this symmetry, $\mathcal{S}^+_{sym}$. The reason behind this construction is clear, when we write the integral relation for a symmetric diamond we get

$$X(a,-a) + X(-b,b) + X(a,b) + X(1+b,a-1) = \int_{-a}^{a} du \int_{-b}^{b} dv,\ c(a,b)$$

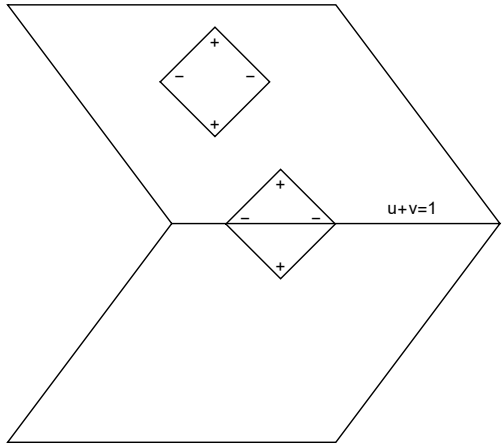

Figure 2.17: An arrow-tail region symmetric with respect to the line $u + v = 1$. The mesh relations defining an ABHY realisation for $\mathcal{B}_{n-1}$ originate from ordinary causal diamonds, the special mesh relations correspond to symmetric diamonds.

which is equivalent to

$$\frac{1}{2}X(a,-a) + \frac{1}{2}X(-b,b) - X(a,b) = \int_{\mathrm{T}} dudv,\ c(a,b) \tag{2.28}$$

where T is half of the original diamond, say the one with $u + v < 1$.

Let us move to the study of the boundary structure of $\mathcal{S}^+_{sym}$. Because of the symmetry we now have to set $X(u,v) = 0$ in *pairs* of points conjugated under the symmetry and for each one draw diamonds as in Fig. 2.11. The usual factorization of arrow-tail regions may produce pairs of conjugated regions that intersect the line $u+v = 1$ in at most one one point, in this case we can forget about one of the regions as the information about the solution $X(u,v)$ is already encoded in the other region. Because of this, we see that the space $\mathcal{S}^+_{sym}$ factorises into itself times ordinary spaces $\mathcal{S}^+$ associated to arrow-tail regions. Obviously this is the continuum limit version of the factorisation of $\mathcal{B}_n$ into copies of itself and $\mathcal{A}_m$. However, there is a crucial novelty. When we impose the vanishing of $X(u,v)$ along some point of the symmetry line $u + v = 1$ the structure of the relevant casual diamonds leave us with a single pair of conjugated regions and therefore this boundary component of $\mathcal{S}^+$ does not factorise at all: it is a single copy of $\mathcal{S}$ for an arrow-tail region. This is the continuum-limit manifestation of the by now well known fact that $\partial\mathcal{B}_{n-1}$ contains n copies of $\mathcal{A}_{n-2}$, which is vital to reproduce the cut properties of the 1-loop integrand.

To recover the convex realisation of $\mathcal{B}$ we apply the usual discretiza-

tion procedure: once again $\mathcal{S}^+_{sym}$ satisfy the projection property, i.e. we can go to finite dimensional subspaces by projecting (or forgetting) most of the points in the left-most edge of the arrow-tail region. Constructing the mesh of light rays, and labelling them in terms of the planar variables - with the notable difference that now we no longer identify $X_{i,j} = X_{j,i}$ and that we have variables X^+_i along the symmetry line - one ends up in the mesh diagrams such as in Fig. 2.15 and thus in the ABHY convex realisation of [34]. To obtain the realisation for $\mathcal{D}$, we now double the variables X^+_i by writing them as $X^+_i = X_i + X'_i$ and we impose the last two relations of (2.26). At first sight this extra ad-hoc step is somewhat unpleasant, in that one would like to see $\mathcal{D}$ automatically emerge from the discretisation of some continuum wave equation problem. On the other hand, the most important difference between the combinatorics of $\partial\mathcal{B}_{n-1}$ and $\partial\mathcal{D}_n$ is that the latter contains facets $\mathcal{A}_{n-1}$ where the former contains facets $\mathcal{A}_{n-2}$ and this difference is clearly lost in the continuum, i.e. when $n \to \infty$. Moreover this fusing/doubling mechanism foreshadows that there should be a simple way to "forget" the extra structure of $\mathcal{D}_n$ and obtain $\mathcal{B}_{n-1}$, a fact which we will understand in more detail in Section 2.3.7.

2.3.6 The polytope $\overline{\mathcal{D}}_n$

The facet structure of the $\mathcal{D}_n$ cluster polytope correctly reproduces the factorizations of a 1-loop planar ϕ^3 integrand. Furthermore, there is a meaningful correspondence between the cuts of the integrand, which are $n+2$ tree level amplitudes, and the *cut* facets $X_i = 0$ and $X'_i = 0$, which are associahedra $\mathcal{A}_{n-1}$. However, this correspondence is less satisfactory, because we do not have the right number of facets in $\mathcal{D}_n$: we have twice as many cut facets as we would like. Going to the other combinatorial extreme, the problem can be understood in terms of vertices of $\mathcal{D}_n$ and Feynman diagrams. The vertices involving only non tagged triangulations correspond to 1-loop Feynman diagrams, the ones involving a pair of tagged and plain radii to tadpole diagrams (by radius we mean an arc going from a vertex of the n-gon to the internal puncture), but then there are also vertices with only tagged radii which we do not know how to interpret.

In a sense our problem is that $\mathcal{D}$ has a symmetry, given by exchanging tagged and plain radii, which has no physical meaning and thus must be modded out. As we discuss in the rest of this section, yet another magical property of the ABHY realization of cluster polytopes is that it allows to do so in an obvious way.

To begin with, we have to promote this symmetry from a purely combinatorial one to a geometrical one. This is done by requiring the mesh

constants c_i and c'_i, which a priori are independent positive numbers to be equal. As a consequence of this, all tadpole vertices now become coplanar, as we will now prove. Firstly, after a moment's thought one realizes that by solving the mesh relations in terms of the initial quiver variables, the variables X_i and X'_i (for $i > 1$) are given by

$$X_i = C - X'_1 + X\,, \quad X'_i = C' - X_1 + X\,, \tag{2.29}$$

where C and C' are combinations of mesh constants which are sent into each other under the swap $c_j \leftrightarrow c'_j$ for all j, and X is a combination of variables $X_{1,a}$. This is a consequence of the underlying combinatorial symmetry of $\mathcal{D}$, encoded in the structure of the mesh relations. It is clear then that the quantity $X_0 = X'_i - X_i = X'_1 - X_1$ does not depend on i, if $c_j = c'_j$ for every j. Therefore the equation $X_0 = 0$ defines a hyperplane on which all tadpole vertices must lie, since any tadpole vertex sits at the intersection of pairs of facets X_i and X'_i. The plane X_0 then cuts the polytope $\mathcal{D}$ in half: on the plane itself we have the tadpole vertices, and on the half-spaces given by $X_0 > 0$ (resp. $X_0 < 0$) we have the plain (resp. tagged) vertices. The formerly purely combinatorial symmetry is now promoted to a geometrical one: the linear map $X_1 \leftrightarrow X'_1$ sends the two half-spaces into each other and, more importantly, a vertex of $\mathcal{D}$ into the one obtained by swapping tagged and plain radii. To mod out this symmetry, we simply restrict ourselves to one of the half-spaces, say $X_0 \geq 0$. By doing so we are led to consider a new polytope, which we call $\overline{\mathcal{D}}$, obtained by adding X_0 to the set of face variables. Note that $\overline{\mathcal{D}}$ is one of the two pieces in which $\mathcal{D}$ is cut into by the plane $X_0 = 0$. The situation is pictured in Fig. 2.18 for the case $n = 3$, the reader is invited to compare it with the Feynman polytope depicted in Fig. 2.3.

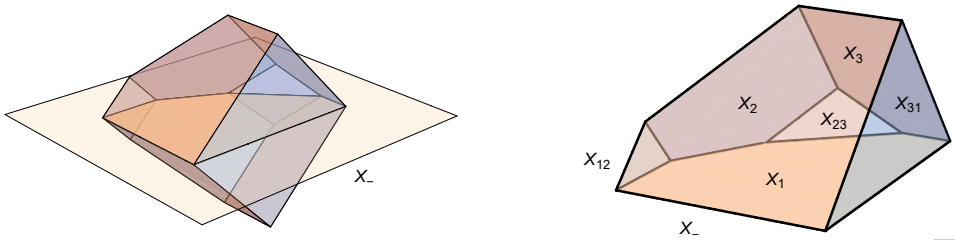

Figure 2.18: Slicing $\mathcal{D}_3$ with the tadpole plane produces two copies of $\overline{\mathcal{D}}_3$

The polytope $\overline{\mathcal{D}}_n$ satisfies all the requirements implied by (1): there is a 1-1 correspondence between its codimension-1 boundaries and the poles of a 1-loop integrand. If we iterate this correspondence down to vertices we find a correspondence between them and 1-loop diagrams, such that adjacent vertices corresponds to diagrams related by a channel

swap. Furthermore, the slicing created new adjacencies between vertices which have a simple diagrammatical interpretation as a tadpole flip.

We end this section with a brief summary of the facets of $\overline{\mathcal{D}}$. The faces $X_{i,j} = 0$ factorise into $\mathcal{A} \times \overline{\mathcal{D}}$, and reproduce the factorisation of the 1-loop integrand. In particular, the faces $X_{i,i+1} = 0$ are given by $\mathcal{A}_{n-3} \times \overline{\mathcal{D}}$ and allow the factorisation of an 2-point function from a tree level amplitude. There are n cut facets $X_i = 0$ which are $(n+2)$-point associahedra $\mathcal{A}_{n-1}$. These faces reproduce the cuts of the integrand, which are tree level amplitudes with an extra pair of particles in the forward limit, coming from the cutted loop propagator. Finally, $X_0 = 0$ is the cyclohedral facet $\mathcal{B}_{n-1}$ on which all tadpole vertices lie. Because of this we will also refer to this variable as the *tadpole variable*.

2.3.7 Projections and the *Forward-limit* Triangulation

It is not difficult to see that ABHY realization of cluster polytopes $\mathcal{B}, \mathcal{C}, \mathcal{D}$ still enjoys the beautiful projection property we described in full detail for $\mathcal{A}$. Since the method to discover and prove such projections is virtually identical to the tree level case, we will not repeat the derivation here. Instead, we will describe an entirely different projection for $\overline{\mathcal{D}}$, which we will call *forward-limit* triangulation for reasons that will become clear later in Chapter 3.

Among the facets of $\overline{\mathcal{D}}_n$ there is an obvious distinguished one, the tadpole facet $X_1 = X_1'$. It is therefore natural to ask ourselves what happens if we project on this facet. To begin with, it is convenient to choose as basis the variables $(X_1, X_1', X_{2,1}, \ldots, X_{n-1,1})$: all other face variables are expressed as linear functions of these basis variables and of the mesh constants. However, the symmetry $X_1' \leftrightarrow X_1$ of $\mathcal{D}$ implies that if X_1 appears in the expression of some variable $X_{i,j}$ then also X_1' appears (with the same sign), and vice versa. Therefore, the dependence of factorization facets on X_1, X_1' is only through the combination $X_+ = X_1 + X_1'$,. This is not true for the variables X_i and X_i', indeed X_i (resp. X_1') depends only on X_1' (resp. X_1). It is therefore natural to introduce a new set of variables:

$$\begin{cases} X_+ &= (X_1 + X_1') \\ X_- &= (X_1 - X_1') \end{cases} \qquad \begin{cases} X_1 &= \frac{1}{2}(X_+ + X_-) \\ X_1' &= \frac{1}{2}(X_+ - X_-) \end{cases} . \tag{2.30}$$

Note that X_- is nothing but the tadpole variable X_0. Using these coordi-

nates, we can define a projection

$$\begin{aligned} \pi_- : \mathcal{D} &\to \mathcal{C} \\ Y = (X_-, X_+, X_{2,1}, \dots) &\mapsto \hat{Y} = (0, X_+, X_{2,1}, \dots), \end{aligned} \tag{2.31}$$

which is a map onto the tadpole facet $\{X_- = 0\}$. Crucially, only the cut facets cast a shadow under the projection: the factorization facets are independent of X_-, thus they are parallel to the direction of the projection and their image is lower dimensional.

As in the case of the soft-limit projection discussed earlier for tree level associahedra $\mathcal{A}$, the projection described here suggests a natural triangulation of $\overline{\mathcal{D}}$. Such triangulation is particularly easy to describe working in the frame defined by $X_\pm$: consider any point $\hat{Y}$ lying on the tadpole facet in the shadow of the facet X_i, in the coordinates (2.30) $\hat{Y}$ is given by

$$\hat{Y} = (0, X_+, X_{2,1}, \dots, X_{n-1,1}), \tag{2.32}$$

we can lift this point by taking all points of the form

$$Y = (X_-, X_+, X_{2,1}, \dots, X_{n-1,1}), \tag{2.33}$$

all these points Y lie in $\overline{\mathcal{D}}$, provided that $X_i \geq 0$. Note that we do not have to check $X_{i,j} \geq 0$ as well, since they are independent of X_-, and they are already positive on $\hat{Y}$. As $\hat{Y}$ moves in the shadow of the cut facet X_i the points Y define a prism with a top facet given by X_i and a bottom facet given by its projection on X_-. Again, it is evident that the bottom and top facet of the prism have the same shape because the projection π_- gives a diffeomorphism between the two. If we denote the i-th prism by $\mathcal{A}_{n+2,i} \times [0, X_i]$, we can schematically write (see Fig. 2.19).

$$\overline{\mathcal{D}}_n = \bigcup_{i=1}^{n} \mathcal{A}_{n+2,i} \times [0, X_i]. \tag{2.34}$$

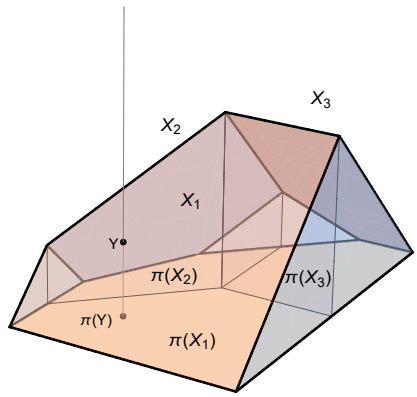

Figure 2.19: The *forward limit* triangulation in the case $n = 3$. The cut facets X_i and their projection $\pi(X_i)$ define three prisms which triangulate $\overline{\mathcal{D}}_3$.

Once more let us give a projective description of the triangulation. Using the coordinates $Y = (1, X_1', X_1, X_{2,1}, \ldots, X_{n-1,1})$ the factorization facets are given by

$$Y \cdot W_{i,j} = 0,$$

with

$$W = \pm(*, 1, 1, *, \cdots, *)^{\mathrm{T}},$$

and they all meet at a point at infinity

$$Z = (0, 1, -1, 0, \cdots, 0)^{\mathrm{T}},$$

since clearly $Z \cdot W_{i,j} = 0$. We can use this point to define a projection on the facet X_-, each cut facet X_i together with its image under this projection on the tadpole facet X_- define the upper and bottom facet of the prisms appearing in the triangulation (2.34).

In Section 3.3.4 we will describe a representation of the 1-loop integrand which is associated to the triangulation $\overline{\mathcal{D}}$ described here. As the reader might expect, all the action will be played by the cut facets which define the prisms composing the triangulation: this explain why we call this the *forward-limit* triangulation.

2.4 Curvy Amplituhedra in 1+2 dimensions

Before concluding this chapter we would like to describe interesting space-time avatars of the geometries understood using the pants decomposition approach to the moduli problem, the Associahedron and the Halohedron. We let ourselves be inspired by the hyperboloid model of the hyperbolic plane to discover these objects in 1+2 dimensional space-time. The hy-

perboloid itself can be re-interpreted as a map relating the two positive geometries, as we will argue. At least at tree level, this map is equivalent to the scattering equations specialised to 1+2 dimensions. These kinematical positive geometries are more complicated than the analogous ones described in the previous sections: they are not polytopes defined by linear inequalities, but rather are curvy objects defined by non-linear constraints analogous to the one satisfied by cross ratios. Because of this, it remains an interesting open question how to compute their canonical differential forms and connect them to scattering amplitudes. Let us stress once again that, only in this section, by kinematical space we will not mean a space of propagators, but rather the space of external and internal momenta.

2.4.1 The kinematical Associahedron

Let us begin with the most natural definition of the kinematical space, namely the set of momenta $(k_1, \dots, k_n)$, with $\sum_{a=1}^{n} k_a = 0$ and $k_a^2 = 0$, up to a common Lorentz transformation. This space has natural boundaries, given by the singular regions where some Mandelstam variable vanishes, that is where $k_I^2 = 0$ with $k_I = \sum_{a\in I} k_a$.

In view of the hyperboloid model, this kinematical space naturally projects to $\mathcal{M}_{\mathbf{D},n}$. Explicitly, the projection map ϕ is constructed as follows: let l_i be a collection of time-like vectors such that $l_i \to k \in L^+$, then the points $l_i/\sqrt{l_i^2}$ on the hyperboloid are mapped by the projection discussed in Section 1.1 to a sequence of points that converge to $z \in \partial\mathbf{D}$, put $\phi(k) \coloneqq z$. Under ϕ the collection of momenta $(k_1, \dots, k_n)$ is mapped to a collection of points $(z_1, \dots, z_n)$ on $\partial\mathbf{D}$ (the ones with negative energy are first mapped to $-k_a$). Note that another set of momenta $k'_a = \Lambda k_a$, with $\Lambda \in \mathrm{SO}^{\uparrow}(1,2)$ is sent to $(z'_1, \dots, z'_n)$ with $z' = \gamma(z)$ for a suitable $\gamma \in \mathrm{Aut}_{\mathbf{D}}$. Thus, ϕ defines a map from the kinematical space to $\mathcal{M}_{\mathbf{D},n}$.

However, note that both k_a and λk_a are sent to the same point in ∂D: the map ϕ, being projective in nature, forgets about the scale of the momenta. Because of this, we re-define our kinematical space to be up to single rescaling of the momenta [10]. Note that the map ϕ does not depend on the momentum conservation requirement, so we can relax this assumption: any set of n null-momenta is a viable choice to represent n light rays.

In summary, we have defined the kinematical space $\mathcal{K}_n$ to be the set of n distinct light rays up to $\mathrm{SO}^{\uparrow}(1,2)$, and definedd a map $\phi : \mathcal{K}_n \to \mathcal{M}_{\mathbf{D},n}$

Note that $\mathcal{K}_n$ is not a compact space, since we removed the configu-

[10] When this does not create confusion we will simply write k_a for its light ray $\{\lambda k \,|\lambda \in \mathbb{R}\}$

rations of collinear light rays. We can compactify this space in a method virtually identical to the moduli space compactification in terms of punctures. Suppose some set of momenta $k_{i\in L}$ is becoming collinear, then move to the reference frame comoving with $k_L = \sum_{i\in L} k_i$. In this frame the momenta $k_j \in R = L^c$ may or not stay at fixed positions as $k_L^2 = 0$. To represent all possible situations we use a diagonal in the Poincaré disk: a diagonal separating k_a into subsets L and R represents a limit where $k_L^2 = 0$ and the particles in R fail to remain at finite positions in the center of mass frame of k_L but rather collapse to a unique light ray. If we stick in the frame comoving with k_R instead, we see the particles in L becoming collinear, and thus we get a natural factorisation of the kinematical space in $\mathcal{K}_{|L|+1} \times \mathcal{K}_{|R|+1}$. Therefore the compactification of the kinematical space is naturally identified with the Associahedron $\mathcal{A}_{n-3}$. It is not difficult to see that ϕ extends to a continuous map from the kinematical Associahedron to the moduli space Associahedron.

We now relate the map ϕ with the scattering equations. We can choose a specific Lorentz frame and write a null momentum k

$$k = \begin{pmatrix} \mathcal{E} \\ \mathcal{E}\vec{\eta} \end{pmatrix}$$

where $\vec{\eta} = (\cos(\theta), \sin(\theta))$ is a unit norm vector and $\mathcal{E}$ may be positive or negative. Such k is sent to $z = \exp(i\theta)$, so we can write the Mandelstam variables as

$$k_a \cdot k_b = \mathcal{E}_a\mathcal{E}_b(1 - \cos(\theta_a - \theta_b)) = \frac{1}{2}\mathcal{E}_a\mathcal{E}_b|z_a - z_b|^2. \tag{2.35}$$

The scattering equations for the kinematics k_a and their images z_a in the disk now are

$$E_a = \sum_{b\neq a} \frac{k_a \cdot k_b}{z_a - z_b} = \frac{1}{2}\sum_{b\neq a} \mathcal{E}_a\mathcal{E}_b(\bar{z}_a - \bar{z}_b) = -\frac{1}{2}(\mathcal{E}_a^2\bar{z}_a - \mathcal{E}_a^2\bar{z}_a) = 0, \tag{2.36}$$

in the last passage we recognised $z_a\mathcal{E}_a$ as the spatial part of k_a and used energy and momentum conservation. Since changing Lorentz frame is equivalent to perform a Moebius map on the punctures z_a and the scattering equations are covariant under Moebius map, our initial choice of frame was uninfluential. We conclude that our map lands in a solution of the scattering equations when it acts on the subset of $\mathcal{K}_n$ where momentum conservation holds [11]. However we noted that the map ϕ is defined

[11] We would like to remark that the solution to the scattering equations provided by

without requiring momentum conservation and thus, in a sense, extends the map given by the scattering equations to other regions of the kinematical space. Moreover, it is guaranteed to land in the Associahedron living in $\mathcal{M}_{\mathbf{D},n}$ as long as the momenta k_a are in the cyclic order $(12\dots n)$. Finally, let us remark that for $n > 5$ there are in general other solutions to the scattering equations other than the one provided by ϕ.

This is a good point to make a remark on the peculiarity of $1+2$ dimensional kinematics. Recall from [29] that in $\mathcal{M}_{\mathbf{D},n}$ the moduli carried by diagonals are essentially cross ratios. Using the hyperboloid model, we can quickly express the moduli of the surface $X = \phi(k_1, \dots, k_n)$, in terms of the momenta k_a. From (2.35) it is immediate to see that

$$(ab|cd) = \sqrt{\frac{k_{ac}k_{db}}{k_{cb}k_{da}}}, \tag{2.37}$$

we call the quantity on the right hand side of (2.37) a space-time cross ratio because of its similarity to a cross ratio. Note that the space-time cross ratios are invariant under rescaling of each single momentum and is thus a function of the light rays, as they should. Equation (2.37) allows us to think of the null momenta k_a as set of *homogeneous coordinates* for the moduli space $\mathcal{M}_{\mathbf{D},n}$. As we discussed earlier, cross ratios have to satisfy the identities (1.4) and because of (2.37) the space time cross ratios have to satisfy these relations as well, which implies that the Mandelstam variable have to satisfy further relations beyond those coming from momentum conservation. Indeed, for any set of 4 null momenta, the first of (1.4) implies

$$\sqrt{k_{12}k_{34}} - \sqrt{k_{13}k_{24}} + \sqrt{k_{14}k_{34}} = 0, \tag{2.38}$$

the combinatorics behind this relation is not new in the world of scattering amplitudes, it appears as Plücker relations in the Grassmannian $\mathrm{Gr}(2,4)$, in the Jacobi identities underlying the colour-kinematics duality and was discovered in [8] to be a condition for the projectivity of a scattering form with numerators. Note that in the particular case where $\sum_{a=1}^{4} k_a = 0$, the condition (2.38) simply reduce to momentum conservation. However, any four momenta k_i have to satisfy (2.38) for the mere reason of being null and in $1+2$ dimensions. Indeed, in three dimensions we can always

the map ϕ is equivalent to the one provided by the spinor helicity formalism.

write

$$\sum_{i=1}^{4} c_i k_i = 0,$$

let us choose $c_4 = 1$, then the massless condition implies

$$\frac{1}{2} k_4 \cdot k_4 = c_1 c_2 k_{12} + c_1 c_3 k_{13} + c_2 c_3 k_{23} = 0, \tag{2.39}$$

but we can also express the coefficients c_i in terms of Mandelstam variables,

$$\begin{aligned} -k_{14} &= c_2 k_{21} + c_3 k_{13}, \\ -k_{24} &= c_1 k_{14} + c_3 k_{23}, \\ -k_{34} &= c_1 k_{13} + c_2 k_{23}, \end{aligned}$$

and together with the massless condition we get

$$\begin{aligned} k_{14} &= \frac{c_2 c_3}{c_1} k_{23}, \\ k_{24} &= \frac{c_3 c_1}{c_2} k_{31}, \\ k_{34} &= \frac{c_1 c_2}{c_3} k_{12}. \end{aligned}$$

Using these, we can re-write (2.38) as

$$|k_{12}| \sqrt{\frac{c_1 c_2}{c_3}} + |k_{23}| \sqrt{\frac{c_2 c_3}{c_1}} - |k_{13}| \sqrt{\frac{c_1 c_3}{c_2}} = 0,$$

if we multiply by $\sqrt{c_1 c_2 c_3}$ we see that this is equivalent to (2.39), if we correctly take into account the relative order of the momenta.

2.4.2 The kinematical Halohedron

We begin by defining the 1-loop kinematical space $\mathcal{K}_{1,n}$. In virtue of what we saw at tree level, we define it to be the set of n light rays with homogeneous coordinates k_a, together with a loop momentum l. We will restrict l to be time-like and bounded in the region $0 < l^2 < 1$. Finally, all is taken up to Lorentz transformations. The time-likeness of l has really no natural justification for now a part the connection with the hyperboloid model.

Having defined our kinematical space, we now need to associate to the

kinematical data $(k_1, \ldots, k_n; l)$ a unique bordered Riemann surface $X = \phi(k_1, \ldots, k_n; l)$. The time momenta has a very naive avatar in the Poincaré disk: its projection. But this construction is too simple, because projecting we loose any information about its mass, and it does not yield a bordered Riemann surface. Another meaningful geometrical object associated to l is a circle, defined by

$$\mathrm{C}_l = \{w \in \mathrm{H} |\ l \cdot w = 1\}.$$

It is easy to see that this is indeed an hyperbolic circle of hyperbolic radius $\cosh(r) = \frac{1}{\sqrt{l^2}}$. We can now can define a bordered Riemann surface simply by cutting away this circle from the Poincaré disk. Of course to the null momenta we keep associating their light-rays and thus the corresponding points in the boundary of $\mathbf{D}$. In conclusion, we have defined a map

$$\begin{aligned} \phi\ &: \mathcal{K}_{1,n} \to \mathcal{M}_{\mathcal{D},1;n} \\ &(k_1, \ldots, k_n; l) \mapsto \mathbf{D} \setminus C_l. \end{aligned}$$

Note that if the kinematical data $(k_a; l)$ are related to another set of kinematical data by an element η of $\mathrm{SO}^{\uparrow}(1,2)$, the associated surfaces are bi-holomorphic. Indeed the transformation of $\mathrm{Aut}_{\mathbf{D}}$ corresponding to η realises the bi-holomorphism. Interestingly the little group of l translates to the automorphism group of the surface X: we can picture the surface $X = \phi(k_1, \ldots, k_n; l)$ in the frame comoving with l, where it looks like an annulus, the little group of l are now rotations around the origin and these are exactly the automorphisms of the annulus. The crucial point of the map ϕ is that when $l^2 \to 0$ the circle C_l becomes a horocycle H_l [12], and thus by normalisation of the surface $\mathbf{D} \setminus H_l$ we obtain a disk with two extra punctures, thus mimicking a forward limit of a cutted integrand.

We now turn to the compactification of the kinematical space. A natural boundary occurs when $l^2 = 1$, that is when l hits the cut-off. In this case the circle C_l shrinks to a point and we get a natural extension of the map ϕ that sends this boundary to the cyclohedral face of the Halohedron H_n in moduli space. Recall that the Cyclohedron paired tadpoles in IR-UV pairs, our choice of names originated from the avatar of the cyclohedral facet in space time which occurs when l hits the cut-off $l^2 = 1$.

The next really new ingredient is that the time-like momentum l can become massless or can become asymptotical to a light ray. We have to add meaningful boundaries to $\mathcal{K}_{1,n}$ reflecting these limits. In space

[12] Recall from section 1.1 that a horocycle is defined by the condition $H_l := \{w \in \mathrm{H} \mid l \cdot w = 1\}$ with $l \in \mathrm{L}^+$

time picture, the redundance $\mathrm{Aut}_{\mathbf{D}}$ is tantamount to choose a Lorentz frame and we now have a new natural choice: the frame comoving with l. Choosing this frame is equivalent to find the element $\Lambda_l \in \mathrm{SO}^{\uparrow}(1,2)$ such that

$$\Lambda_l l = \begin{pmatrix} \sqrt{l^2} \\ 0 \\ 0 \end{pmatrix}.$$

This condition fixes Λ_l up to elements of the little group of l. Suppose now that $l \to p \in \mathrm{L}^+$, in the topology of $\mathbb{R}^{1,2}$, and without loss of generality suppose that the light ray of p is between particles i and $i+1$ with respect to the planar ordering. We can define a canonical Λ_l by

$$\Lambda_l := \eta_l \circ \gamma_1 \circ R_{p,1},$$

where $R_{p,1}$ is a rotation around the origin that sends p to $p_1 = (p^0, p^0, 0)$, γ_l is a parabolic element with fixed point in 1 that sends the center of C_l to the geodetic joining 0 to 1 and finally η_l is an hyperbolic element with fixed points ± 1 that sends the center of C_l to 0. By construction Λ_l sends l to a pure energy vector and the remaining kinematical data are sent to some new positions $\Lambda_l k_a$. In the limit $l \to p$ the light ray associated to $\Lambda_l k_a$ moves to the one associated to the vector

$$p_{-1} = \begin{pmatrix} 1 \\ -1 \\ 0 \end{pmatrix}.$$

Therefore, what l sees around him is a new light cone with a marked ray corresponding to p_{-1}. However the remaining kinematical data k_a may move as $l \to p$, in such a way to compensate the infinite boost η_l, and in this case l would see light rays k_a associated to some "surviving" particles.

We can label all these possible limits with exactly the same combinatorial object we needed to label the facets of the Halohedron, arcs on a marked annulus, and thus compactify $\mathcal{K}_{1,n}$ adding factorised components associated to the contraction of the relevant arc. For example to an arc such as the one in the third row of Table 1.1 we associate the limit where all particles from j to i fail to remain at a finite position when $l \to p$, and we add to the kinematical space a border of the form $\mathcal{K}_{n_L+1} \times \mathcal{K}_{1,n_R+1}$.

A comment is in order for the subtle cut limit that corresponds to an associahedral facet of the kinematical space. This arc represents a situation where all particles survive in the comoving frame of l and therefore we cannot do the limit naively in this way. Accordingly the component that

we have to add is not expressed as a factorisation, it is instead $\mathcal{K}_{n+2,\text{forward}}$ which is defined as the set of $n+1$ light rays - the extra light ray is associated to p - up to transformation under the little group of the extra null momenta. We now motivate this: first, suppose $l \to p$ and define $l' := \lambda l$. In a frame comoving with l (and l') the remaining kinematical data k_a tends to fixed position on the boundary of the disk. We have two surfaces $X = \phi(k_a, l)$ and $X' = \phi(k_a, l')$ which can be represented as annuli with the same punctures but different moduli. However, in the limit $l^2 \to 0$ they both degenerate to the same pinched annuli as shown in Fig. 2.20.

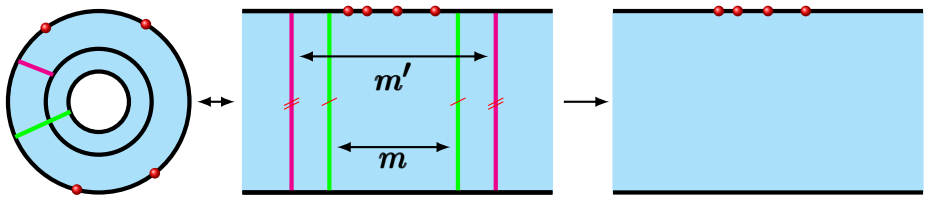

Figure 2.20: On the left are shown two annuli with the same punctures but different moduli. They are equivalent to the strips with identifications depicted in the middle, via the map $\sigma \to \exp \frac{i\sigma}{2\pi m}$. The strips both tend to the same surface as the moduli diverge, which is the infinite strip with punctures on the right.

This explains why we consider the light-ray associated with p rather than p itself. Next consider what happens if we take two surfaces with the same l but kinematical data $k' = \Lambda k$ with Λ an element of the little group of l, which in the disk correspond to an elliptic element with fixed point the center of C_l. If $l \to p$, and we choose a frame where we see $C_l \to H_p$ while the punctures remain at finite positions, Λ tends to an ideal rotation centered at p, but X' and X are always bi-holomorphic and thus they have the same limit: therefore we have to mod out by parabolic elements of the new light ray.prov Note that $\mathcal{K}_{n+2,\text{forward}}$ is not the same as the facet of $\mathcal{K}_{n+2}$ labelled by the arc of Fig. 2.21, as a simple counting of the dimensions proves.

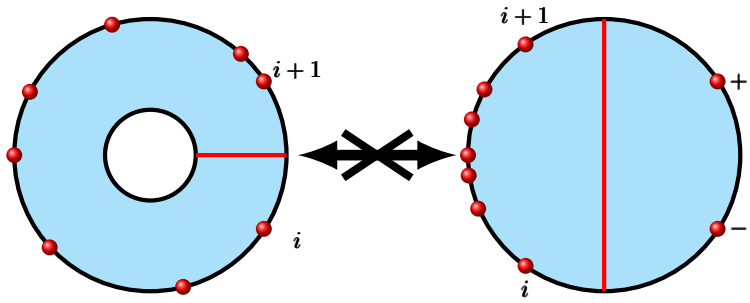

Figure 2.21: These facets of and $\mathcal{K}_{1,n}$ and $\mathcal{K}_{n+2}$ are not equivalent.

In conclusion we defined a compactification $\overline{\mathcal{K}}_{1,n}$ of the kinematical space which is combinatorially equivalent to an Halohedron, the map ϕ is extended by continuity to a map from the kinematical Halohedron onto the moduli space Halohedron.

CHAPTER 3

Amplitudes and Integrands from Positive Geometries

3.1 From Scattering Forms to Scattering Amplitudes

In this section we illustrate the connection between the positive geometries previously discussed and scattering amplitudes, we will for the moment not commit to a particular geometry since the general idea is the same for all of them. At the heart of this connection is the scattering form Ω which was introduced in Section 2.1 as a differential form living in the space of all kinematical variables, i.e. the space of all propagators. More precisely, we are interested in the pull-back of Ω to the m-dimensional subspace H which defines the convex realisation of a specific polytope, where we can write

$$\Omega|_{\mathrm{H}} = \langle Y d^m Y \rangle \underline{\Omega}(Y) = dX_1 \wedge \cdots \wedge dX_m \underline{\Omega}(X), \tag{3.1}$$

where $Y = (Y_0, \ldots, Y_m)$ and $X = (Y_1/Y_0, \ldots, Y_m/Y_0)$ are homogeneous and affine coordinates for H. After the pullback all the information about Ω is then encoded by the rational function $\underline{\Omega}$ and it is this function that we ultimately recognize as a scattering amplitude or, at loop level, as an integrand. Let us briefly comment on the reason of the partial retreat, at loop level, from amplitude to integrand. It is well known that after loop integration scattering amplitudes are expressed in terms of polylogarithmic functions, which have a complicated pattern of branch cuts. To this day, little is known on the physical principles that constrain the nature of these singularities, except in simple cases. On the other hand, an integrand is just a rational function of external and internal momenta and thus can at most develop poles corresponding to some propagator going on-shell. It remains a fascinating open problem to find a precise formula such as (1) for the final amplitude and eventually to understand if and

how the geometrical objects underlying the integrand leave a trace after loop integration. For the sake of brevity, we will not henceforth make difference between tree level scattering amplitudes and loop level scattering integrands and just refer to both as "amplitudes".

After the pullback Ω can be interpreted as the canonical form of the relevant polytope, i.e. is the unique differential form with simple poles along its facets and regular elsewhere such that its residue on the facet F is the canonical form of that facet. By definition it follows that $\underline{\Omega}$ is a rational function with at most *simple* poles, but then it seems implausible that it could reproduce a 1-loop integrand. The reason is that due to diagrams with internal bubbles an integrand can develop higher order poles, as we already discussed in Chapter 2. Nevertheless, one can hope to include rational functions with higher poles in the class of those obtained from canonical forms by deforming these poles into simple ones. For example, one can lift a double pole into a pair of simple poles by introducing a deformation parameter such as in

$$\frac{1}{z^2} = \lim_{\epsilon \to 0} \frac{1}{z(z+\epsilon)}.$$

A priori it is not obvious whether one can consistently define these deformations in more complicated examples, e.g. when the rational function depends on several variables. However the combinatorial structure of the positive geometries we encountered so far suggests a natural way to do so since variables already came in pairs $X_{i,j}$ and $X_{j,i}$. Double poles arise from the equality $X_{i,j} = X_{j,i}$ which is a consequence of momentum conservation at each vertex of a Feynman diagram, but the positive geometries are realized in a larger space where these variables are still distinguished and are attached to different facets. At this stage then, there are no double poles in the rational function $\underline{\Omega}$.

As a consequence of the boundary structure of the involved geometry the rational function $\underline{\Omega}$ satisfies (1), which in turn proves it to be equal to the amplitude. However, let us offer a more pedantic proof which also helps in understanding how the aforementioned lift of double poles is undone and how to get rid of external bubbles and tadpoles, in order to obtain the integrand for the bi-adjoint scalar theory. To pull back Ω we first choose a basis of m variables to parametrize the subspace H where the polytope lives. A convenient choice is to use vertex coordinates of the polytope itself, i.e. the face variables of m facets intersecting at any of its vertices, which we arrange in a projective vector $Y = (1, X_1, \ldots, X_m)$. In terms of this basis all the remaining face variables become affine linear functions on H which we can write introducing a dual projective vector

W_f as

$$X_f = Y \cdot W_f,$$

the pullback of Ω then reads

$$\Omega|_{\mathrm{H}} = \langle Y d^m Y\rangle \sum_{v\in\text{vertices}} \mathrm{sgn}(v) \frac{\langle W^* W_{a_1} \dots W_{a_m}\rangle}{Y\cdot W^* \prod_{i=1}^m Y\cdot W_{a_i}} \tag{3.2}$$

$$= \pm dX_1 \wedge \dots \wedge dX_m \sum_{v\in\text{vertices}} \mathrm{sgn}(v) \frac{\langle W^* W_{a_1} \dots W_{a_m}\rangle}{X_{a_1}\dots X_{a_m}}, \tag{3.3}$$

where we introduced the dual vector $W^* = (1, 0, \dots, 0)$, which represent the line at infinity $Y_0 = 0$. The numerators $\langle W^* W_{a_1} \dots W_{a_m}\rangle$ come from the pullback of the dlog terms of Ω, they could be a priori arbitrary numbers but an important feature of all the convex realisations discussed in Chapter 2 is that they are always ± 1. Furthermore, the signs required for the projectivity of Ω precisely balance those coming from the pullback, so that from (3.3) we immediately read the rational function, up to an overall sign, as

$$\underline{\Omega} = \sum_{v\in\text{vertices}} \frac{1}{X_{a_1}\dots X_{a_m}}. \tag{3.4}$$

Keeping in mind the correspondence between vertices and Feynman diagrams, the RHS of (3.3) basically concludes the identification of $\underline{\Omega}$ with an amplitude. The only subtlety is that now the propagators X_f are written as affine functions on H and they have to be translated back in terms of usual loop and external momenta, we will explain in more details how this is done in each case in the following sections.

3.2 The Halohedron and the integrand of ϕ^3_{BA}

We now specialize the discussion of the previous section to the case of the bi-adjoint scalar integrand, which we will obtain from the Halohedron following [1]. More precisely, this 1-loop integrand is computed summing over all planar 1-loop Feynman diagrams with the exclusion of tadpoles and external bubbles. Recall that the interaction vertex of the theory is $f^{abc}\overline{f}^{\bar{a}\bar{b}\bar{c}}\phi_{a\bar{a}}\phi_{b\bar{b}}\phi_{c\bar{c}}$, the antisymmetry of the structure constants f implies the vanishing of tadpoles. On the other hand, external bubbles contribute with a term proportional to a tree level amplitude which can be removed

from the definition of the integrand [23] [1]. Also, amplitudes and integrands of bi-adjoint are decomposed with respect to both color factors, which defines the so called doubly color ordered amplitudes $m(\alpha, \beta)$ for orderings α and β of the external particles. Considering all planar 1-loop diagrams means that we are computing only the diagonal part of the matrix $m(\alpha, \beta)$. While the off-diagonals elements were computed in [8; 24] at tree level from the Associahedron, it remains an open question if this can be done at loop level.

3.2.1 From the abstract space to the physical space

Following the general idea explained in the previous section, we extract the 1-loop bi-adjoint integrand from the canonical form of the Halohedron. First we show that indeed the numerators appearing on the RHS of (3.3) after the pull back are all "+1". By looking at the form of the face variables defined in (2.15), it is immediately clear that these numerators can only be ± 1. Next, consider two adjacent vertices v and v' of the Halohedron and call X and X' the only two face variables which are not shared by them. We claim that

$$dX \wedge (dX_{a_1} \dots dX_{a_{m-1}}) = -dX' \wedge (dX_{a_1} \dots dX_{a_{m-1}}), \tag{3.5}$$

where in $(dX_{a_1} \dots dX_{a_{m-1}})$ we have gathered all the shared face variables, in the same order. We prove this statement studying case by case the various types of adjacencies.
Cut/Factorisation adjacency. Consider two diagrams such as in figure. The corresponding measures are

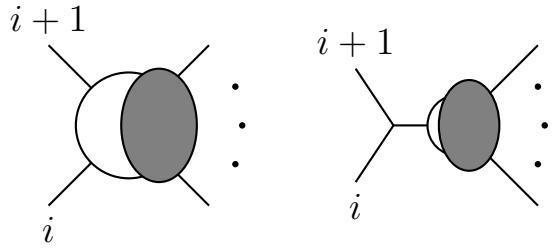

$$dX_i \wedge (\dots),$$

[1] It is not a problem to generate this term as well from the Halohedron, but following [1] we will just throw it away

for the diagram on the left and

$$dX_{(i,i+1)} \wedge (\dots),$$

for the one on the right.
Again, $(\dots)$ denotes the shared variables. Since we have $X_{(i,i+1)} = \epsilon_i - X_i$, (3.5) trivially holds.
IR/UV adjacency. The situation is slightly more complicate for a pair of IR and UV tadpoles. The two diagrams give

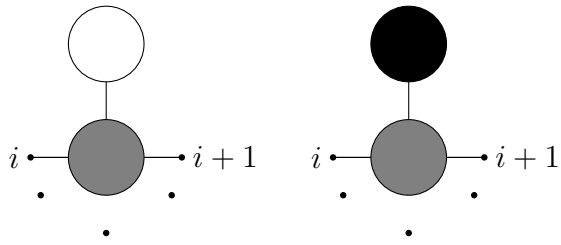

$$dX_i \wedge dX_{(i+1,i+2,\dots,i)} \wedge \dots$$
$$dX_0 \wedge dX_{(i+1,i+2,\dots,i)} \wedge \dots,$$

this time we highlighted one of the shared propagators, which carries the variable

$$dX_{(i+1,i+2,\dots,i)} = -d(X_{i+1} + dX_{i+2} + \dots + dX_{i-1}).$$

Keeping in mind that we are under a wedge with this factor, we can write

$$\begin{aligned} dX_i \wedge dX_{(i+1,i+2,\dots,i)} &= d(X_i + dX_{i+1} + \dots + dX_{i-1}) \wedge dX_{(i+1,i+2,\dots,i)} \\ &= -dX_0 \wedge dX_{(i+1,i+2,\dots,i)} \end{aligned}$$

Tadpole/Bubble adjacency. This adjacency involves two diagrams as in figure.

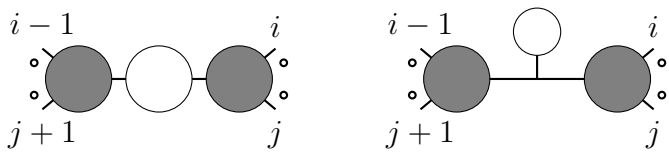

Note that, despite its name, the adjacency swaps a *cut* propagator X_j with a tadpole propagator $X_{(i,\dots,i-1)}$. This time we have to focus on the

two shared propagators at the sides of the bubble, whose variables are

$$\begin{aligned} dX_{(j+1,\dots,i-1)} &= -d(X_{j+1} + \cdots + X_{i-2}) \\ dX_{(i,\dots,j)} &= -d(X_i + \cdots + X_{j-1}), \end{aligned}$$

we have

$$\begin{aligned} dX_{(i,\dots,i-1)} &= -d(\overline{X_i + \cdots + X_{j-1}} + X_j + \overline{X_{j+1} + \cdots + X_{i-1}}) \\ &= -dX_j, \end{aligned}$$

where in the last passage we used the fact that the overlined terms vanish under wedge with the two shared propagators.
s-channel/u-channel adjacency. Finally, we have a adjacency involving tree structures of the diagram. In the figure we drawn the loop part on the leg I_1 but its actual position is irrelevant, only that it is the same in both diagrams. All the four shared variables X_{I_j} have to be kept in consideration, and in particular remember that $dX_{I_1} = -d(X_i + \cdots + X_{j-1})$ [2]. For the diagram on the left we have

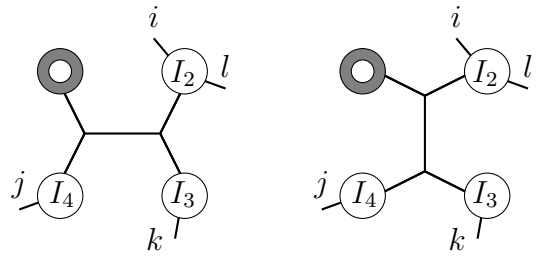

$$\begin{aligned} &\cdots \wedge dX_{I_1} \wedge dX_{I_4} \wedge dX_{I_2 I_3} \\ =&\cdots \wedge dX_{I_1} \wedge dX_{I_4} \wedge d(\overline{X_{I_2 I_3} + X_{I_4} - X_k} + X_k) \\ =&\cdots \wedge dX_{I_1} \wedge dX_{I_4} \wedge dX_k, \end{aligned}$$

we freely added a shared propagator and recognised the overlined term as dX_{I_1}.
Similarly, for the other diagram we get

$$\cdots \wedge dX_{I_3 I_4} = \cdots \wedge dX_l,$$

[2] We made a slight abuse of notation, as we should write $X_{(I_1)^c}$ rather than X_{I_1}

finally we note that

$$\cdots \wedge d(X_k + X_l) = \cdots \wedge d(X_k + X_l + X_{I_2} + X_{I_3} + X_{I_4}) = \cdots \wedge d(X_{I_1}) = 0,$$

thus proving (3.5) also in this case.

Since any two vertices of the Halohedron can be joined by a finite sequence of the above adjacencies, and at each step the sign produced by the pullback balance the one required from projectivity, we conclude that the canonical form of the Halohedron can be written as in (3.3). A convenient choice of "reference" vertex is the one corresponding to the ring diagram, which is the intersection of the n variables X_i dual to the ring propagators. Accordingly the rational function $\underline{\Omega}_{\mathrm{H_n}}$ of the Halohedron is given as in (3.4), i.e. is the sum over all 1-loop diagrams. However, in the sum are involved also UV/IR tadpoles and diagrams with bubbles on external legs. Such unphysical contributions appear with terms $X_0, X_{i,\dots,i+n}$ or $X_{i,\dots,i+n-1}$ in the denominator, which in turn are given by expressions linear in the X_i and in the various ϵ_I. Therefore, we can kill the external bubbles and the tadpoles by taking the limit $\epsilon_I \to \infty$ for $I = 0$ or $|I| = n, n-1$. Finally, we have to translate the remaining face variables in term of the physical propagators. In order to do so we note that each variable X_I carries an ϵ_I term uniquely associated to it. Therefore, we can first solve the ϵ_I for *all* the X_J and, then, the substitution $X_I \to S_I$ can be done unambiguously, even if we have an expression for $\underline{\Omega}_{\mathrm{H}_n}$ where the constants ϵ_I and the variables X_i are not manifestly appearing in a combination from which we can recognise a variable X_I. Finally, we remark that thinking projectively the effect of the limits $\epsilon_I \to \infty$ is to send the corresponding facets at infinity, but in the process the polytope breaks down because we violate the constraints that the constants ϵ have to satisfy.

3.2.2 Standard triangulation of the Halohedron

We understood how to extract the 1-loop integrand from the canonical form of the Halohedron, reproducing the Feynman diagram representation. However, we can obtain new formulae by considering triangulations of the Halohedron to compute its canonical form. In this section we provide an example of this, using a recursion formula for the canonical form of a polytope that works by recycling the canonical forms of its facets. We just sketch this construction here, further details can be found in full generality in [8] and in Appendix A. The idea is to triangulate the polytope using a reference point Z^* in its interior. For each facet $\mathcal{F}$ we take the convex hull $\mathcal{P}_{\mathcal{F}}$ of its vertices with Z^*, together these polytopes triangulate $\mathcal{P}$. The canonical form of $\mathcal{P}_{\mathcal{F}}$ can be obtained by a suitable deformation of the

canonical form of the facet $\mathcal{F}$. In the case of the Associahedron and the Halohedron, these canonical forms can be interpreted as lower points amplitudes, therefore we obtain a geometrically inspired recursion formula.

We will explicitly unwind this procedure for $n = 4$. We choose as reference point the intersection of the cut facets $X^* = (0, 0, 0, 0)$. Therefore, all facets will contribute to the recursion, except for the cut facets for which the convex hull with X^* is 2 dimensional rather than 3 dimensional. The recursion, written directly at the level of the rational functions, reads

$$\underline{\Omega}_{\rm H_4} = \sum_I \underline{\hat{\Omega}}_{X_I}, \tag{3.6}$$

where the sum is over all subsets I of $(1, 2, 3, 4)$ made of cyclically consecutive indices, excluding the singletons $I = \{i\}$, and $\underline{\hat{\Omega}}_{X_I}$ is a deformation of the rational function of the facet X_I obtained as follows. First, we write $X_I = X^0_I + X'_I$, where in X^0_I we gather the constants ϵ and in X'_I the basis variables X_i. The deformation is then defined by replacing each basis variable appearing in $\underline{\Omega}_{X_I}$ with

$$X_i \to \hat{X}_i = -\frac{X^0_I}{X'_I} X_i,$$

and multiplying by the overall factor $(X^0_I/X'_I)^4$. In other words we have that

$$\underline{\hat{\Omega}}_{X_I}(\epsilon|X_i) = \left(-\frac{X^0_I}{X'_I}\right)^4 \frac{\underline{\Omega}_{X_I}(\epsilon| - \frac{X^0_I}{X'_I} X_i)}{X_I}, \tag{3.7}$$

where we emphasized that the rational function $\underline{\Omega}_{X_I}$ depends on both the constants ϵ and the basis variables X_i. We are interested in the limits $\epsilon_J \to \infty$, for $J = 0$ or $|J| = 4, 3$, and which we take in this same order. Recalling the Feynman diagram representation for the rational functions $\underline{\Omega}_{X_I}$, it is easy to understand the effect of this limit on (3.7). If X_I is not one of the facet involved in the limit, i.e. it has $|I| \leq 2$, then tadpoles and external bubbles do not contribute to its rational function. Also, because of the order of the limits, UV tadpoles do not appear in the rational function of an IR tadpole facet, but internal bubbles do. Finally, if I is one of the facet being sent to infinity one has to take into account the diverging pre-factor X^0_I in (3.7). A quick power counting shows that the net effect is that we

are left with

$$\hat{\underline{\Omega}}_{X_I}(\epsilon|X_i) = \frac{\underline{\Omega}_{X_I}(0|X_i)}{X'_I}, \tag{3.8}$$

i.e. we forget the dependence on the constants ϵ of the propagators appearing in $\underline{\Omega}_{X_I}/X_I$.

We now show explicitly the computation for each facet contributing to (3.6), for the sake of brevity we will simply write ϵ_i instead of $\epsilon^2_{(i,i+1)}$.
UV facet. This facet is associated to the variable

$$X_0 = \sum_{i=1}^{4} \epsilon_i - \epsilon_0 - \sum_{i=1}^{4} X_i,$$

therefore

$$X_0^0 = \sum_{i=1}^{4} \epsilon_i - \epsilon_0 \qquad X_0^{'} = -\sum_{i=1}^{4} X_i.$$

The rational function $\underline{\Omega}_{X_0}$ is given by a sum over all 20 UV-tadpole diagrams. If we group those associated with the same IR tadpole propagator, say $X_{(i,i+1,i+2,i+4)}$, we obtain

$$\frac{1}{X_{(i,i+1,i+2,i+4)}}\left(\frac{1}{X_{(i,i+1)}X_{(i+2,i+3)}} + \frac{1}{X_{(i+1,i+2)}X_{(i+1,i+2,i+3)}} + \right.$$
$$\left. \frac{1}{X_{(i,i+1)}X_{(i,i+1,i+2)}} + \frac{1}{X_{(i+1,i+2,i+3)}X_{(i+2,i+3)}} + \frac{1}{X_{(i,i+1,i+2)}X_{(i+1,i+2)}}\right). \tag{3.9}$$

Since this facet is going to infinity, we forget the ϵ dependence of the planar variables appearing in (3.9), after which the terms in the bracket of (3.9) sum up to

$$\frac{X_i + X_{i+1} + X_{i+2}}{X_i X_{i+1} X_{i+2}},$$

the numerator cancels with the denominator outside the bracket leaving us with

$$\frac{1}{X_i X_{i+1} X_{i+2}},$$

and summing over the four IR tadpole propagators we get

$$\underline{\Omega}_{X_0}(0|X_i) = \frac{X_1 + X_2 + X_3 + X_4}{X_1 X_2 X_3 X_4}, \tag{3.10}$$

plugging (3.10) back in (3.8) we finally get the contribution of the UV facet to the recursion

$$\underline{\hat{\Omega}}_{X_0} = \pm \frac{1}{X_1 X_2 X_3 X_4}. \tag{3.11}$$

Tadpole facet. We focus on the facet $X_{(1,2,3,4)}$, the remaining ones are obtained through a cyclic shift. The rational function $\underline{\Omega}_{X_{(1,2,3,4)}}$ is given by a sum over 10 IR and UV tadpole diagrams. However, the UV are killed by the limit $\epsilon_0 \to \infty$ which we take before the limit $\epsilon_{(1,2,3,4)} \to \infty$. Therefore we are left with 5 IR tadpole diagrams, whose contribution is almost identical to (3.9) a part for the prefactor:

$$\frac{1}{X_4}\left(\frac{1}{X_{(1,2)}X_{(3,4)}} + \frac{1}{X_{(2,3)}X_{(2,3,4)}} + \right.$$
$$\left. \frac{1}{X_{(1,2)}X_{(1,2,3)}} + \frac{1}{X_{(2,3,4)}X_{(3,4)}} + \frac{1}{X_{(1,2,3)}X_{(2,3)}}\right), \tag{3.12}$$

again because of the limit the variables in (3.12) lose the ϵ dependence so that $X_{(i,i+1)} \to -X_i$ and $X_{(i,i+1,i+2)} \to -X_i - X_{i+1}$, after some manipulations we get

$$\underline{\Omega}_{X_{(1,2,3,4)}}(0|X_i) = \frac{X_1 + X_2 + X_3}{X_1 X_2 X_3 X_4},$$

and then

$$\underline{\hat{\Omega}}_{X_{(1,2,3,4)}} = \pm \frac{1}{X_1 X_2 X_3 X_4}. \tag{3.13}$$

Bubble facet. Again we consider a specific case, for instance $X_{(1,2,3)} = 0$. Recall that this facet factorises in $\mathrm{H}_{\mathcal{A}} \times \mathcal{A}_1$, $\mathcal{A}_1$ being a 4-point Associahedron. Accordingly, we can write its rational function as

$$\underline{\Omega}_{X_{(1,2,3)}} = \left(\frac{1}{X_{(1,2)}} + \frac{1}{X_{(2,3)}}\right) \times \left(\frac{1}{X_3 X_4} + \dots\right),$$

where in $\dots$ we gathered terms that vanish due to the limits $\epsilon_0, \epsilon_I \to \infty$ with $|I| = 4$, thus in the limit we have

$$\underline{\Omega}_{X_{(1,2,3)}}(0|X_i) = \frac{X_1 + X_2}{X_1 X_2 X_3 X_4},$$

and finally once again

$$\hat{\underline{\Omega}}_{X_{(1,2,3)}} = \pm \frac{1}{X_1 X_2 X_3 X_4}. \tag{3.14}$$

Factorisation Facet. Consider $X_{(1,2)} = \epsilon_1 - X_1 = 0$, there are only two diagrams surviving all the limits so the rational function is given by

$$\underline{\Omega}_{X_{(1,2)}} = \left(\frac{1}{X_2 X_3 X_4} + \frac{1}{X_2 X_4 X_{(3,4)}} \right)$$

which plugging into (3.7) gives

$$\hat{\underline{\Omega}}_{X_{(1,2)}} = \frac{\epsilon_1}{X_1 X_2 X_4 (\epsilon_1 - X_1)} \left(\frac{1}{X_3} + \frac{\epsilon_1}{X_1 \epsilon_3 - \epsilon_1 X_3} \right). \tag{3.15}$$

Note that the denominator $X_1\epsilon_3 - \epsilon_1 X_3$ represents a *spurious* pole, it eventually cancels with a similar contribution coming from the facet $X_{(3,4)} = 0$.

Putting the contributions from the various facets together, and paying attentions to the signs involved, we find that each tadpole contribution cancels with a corresponding bubble. We are left with the UV contribution and the factorisation contributions.

Next, we need to translate back (3.15) into usual loop and external variable. First have to rewrite the constants ϵ_i in terms of the planar variables X_I and then substitute the corresponding propagators:

$$\epsilon_i = X_{(i,i+1)} + X_i \to s_{i,i+1} + \ell_i^2,$$

where $s_{i,j} = 2k_i \cdot k_j$ and ℓ_i^μ is the momentum flowing between particles i and $i+1$, e.g. $\ell_1^\mu = \ell^\mu$, $\ell_2^\mu = \ell^\mu + k_2^\mu$ and so on. After this is done, with a bit of algebra we get the following expression for the 4-point integrand

$$m_4^{1-\text{loop}} = -\frac{1}{\ell_1^2 \ell_2^2 \ell_3^2 \ell_4^2} + \left(\frac{(\ell_1^2 + s_{12})(\ell_3^2 + s_{12})}{s_{12}^2 \ell_2^2 \ell_3^2 \ell_4^2 (\ell_3^2 - \ell_1^2)} + \text{cyclical} \right), \tag{3.16}$$

where the sum is over the remaining three cyclically shifted terms. Note that (3.16) has double poles $s_{12} = 0$ and $s_{23} = 0$ coming from the internal bubbles. If we expand around $s_{12} = 0$ we get

$$\frac{1}{s_{12}^2} \frac{1}{\ell_2^2 \ell_4^2} + \frac{1}{s_{12}} \left(\frac{1}{\ell_1^2 \ell_2^2 \ell_4^2} + \frac{1}{\ell_2^2 \ell_3^2 \ell_4^2} \right) + \dots$$

and from the coefficients of the expansion we read the internal bubble

contribution and the *two* contributions to the residue $s_{12} = s_{34} = 0$.

3.3 ABCD and massive ϕ^3

In the previous section we discussed how to compute amplitudes in bi-adjoint theory using the Halohedron. In particular we learned that integrands with double poles can indeed be treated within the context of positive geometries, by lifting them to pairs of simple poles which are represented by different facets of the polytope. Surprisingly, it is instead the absence of tadpoles and external bubbles which seems to be more in tension with positive geometries since we could not find a polytope whose rational function resembled a sum over Feynman diagrams excluding these topologies. On the other hand, we already saw in Section 2.1 that this is connected with projectivity, it seems impossible to build a 1-loop scattering form without incurring in either tadpoles or external bubbles to compensate the projective variation of more "regular" Feynman diagrams. We are then naturally lead to consider a theory where all such diagrams appear, in order to regulate them we give a common internal mass to all propagators and allow for external particles to be off-shell. By doing so tadpole diagrams share a common propagator $X_0 := -m^2$, while an external bubble on the i-th leg comes with a propagator $X_{i,i+1} := k_i^2 - m^2$. We refer to this theory as the massive ϕ^3 scalar theory. Once again we are interested only in its planar limit and in particular we will compute tree level amplitudes and 1-loop integrands using the cluster polytopes $\mathcal{A}$ and $\overline{\mathcal{D}}$. Although there are strong evidences that the picture carries over to all loop order, it remains an open problem to even fully understand the relevant positive geometries. Finally, we note that the usual ϕ^3_{BA} theory can be recovered from the massive theory discussed here. This is trivial at tree level, where one simply has to take the massless limit $m \to 0$ and $k_i^2 \to 0$. At 1-loop level the situation is slightly subtler since one also has to subtract the diverging terms coming from tadpoles and bubbles. Quite beautifully, however, the geometry of $\overline{\mathcal{D}}$ suggests a simple way to perform the limit and in turn to obtain new results for bi-adjoint theory as well.

3.3.1 From mesh constants to physical space

We begin by proving that, also in the case of cluster polytopes, after the pull-back (3.3) of the scattering form we obtain an expression with unit numerators. We follow the same strategy used for the Halohedron, i.e. we focus on an arbitrary pair of adjacent vertices v and v' and inspect the relation between the corresponding dlog terms. In the language of

cluster polytopes two adjacent vertices correspond to mutated triangulations. If the polytope has dimension d, v and v' lie at the intersection of $d-1$ common facets, which we collectively call $X_{\rm s}$, with two further facets X and X', respectively. As a consequence of the mesh conditions, on the subspace defining the convex realisation of the cluster polytope these variables satisfy

$$dX + dX' = dX_{\rm s},$$

from which is evident that expressing the dlog term of, say v', in the vertex coordinates of v we gain an overall minus sign which is balanced by the one coming from projectivity, as expected. The result is generalized to an arbitrary pair of vertices, since they are always connected by a sequence of mutations. A convenient choice of vertex coordinates are those associated to the left-most edge of the region for the wave equation, which correspond to planar variables $[X_{1,3},\ldots,X_{1,n-1}]$ for the standard ABHY realization of $\mathcal{A}_{n-3}$ or to the planar variables $[X_1, X_1', X_{1,2},\ldots,X_{1,n-1}]$ for the standard ABHY realization of $\mathcal{D}$ and $\overline{\mathcal{D}}$. For these latter polytopes, we will refer to their associated basis as *tadpole basis* since the basis variables are dual to a tadpole. Another convenient choice is the *ring diagram* vertex corresponding to the variables $[X_1,\ldots,X_n]$.

We have now proved that the rational function of all cluster polytopes is given by (3.4), that is as a sum over Feynman diagrams, each one contributing with the inverse product of its dual variables. We now turn to the translation of the planar variables, which at this stage are linear functions of mesh constants and the chosen basis variables, to their usual representation in terms of external and internal momenta. This will also have the effect of undo the double poles deformation and restore momentum conservation. As in the case of the Halohedron, this can be done by inspecting the solution of the mesh relations, say in the tadpole basis, which schematically can be written as

$$X_f = C_f + X_{\rm basis}.$$

One then invert these relations to express the constants C_f (which are linear combinations of mesh constants) as a function of the planar variables X_f and the basis variables $X_{\rm basis}$, which are immediately expressed

Basis Elements	Mesh constants	Effect
$X_1 \to \ell^2 - m^2$	$c_i \to \ell_i^2 + \ell_{i+1}^2 - k_i^2 - 2m^2$	$X_0 \to -m^2$
$X_1' \to \ell^2 - 2m^2$	$c_{i,j} \to -2k_i \cdot k_j$	$X_i \to \ell_i^2 - m^2$
$X_{1,2} \to k_1^2 - m^2$	$c_{i,i+1} \to -2\ell_i^2 - 2k_i \cdot k_{i+1} + m^2$	$X_{i,i+1} \to k_i^2 - m^2$
$X_{1,j} \to \left(\sum_{a=1}^{j-1} k_a\right)^2 - m^2$	$c_{i+2,i} \to k_{i+1}^2 - 2k_i \cdot k_{i+2} - m^2$	$X_{i,j} \to \left(\sum_{a=i}^{j-1} k_a\right)^2 - m^2$

Table 3.1: Replacement rules for $\overline{\mathcal{D}}_n$ an their effects on the planar variables

in terms of loop and external momenta as

$$\begin{aligned} X_i &= \left(\ell + \sum_{a=1}^{i-1} k_a\right)^2 - m^2, \\ X_{i,j} = X_{j,i} &= \left(\sum_{a=i}^{j-1} k_a\right)^2 - m^2 \\ X_0 &= -m^2 \\ X_1' &= X_0 + X_1 = \ell^2 - 2m^2. \end{aligned} \tag{3.17}$$

Clearly, at this step we restore the double poles by imposing $X_{i,j} = X_{j,i}$. For future convenience, we also introduce the short-hand notation

$$\ell_i = \left(\ell + \sum_{a=1}^{i-1} k_a\right).$$

In practice, it is easier to work with the mesh constants directly rather than with their combinations C_f. One can read off the substitution of mesh constants in terms of physical propagators directly from mesh relations. For example, the typical relation

$$c_{i,j} = X_{i,j} + X_{i+1,j+1} - X_{i,j+1} - X_{i+1,j},$$

implies that we have to substitute $c_{i,j} \to= -k_i \cdot k_j$. For convenience, the set of replacements when working in the tadpole basis $(X_1, X_1', X_{1,2}, \ldots X_{1,n-1})$ is listed in table (3.1); a similar set of rules can be derived when working in the ring basis $(X_1, \ldots, X_n)$. In conclusion, we shown that amplitudes and integrands of massive ϕ^3 theory can be extracted from the rational

function of ABHY polytopes by

$$m_n^{\text{tree}} = \underline{\Omega}_{\mathcal{A}_{n-3}}(c(X)|X), \quad m_n^{1-\text{loop}} = \underline{\Omega}_{\overline{\mathcal{D}}_n}(c(X)|X), \tag{3.18}$$

using the rules of Tab. (3.1) for the constants $c = c(X)$.

As anticipated we can also obtain the massless integrand for the bi-adjoint theory from $\overline{\mathcal{D}}_n$. In order to do so, one first expresses all variables in terms of the ring basis. In this basis the tadpole variable is given by $X_0 = C_0 - X_1 - X_n$, see (B.8), so that sending $C_0 \to \infty$ kills the tadpole contributions. In principle other planar variables might depend on C_0 when expressed in the ring basis, but in Appendix B we show that this is not the case, thus the limit removes *precisely* the tadpole contributions. Depending on the definition of the integrand for bi-adjoint theory, external bubbles can be removed in the same way. Finally one performs a similar set of replacements as those described above, with the difference that now we want massless propagators and thus we replace $X_i \to \ell_i^2$.

Let us now see a few simple examples. The simplest case is the four point tree level amplitude, which correspond to the cluster polytope $\mathcal{A}_1$. We choose $X_{1,3}$ as basis variable, there is a single mesh relation

$$X_{1,3} + X_{2,4} = c_{1,3}, \tag{3.19}$$

whose solution yields

$$X_{2,4} = c_{1,3} - X_{1,3}. \tag{3.20}$$

The rational function is therefore

$$\underline{\Omega}_{\mathcal{A}_1} = \frac{1}{X_{1,3}} + \frac{1}{c_{1,3} - X_{1,3}}. \tag{3.21}$$

Following the prescription (3.18), we now substitute (3.19) in (3.21) obtaining

$$m_4 = \underline{\Omega}_{\mathcal{A}_1}(c_{1,3}|X_{1,3})\big|_{c\to c(X)} = \frac{1}{X_{1,3}} + \frac{1}{X_{2,4}}. \tag{3.22}$$

At this point one might accuse us of being over pedantic: why we do not simply call $c_{1,3} - X_{1,3} = X_{2,4}$ and be done with it? The reason is that we might get to expressions for the rational function where mesh constants and basis variable do not appear in a way that makes manifest how to

recognize them as other planar variables, such as in

$$\underline{\Omega}_{\mathcal{A}_1} = \frac{c_{1,3}}{X_{1,3}(c_{1,3} - X_{1,3})},$$

however we can still follow (3.18) and obtain

$$m_4 = \underline{\Omega}_{\mathcal{A}_1}(c_{1,3}|X_{1,3})\big|_{c\to c(X)} = \frac{X_{1,3} + X_{2,4}}{X_{1,3}X_{2,4}}. \tag{3.23}$$

Indeed, this will be the case when we will compute the canonical form of ABHY polytopes using triangulations.

Let us now move to a 1-loop example, the simplest case is $\overline{\mathcal{D}}_2$ which gives the 1-loop 2-point amplitude. Again there is a single mesh relation

$$X_1' + X_2 = c_1, \tag{3.24}$$

and therefore we find the replacement rule $c_1 \to \ell_1^2 + \ell_2^2 - 3m^2$, [3]. Since $\overline{\mathcal{D}}_2$ is just a triangle, we can immediately write down its rational function

$$\underline{\Omega}_{\overline{\mathcal{D}}_2}(c|X_1, X_1') = \frac{c_1}{X_1(c_1 - X_1')(X_1' - X_1)}, \tag{3.25}$$

and applying (3.18) we get the 1-loop integrand

$$\begin{aligned} m_2^{1-\text{loop}} &= \underline{\Omega}_{\overline{\mathcal{D}}_2}(c|X_1, X_1')\big|_{c_1=\ell_1^2+\ell_2^2-3m^2} = \frac{\ell_1^2 + \ell_2^2 - 3m^2}{(\ell_1^2 - m^2)(\ell_2^2 - m^2)(-m^2)} \\ &= \frac{1}{(\ell_1^2 - m^2)(\ell_2^2 - m^2)} + \frac{1}{(\ell_1^2 - m^2)(-m^2)} + \frac{1}{(\ell_2^2 - m^2)(-m^2)}. \end{aligned}$$

Note that if we take the residue at $X_1 = 0$ or equivalently at $\ell_1^2 - m^2 = 0$ we are left with a 4-point amplitude in the forward limit,

$$\text{Res } m_2^{1-\text{loop}}\Big|_{\ell^2=m^2} = \frac{1}{-m^2} + \frac{1}{(\ell + k_1)^2 - m^2} = m_4^{\text{tree}}(1, -, +, 2) \tag{3.26}$$

We take advantage of this simple example to show also how the massless limit works. The basis ring is just (X_1, X_2) and it is trivial to move to this basis since the mesh relation tells us $X_1' = c_1 - X_2$, therefore the tadpole constant is just c_1 because $X_0 = X_1' - X_1 = c_1 - X_1 - X_2$. If we send $c_1 \to \infty$

[3] This rule is slightly different from the general one of table (3.1) because in this simple case the mesh relation does not have $X_{i,i+1}$ on the RHS, as it would be for general n.

we get

$$\underline{\Omega}_{\overline{\mathcal{D}}_2}(c|X_1,X_2)=\frac{c_1}{X_1X_2(c_1-X_1-X_2)}\to\frac{1}{X_1X_2}, \tag{3.27}$$

the replacement rules are simply $X_i\to\ell_i^2$ and thus we get the two point bi-adjoint function: $\frac{1}{\ell_1^2\ell_2^2}$.

3.3.2 Standard Triangulation for $\overline{\mathcal{D}}_n$

We begin with the simplest possible triangulation, which works for any polytope $\mathcal{P}$, and that we already used for the Halohedron: choose any point $Z^*\in\mathcal{P}$, for any facet X_f take its convex hull with Z^*, i.e. define the polytope

$$\hat{X}_f=\text{Conv}(Z^*,X_f),$$

the union of all such polytopes give a triangulation of $\mathcal{P}$, i.e.

$$\mathcal{P}=\bigcup_{f\in\text{facets}}\hat{X}_f, \tag{3.28}$$

and all these polytopes interiors do not overlap. If facets are not simplices, one simply has to iterate the procedure. Furthermore, if at each step we choose the point Z^* to be one of the vertices, there is no need to take convex hulls with the facets intersecting at that vertex.

As first described in [8], this triangulation translates into a recursive expression for the canonical form of $\mathcal{P}$ built up from the canonical form of its facets. For the sake of self-containedness let us quickly review here how this formula goes. To begin with, we send Z^* to some vertex Z of $\mathcal{P}$ and choose as basis the variables X intersecting at that vertex. Now pick any facet f to which Z does not belong. Choose any vertex $Z_f\in X_f$ and the variables χ intersecting there as a basis for the subspace $X_f=0$. The rational function of the facet X_f is a function of χ and of the various constants c_f appearing in the face variables,

$$\underline{\Omega}_{X_f}=\underline{\Omega}_{X_f}(c_f|\chi).$$

To get the canonical form of $\hat{X}_f$, one has to perform a *pullback* on the larger space $X_f\neq 0$ which in practice requires to express the χ variables in the X basis obtaining a new function which we denote by the same symbol for sake of brevity

$$\underline{\Omega}_{X_f}=\underline{\Omega}_{X_f}(c_f|X).$$

Then one has to perform the *replacement trick*, which consists in introducing a deformation parameter ϵ_f read from the expression of X_f in the basis X:

$$X_f = X_f^0 + X_f' \;\Rightarrow\; \epsilon_f := -\frac{X_f^0}{X_f'},$$

where X_f' is a linear expression in X and X_f^0 is a constant. Then the rational function of $\hat{X}_f$ is given by

$$\underline{\Omega}_{\hat{X}_f}(c|X) = \left(\frac{X^0}{X'}\right)^d \frac{\underline{\Omega}_{X_f}(c_f| - \epsilon_f X)}{X_f}, \tag{3.29}$$

where d is the dimension of $\mathcal{P}$.

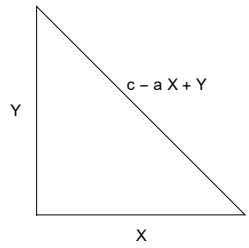

Figure 3.1: A triangle with faces given by $x = 0$, $y = 0$ and $c - ax + y = 0$.

To fix ideas, let us give a simple application of this formula to compute the canonical form of the triangle in figure. We choose the origin as Z^*, therefore only the facet $X_f = c - ax + y = 0$ contributes, it lives in a subspace where we can use a coordinate $0 \leq x \leq c/a$, in terms of which the rational function of $X_f = 0$ is

$$\underline{\Omega}_{X_f}(a, c|x) = \frac{c/a}{x(c/a - x)},$$

the deformation parameter is $\epsilon_f = \frac{c}{ax-by}$, therefore the canonical form of the triangle as computed from (3.29) is

$$\underline{\Omega}_{X_f}(a, c|-\epsilon_f x) = \left(\frac{cx}{ax - y}\right)^2 \frac{c/a}{\frac{cx}{ax-y}\left(c/a - \frac{cx}{ax-y}\right)(c - ax + y)} = \frac{c}{xy(c - ax + y)},$$

which is what we would get from the usual formula for a simplex.

As was firstly discussed in [8] and studied in more detail in [22] the triangulation can be used to set up recursion relation for tree level amplitudes: indeed, as it should be clear from the example above, the formula

works by recycling the information of the canonical form of the facets and in the case of $\mathcal{A}_n$ polytopes these are lower point amplitudes, expressed as rational functions of planar basis and mesh constants. Note that for the triangulation formula to work as a *recursion* formula it is crucial the fact that ABHY realization of cluster polytopes is closed upon taking boundaries, i.e. not only boundaries are again cluster polytopes, but moreover they are ABHY-realized with effective charges as described in Section 2.3.1. The recursion of the mesh constants has to be fed in the recursion.

As it should be clear, the triangulation (3.28) does not rely on any particular geometrical or combinatorial property of $\mathcal{P}$ (other than being a polytope), and it is therefore interesting that it is enough to learn something new about amplitudes, when applied to ABHY polytopes.. This is even more striking when applied to $\overline{\mathcal{D}}_n$: send Z^* to the "ring diagram" vertex, which is in the intersection of the n cut facets. Thus we can set up a recursion formula which does not require the knowledge of $n+2$ tree level amplitudes, which is quite surprising from the point of view of (1). Remember, however, the presence of the tadpole facet which gives an extra term. Specifically, the recursion formula reads

$$\begin{aligned}\overline{\Omega}_{\overline{\mathcal{D}}_n}(X_i) = &\sum_{i+1<j}\left(\frac{X^0_{i,j}}{X'_{i,j}}\right)^n \frac{1}{X_{i,j}}\underline{\Omega}_{\mathcal{A}_{n_L}}(\hat{X}_L|\hat{c}_L)\times\overline{\Omega}_{\overline{\mathcal{D}}_{n_R}}(\hat{X}_R|\hat{c}_R)\\ &+\sum_{j<i}\left(\frac{X^0_{i,j}}{X'_{i,j}}\right)^n \frac{1}{X_{i,j}}\overline{\Omega}_{\overline{\mathcal{D}}_{n_L}}(\hat{X}_L|\hat{c}_L)\times\overline{\Omega}_{\mathcal{A}_{n_R}}(\hat{X}_R|\hat{c}_R)\\ &+\left(\frac{X^0_0}{X'_0}\right)^n \frac{1}{X_0}\overline{\Omega}_{\mathcal{B}_{n-1}}(\hat{X}_B),\end{aligned} \tag{3.30}$$

where the various hats remind us that we have to use deformed basis variables and effective mesh constants. One might argue that the presence of the tadpole facet make so that the above is not really a recursive formula for the 1-loop integrand, however the tadpole facet is nothing but an ABHY $\mathcal{B}_{n-1}$ polytope, therefore we can set up the same recursion formula to compute its rational function. However, no matter to which vertex we send Z^* in this recursion, we will not avoid the fact that some $n+1$ tree level associahedra appears in the triangulation [4]. Therefore, we will need tree level amplitudes with up to $n+1$ external legs to compute the 1-loop integrand in this way. It is quite interesting that, in this representation of the 1-loop integrand, the truly higher point contribution to

[4]These associahedra show up as the intersection of the previous cut associahedra, which were $(n+2)$-pt tree, with the tadpole facet.

the integrand originates from tadpoles.

For illustration purposes, in Fig. 3.2 is shown the triangulation for $n = 3$. There are three pieces coming from the bubble factorization facets $X_{i,i+1}$ which are just simplices and a pyramid whose hexagonal base is the tadpole facet of $\overline{\mathcal{D}}_3$. Notice how the three pentagonal cut facets do not contribute: taking their convex hulls with the ring vertex does not produce a three dimensional polytope. Before ending this section, let

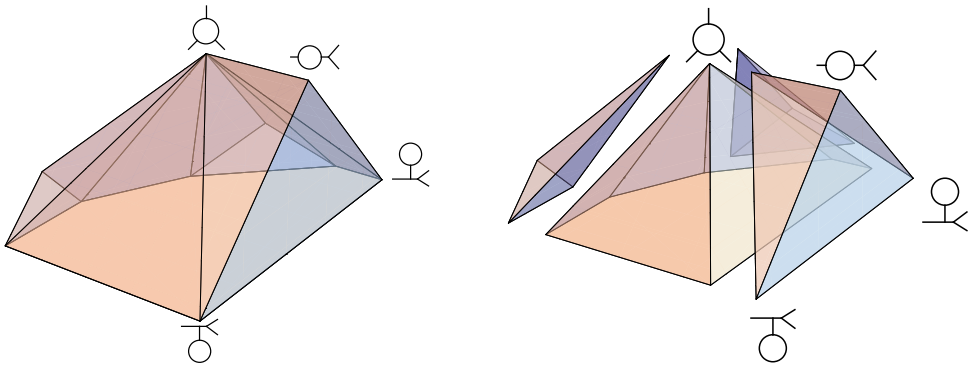

Figure 3.2: $\overline{\mathcal{D}}_3$ triangulated by taking convex hulls of its facets with the ring vertex

us make a few further comments on the formula (3.30). To begin with, note that the usual Feynman-diagrammatic expansion involves roughly speaking $n!$ terms, whilst (3.30) sum over roughly n^2 terms. However, when one tries to solve the recursion relation one ends up in a factorial growth again. Moreover, (3.30) has spurious poles which have to cancel in a very intricate way in order to give the correct results. As studied in [22], these spurious poles become highly non-linear as n increases, a fact reminiscent of BCFW recursion formula for tree level NMHV amplitudes in $\mathcal{N} = 4$ SYM.

3.3.3 Projection and soft limit formula for $\mathcal{A}_{n-3}$

Recall that in Subsection 2.3.3 we described a remarkable property of the tree level Associahedron $\mathcal{A}_n$: there is a natural projection of the n-point Associahedron onto the $(n-1)$-point Associahedron. Furthermore, this projection suggested a beautiful decomposition of $\mathcal{A}_n$ into *prisms*, i.e. polytopes with "bottom" and "top" facets given by (product of) lower point associahedra and "side" facets which are parallel to the direction of the projection.

We have a prism $\mathcal{P}_i$ for each of the facet $X_{2,i} = 0$, with $i = 4, \ldots, n-3$. We can compute its canonical form as described in Appendix A. In our case the vertex Z is given by $Z = (0, 1, 0, \ldots, 0)$, $Y \cdot W_{\mathcal{U}} = X_{2,i}$, $Y \cdot W_{\mathcal{B}} = X_{1,3}$ and $Z \cdot W_{\mathcal{B}} = -Z \cdot W_{\mathcal{U}} = 1$. Putting all together we have

$$\Omega_{\mathcal{P}_i} = \langle Y d^n Y \rangle \left(\frac{1}{X_{1,3}} + \frac{1}{X_{2,i}} \right) \underline{\Omega}_{X_{2,i}} (Y + X_{2,i} Z) \,,$$

the rational function $\underline{\Omega}_{X_{2,i}}$ is the lower data that we have to feed in the recursion, given by a product of lower point amplitudes, and evaluating in it $Y + X_{2,i}Z$ means that we first have to express the original variables used to compute them (associated to the diagonals of the two smaller n-gons) in terms of the new variables $X_{1,3}, \ldots, X_{1,n-1}$ and then substitute $X_{1,3} \to X_{1,3} + X_{2,i} = \sum_{a=3}^{i-1} c_{1,a} + X_{1,i}$. Summing over all prisms we can compute the canonical form of the n point Associahedron,

$$\underline{\Omega}_{\mathcal{A}_{n-3}}(c|X) = \sum_{i=4}^{n} \underline{\Omega}_{\mathcal{A}_L}(c_L|\hat{X}_L) \underline{\Omega}_{\mathcal{A}_R}(c_R|\hat{X}_R) \left(\frac{1}{X_{1,3}} + \frac{1}{X_{2,i}} \right) , \tag{3.31}$$

where the hats denote the deformations implied by the projection: translate the coordinate basis of the lower point associahedra to $X_{1,i}$ with $i = 3, \ldots, n-1$, and then substitute $X_{1,3} \to \sum_{a=3}^{i-1} c_{1,a} + X_{1,i}$.

The recursive formula (3.31) for the rational function of $\mathcal{A}_{n-3}$ descends to a recursive formula for tree level amplitudes, which is particularly simple when written directly in terms of planar variables rather than mesh constants. Let us temporarily restore particles labels in amplitudes by $m_n(1, 2, \ldots, n)$, then the recursion is

$$\boxed{m_n(1, 2, \ldots, n) = \sum_{i=4}^{n} \left(\frac{1}{X_{1,3}} + \frac{1}{X_{2,i}} \right) \hat{m}_{n_L}(2, 3, \ldots, i) \hat{m}_{n_R}(1, 2, i, i+1, \ldots, n)} \tag{3.32}$$

the deformations of (3.31) appear as a deformation of the amplitudes $\hat{m}$ on the RHS of (3.32) which consists in the replacement $X_{2,a} \to X_{2,a} - X_{2,i}$. Let us write this formula explicitly for the amplitude m_5 from $\mathcal{A}_2$. The basic building block is the 4-point amplitude which we write for generic external particles as

$$m_4(A, B, C, D) = \frac{1}{X_{A,C}} + \frac{1}{X_{B,D}} \,. \tag{3.33}$$

As shown in Fig. 2.13 we only have two prism. The first prism is given by the top facet $X_{2,4}$ which is the product of a left point-like Associahedron and a right Associahedron built on the 4-gon with vertices $(1,2,4,5)$. Therefore this prism contributes with the deformed amplitude

$$\hat{m}_4(1,2,4,5) = \frac{1}{X_{1,4}} + \frac{1}{X_{2,5} - X_{2,4}}\,,$$

The second prism is given by the top facet $X_{2,5}$ which is the product of a left Associahedron built on the 4-gon with vertices $(2,3,4,5)$ and of a right point-like Associahedron. For the left factor, we can use again the basic formula (3.33), which after the deformation gives

$$\hat{m}_4(2,3,4,5) = \frac{1}{X_{2,4} - X_{2,5}} + \frac{1}{X_{3,5}}\,. \tag{3.34}$$

Putting all together we get

$$m_5 = \left(\frac{1}{X_{2,4}} + \frac{1}{X_{1,3}}\right)\left(\frac{1}{X_{2,5} - X_{2,4}} + \frac{1}{X_{1,4}}\right) + \left(\frac{1}{X_{2,5}} + \frac{1}{X_{1,3}}\right)\left(\frac{1}{X_{3,5}} + \frac{1}{X_{2,4} - X_{2,5}}\right).$$

Similarly we can write down the result for m_6 from the triangulation of $\mathcal{A}_3$. As shown in Fig.(2.13) there are three prisms, we recycle the results from m_5 and m_4 to obtain

$$\begin{aligned} m_6 = &\left(\frac{1}{X_{2,5}} + \frac{1}{X_{1,3}}\right)\left(\frac{1}{X_{2,6} - X_{2,5}} + \frac{1}{X_{1,5}}\right)\left(\frac{1}{X_{3,5}} + \frac{1}{X_{2,4} - X_{2,5}}\right) + \\ &+ \left(\frac{1}{X_{2,4}} + \frac{1}{X_{1,3}}\right)\left[\left(\frac{1}{X_{2,5} - X_{2,4}} + \frac{1}{X_{1,4}}\right)\left(\frac{1}{X_{2,6} - X_{2,5}} + \frac{1}{X_{1,5}}\right) + \left(\frac{1}{X_{2,6} - X_{2,4}} + \frac{1}{X_{1,4}}\right)\left(\frac{1}{X_{4,6}} + \frac{1}{X_{2,5} - X_{2,6}}\right)\right] \\ &+ \left(\frac{1}{X_{2,6}} + \frac{1}{X_{1,3}}\right)\left[\left(\frac{1}{X_{3,5}} + \frac{1}{X_{2,4} - X_{2,6}}\right)\left(\frac{1}{X_{3,6} - X_{3,5}} + \frac{1}{X_{2,5} - X_{2,6}}\right) + \left(\frac{1}{X_{3,6}} + \frac{1}{X_{2,4} - X_{2,6}}\right)\left(\frac{1}{X_{4,6}} + \frac{1}{X_{3,5} - X_{3,6}}\right)\right] \end{aligned}$$

Note that in general the soft-limit recursive formula requires to sum over $n-3$ terms and is therefore much more efficient than the standard triangulation formula described in the previous subsection. Furthermore, the spurious poles are always linear functions of planar variables and mesh constants. Finally, it is not difficult to solve the recursion and obtain a closed formula for the n-point amplitude which requires to sum over (n-1)-th Catalan numbers of terms cleanly factorized in the various height functions we get when we iterate the projections.

3.3.4 Projection and Forward-limit formula for $\overline{\mathcal{D}}_n$

In this section we describe how to use the triangulation described in Subsection 2.3.7 to derive a recursion formula strongly reminiscent of the for-

mula (1.5), which was inspired by the forward limit properties of scattering integrands. The starting point is the triangulation (2.34), it is again a triangulation built out of prisms and therefore we can derive from it an expression for the canonical form using the results described in Appendix A.

We use (A.5) working in coordinates $Y = (1, X_1, X_1', X_{2,1}, \ldots, X_{n-1,1})$. In our case the projection point is then $Z = (0, 1, -1, 0, \ldots, 0)$. We have a prism for each cut facet $X_i = X_i^0 - X_1' = 0$, where in X_i^0 we gathered all terms independent on X_1' [5], obviously for the first prism the facet is given by $X_1 = 0$ instead. The projected vector appearing in (A.5) is then

$$Y_{\mathcal{U}_i} = \begin{cases} (1, X_1 + X_1' - X_i^0, X_i^0, X_{2,1}, \ldots, X_{n-1,1}), & i \neq 1 \\ (1, 0, X_1 + X_1', X_{2,1}, \ldots, X_{n-1,1}) & i = 1. \end{cases} \tag{3.35}$$

Applying (A.5) for each prism and summing over them we get the canonical form of $\overline{\mathcal{D}}_n$:

$$\Omega_{\overline{\mathcal{D}}_n} = \langle Y d^n Y \rangle \sum_{i=1}^{n} \left(\frac{2}{X_1' - X_1} + \frac{1}{X_i} \right) \underline{\Omega}_{X_i}(Y_{\mathcal{U}_i}). \tag{3.36}$$

At this level (3.36) is a recursive formula where the seeds are given by the canonical form of tree level, $n+2$ points associahedra. Translating back to physical propagators, it descends to the *forward limit* formula for the 1-loop integrand of massive ϕ^3

$$\boxed{m_n^{1-\text{loop}} = \sum_{i=1}^{n} \left(\frac{2}{-m^2} + \frac{1}{\ell_i^2 - m^2} \right) \hat{m}_{n+2}^{\text{tree}}(1, \ldots, i, -, +, \ldots, n),} \tag{3.37}$$

where once again the hat represents the deformation dictated by the projection, which has a very simple interpretation in terms of planar variables. Any propagator $X_{a,b}$ associated to a factorization facet is left invariant by the i-th deformation,

$$X_{a,b} = \cdots - (X_1 + X_1') \xrightarrow{\text{deformation}} \cdots - (X_1 + X_1' - X_i^0 + X_i^0) = X_{a,b},$$

where the dots represent terms independent on X_1, X_1' and thus untouched by the deformation. On the other hand, a ring propagator X_a associated

[5] We caution the reader that unlike in the case of the standard triangulation X_i^0 is not a constant

to a cut facet is deformed to

$$X_a = X_a^0 - X_1' \xrightarrow{\text{deformation}} X_a^0 - X_i^0 = X_a - X_i,$$

finally the tadpole propagator becomes

$$X_0 = X_1' - X_1 \xrightarrow{\text{deformation}} 2X_i^0 - X_1' - X_1 = 2X_i + X_0.$$

Let us also study the massless limit, by switching to the radii basis and sending the tadpole constant $C_0 \to \infty$ (B.8). Both the ring and factorization propagators, after the deformation, are still independent on C_0 and therefore again survive the limit. On the other hand, both the non-deformed and deformed tadpole propagator, when expressed in the radii basis have C_0 as constant and therefore go to infinity in the limit, which therefore kills again all tadpole diagrams. After this limit, and translating back to the massless physical propagators, we obtain from (3.37) a forward limit formula for the integrand of bi-adjoint theory

$$\boxed{m_n^{1-\text{loop}} = \sum_{i=1}^{n} \left(\frac{1}{\ell_i^2}\right) \hat{m}_{n+2}^{\text{tree}}(1,\ldots,i,-,+,\ldots,n)}, \tag{3.38}$$

since tadpoles contributions disappeared from the tree level deformed amplitude $\hat{m}_{n+2}^{\text{tree}}(1,\ldots,i,-,+,\ldots,n)$, the only dependence on the loop momenta ℓ is through the deformed ring propagators which now read

$$X_a - X_i = \left(\ell + \sum_{b=1}^{a-1} k_b\right)^2 - \left(\ell + \sum_{b=1}^{i-1} k_b\right)^2 = \left(\ell_i + \sum_{b=i}^{a-1} k_b\right)^2 - \ell_i^2 \tag{3.39}$$

therefore the amplitude is effectively computed as if we had a pair of massless momenta $\pm\ell_i$ in positions "-" and "+": the mass of ℓ_i is removed by the subtraction in (3.39). Also, note that external cutted bubbles on leg i and $i+1$ are still present and regulated by the massive momenta k_i and k_{i+1}. Finally, if we perform a shift $\ell \to \ell - \left(\sum_{b=1}^{i-1} k_b\right)$ for each of the terms of (3.38), we obtain precisely formula (13) of [23].

Let us see explicitly how these formulae look in the simplest case, $n = 2$. $\overline{\mathcal{D}}_2$ is just a triangle and the two cut facets contributing to the recursion

are 4-point tree level associahedra, we have

$$\hat{m}^{\text{tree}}(1,-,+,2)_4 = \frac{1}{X_2 - X_1} + \frac{1}{2X_1 + X_0}$$
$$\hat{m}^{\text{tree}}(2,-,+,1)_4 = \frac{1}{X_1 - X_2} + \frac{1}{2X_2 + X_0}$$

therefore (3.38) gives

$$m_2^{1-\text{loop}} = \left(\frac{2}{X_0} + \frac{1}{X_1}\right)\left(\frac{1}{X_2 - X_1} + \frac{1}{2X_1 + X_0}\right) + \left(\frac{2}{X_0} + \frac{1}{X_1}\right)\left(\frac{1}{X_1 - X_2} + \frac{1}{2X_2 + X_0}\right),$$

or in terms of usual loop momenta, using $X_i = \ell_i^2 - m^2$ and $X_0 = -m^2$,

$$m_2^{1-\text{loop}} = \left(\frac{2}{-m^2} + \frac{1}{\ell_1^2 - m^2}\right)\frac{\ell_1^2 + \ell_2^2 - 3m^2}{(2\ell_1^2 - 3m^2)(\ell_2^2 - \ell_1^2)} + \left(\frac{2}{-m^2} + \frac{1}{\ell_2^2 - m^2}\right)\frac{\ell_1^2 + \ell_2^2 - 3m^2}{(\ell_1^2 - \ell_2^2)(2\ell_2^2 - 3m^2)}.$$

Finally we turn to the massless limit. From (3.38) we have

$$m_2^{1-\text{loop}} = \frac{1}{X_1}\frac{1}{X_2 - X_1} + \frac{1}{X_2}\frac{1}{X_1 - X_2} = \frac{1}{X_1 X_2} \tag{3.40}$$

then by substituting $X_i \to \ell_i^2$ we get the bi-adjoint integrand $m_2^{1-\text{loop}} = \frac{1}{\ell_1^2 \ell_2^2}$, if we also perform a shift in the loop momentum $\ell^\mu \to \ell^\mu - k_1^\mu$ in the second term of (3.40) we get the same result in the representation given in [23]

$$m_2^{1-\text{loop}} = \frac{1}{\ell^2}\left(\frac{1}{\ell^2 - (\ell - k_1^2)} + \frac{1}{\ell^2 - (\ell - k_2^2)}\right).$$

In the same way it is also possible to prove a partial fraction identity that represent the n point ring diagram as a sum of n tree level ladder diagrams, of which the above is the simplest example, [23]. Finally, we can combine the forward limit formula with the soft-limit formula to compute

a three point 1-loop integrand,

$$
\begin{aligned}
m_3^{1-\text{loop}} &= \left(\frac{1}{X_1}+\frac{2}{X_0}\right)\left[\left(\frac{1}{X_2-X_1}+\frac{1}{X_0+2X_1}\right)\left(\frac{1}{X_{1,2}}+\frac{1}{X_3-X_2}\right)+\left(\frac{1}{X_3-X_1}+\frac{1}{X_0+2X_1}\right)\left(\frac{1}{X_{3,1}}+\frac{1}{X_2-X_3}\right)\right] \\
&+\left(\frac{1}{X_2}+\frac{2}{X_0}\right)\left[\left(\frac{1}{X_3-X_2}+\frac{1}{-X_{2,3}+X_0+2X_2}\right)\left(\frac{1}{X_{2,3}}+\frac{1}{X_1-X_2}\right)+\left(\frac{1}{X_0+2X_2}+\frac{1}{X_1-X_2}\right)\left(\frac{1}{X_{2,3}-X_0-2X_2}+\frac{1}{X_{1,2}}\right)\right] \\
&+\left(\frac{1}{X_3}+\frac{2}{X_0}\right)\left[\left(\frac{1}{X_{2,3}-X_2+X_3}+\frac{1}{X_1-X_3}\right)\left(\frac{1}{X_{3,1}}+\frac{1}{X_2-X_3}\right)+\left(\frac{1}{-X_{2,3}+X_2-X_3}+\frac{1}{X_0+2X_3}\right)\left(\frac{1}{X_{2,3}}+\frac{1}{X_{3,1}}\right)\right]
\end{aligned}
$$

Conclusions

Summary

The central topic of this thesis was the pursuit of positive geometries of interest for the physics of scattering amplitudes. Our guiding principle has been that the boundaries of such geometries should solve the famous equation (1), which encodes how Locality and Unitarity manifest in the singularity structure of amplitudes and integrands. In other words, any family of geometrical objects $\mathcal{A}_n$ which factorizes into itself upon taking boundaries as in

$$\partial\mathcal{A}_n = \mathcal{A}_{n_L} \times \mathcal{A}_{n_R}, \tag{3.41}$$

is expected to be of relevance for tree level amplitudes. Starting at 1-loop, in order to capture cuts of integrands, in addition to factorization meaningful geometries should also allow for boundaries given by the geometries found at lower loop level, as in

$$\partial\mathcal{A}_n^{1-\text{loop}} = \mathcal{A}_{n+2}^{\text{tree}}.$$

The moduli space of Riemann surfaces, $\overline{\mathcal{M}}_{g,n}$, represents a natural starting point for this exploration since, as it has been known for long time, its boundary structure reproduces both factorization and cuts. In Chapter 1 we described important examples of positive geometries which live in various moduli spaces, some of which were already known, some of which were not. We proposed hyperbolic geometry as the natural language to study the connection of moduli spaces with positive geometries, since it makes manifest the boundary structure of $\overline{\mathcal{M}}_{g,n}$. Accordingly, we followed the two main approaches - pants decompositions and triangula-

tion - and studied the simplest examples of surfaces. Using pants decompositions, the first new interesting geometry encountered is the Halohedron which is of evident importance for 1-loop integrands. The triangulations approach is deeply connected with cluster algebras, and leads to the study of finite type cluster polytopes: $\mathcal{A}, \mathcal{B}, \mathcal{C}, \mathcal{D}$. The inherent simplicity of cluster mutations, much easier than the corresponding change of coordinates in the pants decomposition approach, allows to make manifest the boundary structure of the simplest moduli spaces by means of certain equations, which were first pointed out in the context of positive geometries in [8] [6].

The study of moduli spaces puts into the spotlight two new positive geometries relevant for 1-loop integrands, the Halohedron and $\mathcal{D}_n$. However to make connection with amplitudes one either needs a map from kinematical space to the moduli space, such as the scattering equations, or a realisation of these geometries directly in kinematical space. In Chapter 2 we focused on the latter. Firstly, we illustrated a convex realisation of the Halohedron in an *abstract* kinematical space, following [29]. Secondly we discussed the ABHY realization of all cluster polytopes. In particular, we described a surprising connection with the wave equation in 1+1 dimensions. On one hand, this connection makes completely manifest the origin of the factorization of the boundaries. On the other hand, it guided us to the discovery of certain projection properties of ABHY polytopes which can be used to triangulate them efficiently.

The results of the previous chapters found their ultimate justification in Chapter 3, where amplitudes and integrands are finally computed. The first interesting result is that, although at 1-loop integrands develop higher order poles, one does not have to leave the world of positive geometries and logarithmic canonical forms to treat them. Indeed, the positive geometries we studied suggest a natural way to deform these double poles into pair of simple poles. One can then compute canonical forms in the abstract space where the geometries are realised, and then translate back to ordinary kinematical space, restoring double poles and momentum conservation in the integrands. We then provided a few examples of new formulae, up to 1-loop integrand of bi-adjoint theory and of massive ϕ^3 theory. These include a remarkably efficient formula for tree level amplitudes, and forward-limit formulae for both integrands. Also, a by-product of our construction is a regularised massless limit to connect massive ϕ^3 theory and bi-adjoint theory.

[6] I am particularly grateful, for sharing their hindsights on this idea with me, to Arkani-Hamed, Song He and his students.

Future Directions

The present thesis opens a number of interesting questions, which hopefully will lead into new hindsights on scattering amplitudes in the near future.

All loop ϕ^3. The first and most pressing question is to complete the amplituhedral formulation for the S-matrix in bi-adjoint, or massive ϕ^3, at all loop orders. As we elaborated in Chapter 1, a natural starting point are either the moduli space of higher genera surfaces in the pants decomposition approach, or of the disk with several interior punctures in the triangulation-based approach. As we briefly mentioned, both strategies face immediate obstacles: in the first case moduli spaces cease to be polytopes, in the second case we encounter the cluster algebra infinity. At the origin of both problems seems to be the fact that these surfaces begin to have a non-trivial mapping class group, whose action on pants and triangulations has to be modded out. Interestingly, in terms of dual variables this action translates into the permutation of the loop momenta, which is physically meaningless. Could it be that, in the case of triangulations, might be enough to tame the infinity and produce a well defined polytopal positive geometry at higher loop?

While we do not have yet an answer to this question, in an on-going collaboration with Arkani-Hamed and Hadleigh Frost we did an encouraging step forward at the level of the scattering form. Using the infinite cluster algebra associated to disks with several interior punctures, it is possible to define a projectively invariant scattering form following the usual sign rule. Obviously, this form is a rather formal object since it is given by the sum of infinitely many dlog terms. However, upon identifying those variables which are sent into each other by the action of the mapping class group, we are left with a finite, projectively invariant, scattering form. This is a very promising result, especially in light of the discussion of 2.1.2.

Loop Integration. Notwithstanding the fascinating connections discovered between integrands and positive geometries, first in $\mathcal{N} = 4\,\mathrm{SYM}$ and now in ϕ^3, similar results at the level of the integrated amplitude are still missing. It seems suspicious that such a rich interplay between geometry and physics may exists at the integrand level without leaving an imprint of itself on the final answer. In order to address this question, a first interesting observation is the analogy between volume formulae for the canonical form of polytopes and the familiar Feynman trick. Namely we can write the rational function of a polytope $\mathcal{P}$ as an integral over its

dual

$$\overline{\Omega}(Y) = \int_{\mathcal{P}*} \frac{\langle W d^d W \rangle}{(Y \cdot W)^{d+1}},$$

which can be proven by first reducing by triangulations to the case of a simplex, in which case the above integral can be recognized as the usual Feynman trick. Therefore, using the results of this thesis we can use $\overline{\mathcal{D}}^*$ as a *Feynman parameters polytope* and perhaps learn something new about the integrated amplitude.

Beyond ϕ^3 By now there is more and more evidence that the S-matrix of many other theories admits a formulation in terms of positive geometries. A large class of polytopes called Stokes polytopes seems to be connected with amplitudes in planar ϕ^4 [36], and an even larger class of polytopes known as accordiohedra with ϕ^p [37] and even with general polynomial interactions, such as $\lambda_3\phi^3 + \lambda_4\phi^4$ [38]. Finally, also non-planar amplitudes seem tractable [21].

Another immediate direction of investigation is offered by a class of polytopes known as graph cubeahedra and graph associahedra [29], [30] which further generalize the Halohedron and the Associahedron. The boundary structure of these polytopes satisfy interesting factorization and cut properties, but so far it is not clear whether they can be understood as factorizations and cuts of integrands. Amusingly, the only real obstacle in this investigation is purely combinatorial: it is unclear whether it is possible to translate the language of *tubings* used to defined these polytopes in terms of familiar Feynman diagrams.

Another, somewhat indirect, clue that many other theories should admit a positive geometry formulation is the vast plethora of theories which can be treated within the CHY formalism. At the heart of this formalism are the scattering equations, which were given a new interpretation in [8] as a map between the kinematical Associahedron and the moduli space Associahedron In particular, the CHY formula for bi-adjoint theory was understood as a pushforward of the corresponding canonical forms. Is it possible to extend this picture to other theories, and is it possible to find "scattering equations" between the moduli space positive geometries described here and their kinematical counterparts? For advances in this direction, see also [19], [3] and [20].

New results for ϕ^3. Somewhat more straightforward questions are still open in the domain of ϕ^3 and its positive geometries. In Chapter 3 we focused on representation of amplitudes which can be obtained upon triangulation of the corresponding polytopes. However, using the volume formula mentioned earlier one can obtain entirely different formulae by

triangulating the duals of these polytopes. This produce *local* representation, i.e. without spurious poles, since one does not introduce spurious boundaries in the interior of the direct polytopes. These representations are especially interesting at loop level, where spurious poles present a problem for the integration over loop momenta. Finally, when considering 1-loop bi-adjoint theory we only focused on its diagonal part, i.e. assuming the same ordering for both color factor. It would be desirable to complete the picture including different orderings, also in connection with [12].

Appendices

APPENDIX A

Projections, Triangulations and canonical form of a Prism

We review here some facts about projective geometry and canonical forms of polytopes.

One of the most natural geometrical construction in projective geometry is the projection to a plane through a point. Let Z be a point in $\mathbb{P}$ and H an $n-1$ dimensional hyperplane given by $Y \cdot W = 0$. Given any point Y, consider the unique line L that passes through Y and Z and call $\bar{Y}$ its intersection with H: this point is the projection of Y to H through Z. We can think of Y as giving a coordinate on H, at the cost of introducing a $GL(1)$ redundancy, since many points Y belong to the same line L. This $GL(1)$ is the "little group" of the line. Concretely we can write

$$\overline{Y} = Y - \frac{Y \cdot W}{Z \cdot W} Z, \tag{A.1}$$

note that the right hand side of (A.1) indeed has a new $GL(1)$ redundancy: $Y \to Y + \alpha Z$.

Suppose that $\overline{A}_i \in H$ are the projections of certain points A_i, then we have the basic formula:

$$\langle \overline{A}_1 \dots \overline{A}_{n-1} \rangle = \frac{\langle Z A_1 \dots A_{n-1} \rangle}{Y \cdot W} = \frac{\langle Z A_1 \dots A_{n-1} \rangle}{\langle Z Z_1 \dots Z_{n-1} \rangle}, \tag{A.2}$$

where $Z_1, \dots Z_{n-1}$ is any generic set of points in H. This formula can be proven by first picking a chart where $Y \cdot W = Y_0$ and then exploiting the variance of determinants and covariance of W.

Projections play a central role in the computation of the canonical forms of polytopes. The basic fact is that if a polytope $\mathcal{P}$ lives in H and its canonical form is given by

$$\Omega_{\mathcal{P}} = \langle \overline{Y} d^{n-1} \overline{Y} \rangle \underline{\Omega}_{\mathcal{P}} \left(\overline{Y} \right),$$

then the canonical form of

$$\hat{\mathcal{P}} = \mathrm{Conv}(Z, \mathcal{P})$$

is given by

$$\Omega_{\hat{\mathcal{P}}} = \langle Y d^n Y \rangle \frac{Z \cdot W}{Y \cdot W} \underline{\Omega}_{\mathcal{P}} \left(Y - \frac{Y \cdot W}{Z \cdot W} Z \right), \tag{A.3}$$

this fact is easily proven for the case of a simplex using (A.2) and then generalized by triangulation for any polytope $\mathcal{P}$. In the case of physical applications, the polytope $\mathcal{P}$ is associated to some lower loop/point computation and the convex hull $\hat{\mathcal{P}}$ is part of a triangulation of some higher level computation. Formula (A.3) then allows to set up recursive relations, since the only non trivial part is given by $\Omega_{\mathcal{P}}$ replacing $\Omega_(\mathcal{P})$ which has supposedly been already computed.

In this paper we encountered a remarkable kind of triangulation which involved prisms, i.e. a polytope $\mathcal{P}$ characterized by an $\mathcal{U}$pper facet, a $\mathcal{B}$ottom facet and a collection of $\mathcal{S}$ide facets that meet at a common vertex Z. Such a prism is easily triangulated by taking the convex hull $\hat{\mathcal{B}} = \mathrm{Conv}(Z, \mathcal{B})$ and removing the convex hull $\hat{\mathcal{U}} = \mathrm{Conv}(Z, \mathcal{U})$. We apply (A.3),

$$\Omega_{\hat{X}} = \langle Y d^n Y \rangle \frac{Z \cdot W_X}{Y \cdot W_X} \underline{\Omega}_X \left(Y - \frac{Y \cdot W_X}{Z \cdot W_X} Z \right), \tag{A.4}$$

where $X = \mathcal{U}, \mathcal{B}$. The projection through Z also gives a diffeomorphism π of positive geometries between the two polytopes $\mathcal{U}$ and $\mathcal{B}$, therefore it relates their canonical forms by pullback [1]:

$$\pi^*(\Omega_{\mathcal{B}}) = \Omega_{\mathcal{U}}.$$

We can give an explicit proof of this fact in the case where both $\mathcal{U}$ and $\mathcal{B}$ are simplices with vertices $Z_{\mathcal{B}}$ and $Z_{\mathcal{U}}$; the general case follows again by triangulation. The canonical form of the bottom facet in this case is given by

$$\frac{\langle Y_B d^{n-1} Y_B \rangle \langle Z_{\mathcal{B}_1} \dots Z_{\mathcal{B}_n} \rangle^n}{\prod_{i=1}^{n} (-1)^i \langle Y_{\mathcal{B}} Z_{\mathcal{B}_1} \dots \hat{Z}_{\mathcal{B}_i} \dots Z_{\mathcal{B}_n} \rangle},$$

[1] One usually push-forward rather than pull-back canonical forms of positive geometries, but since π is linear the two are equivalent

we write

$$Y_{\mathcal{B}} = Y_{\mathcal{U}} - \frac{Y_{\mathcal{U}} \cdot W_{\mathcal{B}}}{Z \cdot W_{\mathcal{B}}} Z,$$

and repeatedly use (A.2):

$$\langle Y_{\mathcal{B}} d^{n-1} Y_{\mathcal{B}} \rangle = \frac{\langle Z Y_{\mathcal{B}} d^{n-1} Y_{\mathcal{B}} \rangle}{Z \cdot W_{\mathcal{B}}} = \frac{\langle Z Y_{\mathcal{U}} d^{n-1} Y_{\mathcal{U}} \rangle}{Z \cdot W_{\mathcal{B}}} = \frac{Z \cdot W_{\mathcal{U}}}{Z \cdot W_{\mathcal{B}}} \langle Y_{\mathcal{U}} d^{n-1} Y_{\mathcal{U}} \rangle,$$

we get a factor $\frac{Z \cdot W_{\mathcal{U}}}{Z \cdot W_{\mathcal{B}}}$ in converting the remaining determinants but they cancel overall, so we are left with the canonical form for the upper simplex. Therefore the canonical form of the prism is given by

$$\Omega_{\mathcal{P}} = \langle Y d^n Y \rangle \left(\frac{Z \cdot W_{\mathcal{B}}}{Y \cdot W_{\mathcal{B}}} - \frac{Z \cdot W_{\mathcal{U}}}{Y \cdot W_{\mathcal{U}}} \right) \underline{\Omega}_{\mathcal{U}} \left(Y - \frac{Y \cdot W_{\mathcal{U}}}{Z \cdot W_{\mathcal{U}}} Z \right). \tag{A.5}$$

APPENDIX B

Solution of the mesh relations

In this appendix we describe the solutions of the mesh relations in a closed form valid for arbitrary n.

B.1 Type $\mathcal{A}$

For the right triangle region, which is equivalent to the standard ABHY realisation of $\mathcal{A}_{n-3}$, the mesh diagram of Fig. (2.5) makes immediate to solve every variable $X_{i,j}$ in terms of the basis given by the variables $X_{1,i}$, $i = 3, \ldots, n-1$. Given any variable $X_{i,j}$, construct the causal diamond with variables $X_{1,i}, X_{1,j}, Xi, j$ and $X_{j-1,j}$ at its left, bottom, right and top corners. All the mesh relations in the small causal diamonds contained in the larger diamond sum up telescopically to

$$X_{1,i+1} + X_{i,j} - X_{1,j} = C_{i,j},$$

where $C_{i,j}$ is the total charge of this region. We can therefore easily express $X_{i,j}$ in the basis, and explicitly we get

$$X_{i,j} = \sum_{\substack{a=1 \\ b=i+1}}^{\substack{a=i-1 \\ b=j-1}} c_{a,b} + X_{1,j} - X_{1,i+1}. \tag{B.1}$$

It is straightforward to generalize this construction to other domains, such as the arrow-tail region.

B.2 Type $\mathcal{D}$

The same strategy used at tree level extends to type $\mathcal{D}$ and $\overline{\mathcal{D}}$. The natural basis to use is the "tadpole basis" given by variables $X_1, X_1', X_{1,2}, \ldots, X_{1,n-1}$.

We also recall that in the main text we introduced a new set of variables,

$$X_{\pm,i} := X'_i \pm X_i, \tag{B.1}$$

in terms of which the original variables are given by

$$X_i = \frac{1}{2}\left(X_{+,i} + X_{-,i}\right), \tag{B.2}$$

$$X'_i = \frac{1}{2}\left(X_{+,i} + X_{-,i}\right). \tag{B.3}$$

The advantage of these variables is that they satisfy a set of ABHY conditions similar to the tree level one. Indeed, we have

$$X_{+,i} + X_{+,i+1} - 2X_{i,i+1} = 2c_i, \tag{B.4}$$

$$\tag{B.5}$$

so if we rescale all the remaining variables, and the mesh constants, by a factor of two we can arrange all the variables in a causal diamond. Variables at the vertices of smaller diamonds satisfy ABHY relations with the usual signs see Fig. B.1. Note that for diamonds with a vertex on the

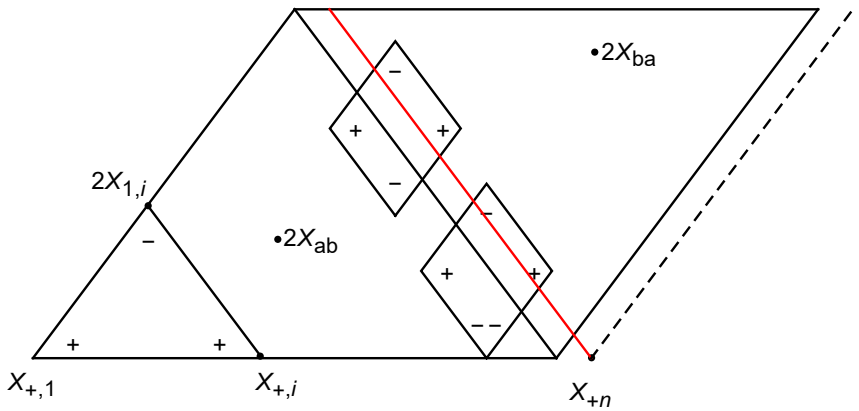

Figure B.1: Some examples of diamonds, with the signs for the relevant ABHY condition indicated. On the leftmost line live the variables $X_{+,1}, X_{1,2}, \ldots$, on the bottom one the variables $X_{+,i}$, on the red line the variables $X_{j,n}$ and in the dashed line the variables $X_{+,n}, X_{n,1}, \ldots$. The picture is not in scale.

lower line, we need a factor of "-2" in the corresponding ABHY relation, as indicated by the double minus in the figure. Also note that the variables $X_{-,i}$ actually do not depend on i, because by taking the difference

of the original ABHY conditions we get

$$X_{-,i} = X'_i - X_i = X'_{i+1} - X_{i+1} = X_{-,i+1},$$

we can therefore forget the index "i" and call this quantity simply X_-: as described in Section 2.3.6 it is the face variable of the *tadpole facet*. Now we can devise for any variable X a system of light rays that make manifest its solution in terms of the tadpole basis. The three possible situations are described in Fig. B.2 and Fig. B.3, from which it is clear that we get

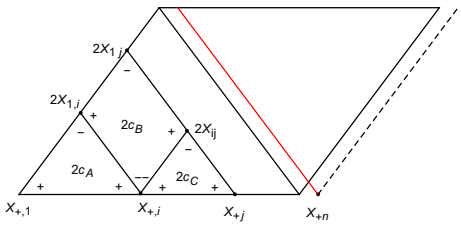

Figure B.2: System of light rays for variables $X_{+,i}$ and $X_{i,j}$ below the red line

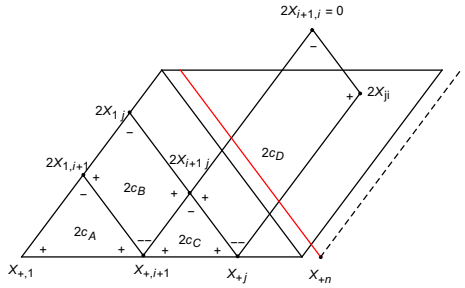

Figure B.3: System of light rays for variables on and above the red line

(B.6)

$$\begin{aligned}
X_{+,j} = 2c_A + 2X_{1,j} - X_{+,1} &\Leftrightarrow X_i = c_A + X_{1,j} - X'_1, \\
2X_{i,j} = 4c_A + 2c_B + 2X_{1,j} + 2X_{1,i} - 2X_{+,1} &\Leftrightarrow X_{i,j} = 2c_A + c_B + X_{1,i} + X_{1,j} - X_1 - X'_1 \\
2X_{j,i} = 2c_D + 2c_C + X_{+,j} - X_{+,i+1} &\Leftrightarrow X_{j,i} = c_D + c_B + 2c_C + X_{1,j} - X_{1,i+1},
\end{aligned}$$

and (B.6) together with $X'_i - X_i = X_- = X'_1 - X_1$ is sufficient to solve for all the variables of $\mathcal{D}_n$.

Let us now make a few comments on $\overline{\mathcal{D}}_n$. From (B.6) we see that each face variable, including the tadpole variable $X_- = X'_1 - X_1$, is expressed as a linear function of the tadpole basis elements with a specific combination of mesh constants, *uniquely associated to that facet*. This guarantees that one can perform the shifts described in Section 3.3.1 which convert face variables to physical propagators. One first rewrites X'_1 as $X_- + X_1$, then rearrange (B.6) so that the constants are on the right hand side and the face variables on the left hand side. Because the combinations of mesh constants are unique to each facet, we can solve these equations for the mesh constants in terms of *all* the face variables. Since the latter have an immediate meaning as physical propagators, this give meaning to the mesh constants as well.

Finally we turn to the *massless limit*, which allows to obtain the 1-loop integrand for the bi-adjoint scalar theory. It is convenient to switch to the basis given by the planar variables X_i, for $i = 1, \dots, n$. Dually, these variables correspond to the propagators of the ring diagram, therefore we will refer to this as the *ring basis*. To express the planar variables in terms of the ring basis we first find the expression for the tadpole basis elements and then plug it into (B.6). We can use the first of (B.6) with $n = i$ to find

$$X_1' = C_0 - X_n, \tag{B.7}$$

where C_0 is the total charge on the left of the red line of figures (B.2) and (B.3). Note that this is also the constant of the tadpole variable in the ring basis:

$$X_0 = X_1' - X_1 = C_0 - X_1 - X_n. \tag{B.8}$$

Sticking to the notation of such figures, if we plug (B.7) in the remaining equations of (B.6) we get

$$\left.\begin{array}{ll} X_{1,i} & = C_0 - C_A + X_i - X_n \\ X_{1,j} & = C_0 - C_A - C_B - C_C + X_j - X_n \end{array}\right\} \Rightarrow X_{i,j} = (C_0 - C_C) - X_n - X_1 + X_i + X_j, \tag{B.9}$$

and

$$X_{j,i} = C_C + C_D + X_j - X_{i+1}. \tag{B.10}$$

From the rational function of $\overline{\mathcal{D}}_n$ expressed in the ring basis, one can obtain the 1-loop integrand for the bi-adjoint theory by first sending $C_0 \to \infty$, which has the only effect of killing the contribution of the tadpole vertices. Then one translates to the *massless* propagators by replacing $X_i \to \ell_i^2$, $X_{i,j}, X_{j,i} \to \left(\sum_{a=i}^{j-1} k_a\right)^2$ and $X_{i,i+1} \to k_i^2$, and inverting (B.9),(B.10) to read of the physical meaning of the surviving face constants, in the same way as done before for the full massive integrand.

Note that while the original ABHY constants were subjected only to the positivity constraint, the face constants in the ring basis satisfy non trivial equalities. Let us denote $C_{i,j}$ the constant for the variable $X_{i,j}$, an obvious consequence of (B.9),(B.10) is that $C_{i,j} > 0$ for any face variable (including C_0). In addition, we also see that

$$C_0 < C_{i+1,j} + C_{j,i},$$

therefore it is impossible to send $C_0 \to \infty$ without either breaking the positivity requirement for some C or sending it to infinity as well. This means that, although the limiting procedure at the level of rational function is well defined and reproduces the massless integrand after the translation to physical propagators, the final result can no longer be interpreted as the canonical function of a polytope, since the positivity requirement has been violated. A similar phenomenon happens in the case of the Halohedron when eliminating external bubbles and tadpoles.

APPENDIX C

Graph Associahedra and Cubeahedra

In this Appendix we describe two large families of polytopes called *Graph Associahedra* and *Graph Cubeahedra* and their realisations as convex polytopes. These polytopes were introduced in [29], where their convex realisations were also provided. We report this construction here for the sake of self-containedness and to provide explicit details which are useful for the computation of amplitudes.

C.1 Graph Associahedra

Graph Associahedra are a family of polytopes labelled by connected graphs, they include the classical Associahedron $\mathcal{A}$ and the Cyclohedron $\mathcal{B}$ which correspond to the graph being a path or a cycle respectively. More generally, to each connected graph $\mathcal{G}$ we can associate a graph Associahedron $\mathcal{A}_\mathcal{G}$. At the combinatorical level the Associahedron $\mathcal{A}_\mathcal{G}$ is the poset of tubings of $\mathcal{G}$, which we now define. A *tube* on $\mathcal{G}$ is a proper connected subset $\mathcal{T}$ of $\mathcal{G}$ which we represent as a yellow tube around some nodes of $\mathcal{G}$ as in Fig. C.5. We say that two tubes $\mathcal{T}$ and $\mathcal{T}'$ are adjacent if they are disjoint and their union is another tube on $\mathcal{G}$. We define two tubes to be compatible if either 1) one is a subset of the other or 2) they are disjoint and not adjacent. Finally, we define a *tubing* on $\mathcal{G}$ to be a (possibly empty) collection of pairwise compatible tubes and a partial ordering on the set of tubings given by the usual set-theoretical inclusion $\subset$.

When $\mathcal{G}$ is a path with m nodes the corresponding Associahedron $\mathcal{A}_\mathcal{G}$ is just the classical Associahedron $\mathcal{A}_{m-1}$, instead if $\mathcal{G}$ is a cycle with m nodes one obtains the cyclohedron $\mathcal{B}_{m-1}$, in Fig. C.1 are shown two-dimensional examples. The proof is entirely combinatorical and it boils down to translating the language of tubings to that of triangulations or pants decomposition, it can be found in [29].

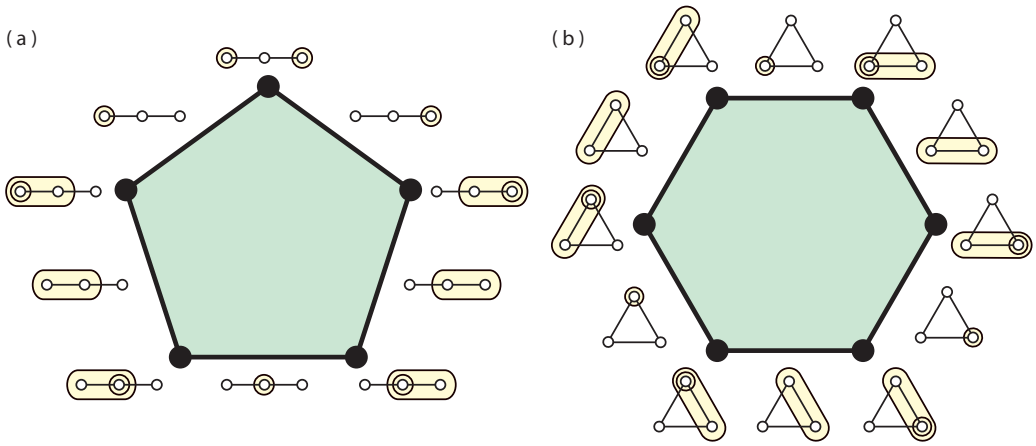

Figure C.1: The Associahedron $\mathcal{A}_2$ (a) and Cyclohedron $\mathcal{B}_2$ (b) as particular instances of graph associahedra $\mathcal{A}_\mathcal{G}$. The picture is a courtesy of Prof. Satyan Devadoss and it is taken from [29].

Graph associahedra constitute a family of polytopes which are closed upon taking boundaries, i.e. every face [1] of a graph associahedra is combinatorially equivalent to a product of graph associahedra. This factorization is conveniently described in terms of the underlying graph: suppose that $\mathcal{T}$ is a tube on $\mathcal{G}$, and let $\mathcal{G}'_a$ for $a = 1, \dots N$ denote the connected components of $\mathcal{G}' = \mathcal{G} \setminus \mathcal{T}$, i.e. of the subgraph of $\mathcal{G}$ obtained by removing all the nodes contained in $\mathcal{T}$ together with the edges incident on them. Then the face of $\mathcal{A}_\mathcal{G}$ corresponding to $\mathcal{T}$ is given by

$$\partial_\mathcal{T} \mathcal{A}_\mathcal{G} = \mathcal{A}_\mathcal{T} \times \mathcal{A}_{\mathcal{G}'_1} \cdots \times \mathcal{A}_{\mathcal{G}'_N}. \tag{C.1}$$

The mechanism behind this factorization is straightforward: all tubes contained in $\mathcal{T}$ are compatible with it and thus they are responsible for the first factor in the RHS of (C.1). If a tube contained in some component $\mathcal{G}'_a$ is adjacent to $\mathcal{T}$ then we can make it compatible with $\mathcal{T}$ by taking its union with $\mathcal{T}$, so the tubes of $\mathcal{G}'_a$ give rise to the corresponding factor in (C.1).

Next we turn to the convex realisation of a graph associahedra $\mathcal{A}_\mathcal{G}$ for an arbitrary graph $\mathcal{G}$ with m nodes. The realisation is based on the truncations of a simplex and was first presented in [30]. The truncation can be defined in many ways, we present here a particularly simple one. In a projective space is $\mathbb{P}^{m-1}$ we consider an $(m-1)$-simplex $\Delta_\mathcal{G}$ defined by the positivity of m functions $X_{(i)}$ with $i = 1, \dots, m$. Note that, in order

[1] We slightly abuse notation in referring to "boundaries" and "faces" since at this level the discussion is purely combinatorical, hopefully this will not generate confusion

for these functions to define a simplex, they have to satisfy

$$\sum_{i\in\mathcal{G}} X_{(i)} = \epsilon_{\mathcal{G}} > 0, \tag{C.2}$$

where $\epsilon_{\mathcal{G}}$ is an arbitrary non-vanishing constant. Implicitly, in (C.2) we thought of the facets $X_{(i)} = 0$ of $\Delta_{\mathcal{G}}$ as labelled by tubes (i) around the i-th node of the graph. We can similarly label all the lower dimensional faces of the $\Delta_{\mathcal{G}}$ by the subset $\mathcal{S}$ of nodes whose associated facets $X_{(i)}$ intersect there. We stress that $\mathcal{S}$ may or may not be a tube depending on the connectivity of $\mathcal{G}$. The simplex $\Delta_{\mathcal{G}}$ is then truncated by shaving off those faces which are labelled by tubes, in order of increasing dimensions. Concretely, if a face of $\Delta_{\mathcal{G}}$ is labelled by a tube $\mathcal{T}$ we intersect the original simplex with the half-space defined by

$$X_{\mathcal{T}} = \sum_{a\in\mathcal{T}} X_{(a)} - \epsilon_{\mathcal{T}} \geq 0, \tag{C.3}$$

where $\epsilon_{\mathcal{T}}$ is a positive constant. We claim that the polytope

$$\mathcal{A}_{\mathcal{G}} = \{Y \in \mathbb{P}^{m-1} | X_{\mathcal{T}}(Y) \geq 0, \quad \forall \mathcal{T} \in \text{tubes of } \mathcal{G}\}$$

is the graph Associahedron of $\mathcal{G}$, provided that the constants ϵ appearing in (C.3) satisfy the conditions

(i) $\epsilon_{\mathcal{T}} < \epsilon_{\mathcal{G}}$ for all $\mathcal{T}$.

(ii) $\epsilon_{\mathcal{T}} + \epsilon_{\mathcal{T}'} < \epsilon_{\mathcal{T}\cup\mathcal{T}'} + \epsilon_{\mathcal{T}\cap\mathcal{T}'}$ for all $\mathcal{T}, \mathcal{T}'$ such that $\mathcal{T}\cup\mathcal{T}'$ is a tube.

Before proving this claim let us point out that, indeed, intersecting $\Delta_{\mathcal{G}}$ with the half-space defined by (C.3) has the effect of truncating the face associated to $\mathcal{T}$, since $X_{\mathcal{T}}$ is *negative* there, and creating a new facet $X_{\mathcal{T}} = 0$. The constants ϵ modulate the depths of all these cuts and they have to satisfy i) and ii) to guarantee that none is too deep and they are taken in order of increasing dimension of the faces, as shown in Fig. C.2 We now prove the correctness of the convex realisation of $\mathcal{A}_{\mathcal{G}}$, in order to do so we will first prove that non compatible tubes are associated to non intersecting facets and then show that each facet of $\mathcal{A}_{\mathcal{G}}$ factorizes accordingly to (C.1). Let $\mathcal{T}$ and $\mathcal{T}'$ be non compatible tubes, i.e. either adjacent or such that $\mathcal{T}\cap\mathcal{T}' \neq 0$. In both cases, $\mathcal{T}\cup\mathcal{T}'$ is a tube and so it is associated to a face variable $X_{\mathcal{T}\cup\mathcal{T}'}$, on the other hand we define $X_{\mathcal{T}\cap\mathcal{T}'} = 0$ if they are adjacent. Recalling (C.3) we have

$$X_{\mathcal{T}\cup\mathcal{T}'} + X_{\mathcal{T}\cap\mathcal{T}'} - X_{\mathcal{T}} - X_{\mathcal{T}'} < \epsilon_{\mathcal{T}} + \epsilon_{\mathcal{T}'} - \epsilon_{\mathcal{T}\cup\mathcal{T}'} - \epsilon_{\mathcal{T}\cap\mathcal{T}'} < 0, \tag{C.4}$$

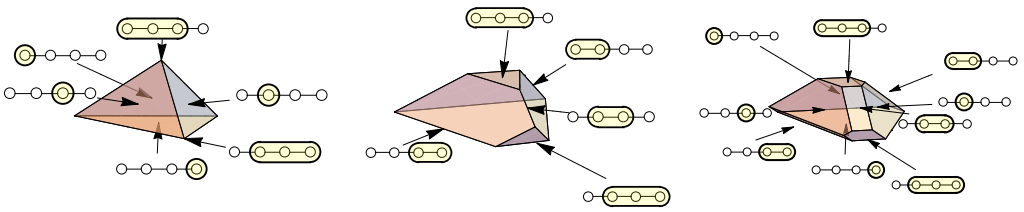

Figure C.2: Sequence of truncations producing $\mathcal{A}_3$. From the leftmost to the central figure two vertices are truncated, from the central to the rightmost three edges.

from which it is clear that $X_{\mathcal{T}}$ and $X_{\mathcal{T}'}$ cannot be simultaneously zero without breaking the positivity of either $X_{\mathcal{T}\cup\mathcal{T}'}$ or $X_{\mathcal{T}\cap\mathcal{T}'}$, in other words the corresponding facets do not intersect. Next, consider a tube $\mathcal{T}$ and for simplicity assume that $\mathcal{G}' = \mathcal{G} \setminus \mathcal{T}$ is connected (the general case is a straightforward generalization), then we wish to prove that the facet $X_{\mathcal{T}} = 0$ factorizes into $\mathcal{A}_{\mathcal{T}} \times \mathcal{A}_{\mathcal{G}'}$. On this facet, the variables associated to the nodes of $\mathcal{T}$ define a smaller simplex $\Delta_{\mathcal{T}}$, since

$$X_{\mathcal{T}} = 0 \Rightarrow \sum_{i\in\mathcal{T}} X_{(i)} = \epsilon_{\mathcal{T}}, \tag{C.5}$$

which should be compared with the condition (C.2), note that the latter also implies that

$$\sum_{i\in\mathcal{G}'} X_{(i)} = \epsilon_{\mathcal{G}} - \epsilon_{\mathcal{T}} > 0. \tag{C.6}$$

Recall that the factor $\mathcal{A}_{\mathcal{G}'}$ is due to tubes on $\mathcal{G}'$ which, if they are adjacent to $\mathcal{T}$ as tubes on $\mathcal{G}$, have to be united to $\mathcal{T}$. Accordingly, we associate to a tube $\mathcal{T}'$ in $\mathcal{G}'$ either the function $\mathbf{X}_{\mathcal{T}'} = X_{\mathcal{T}'}$ or the function $\mathbf{X}_{\mathcal{T}'} = X_{\mathcal{T}\cup\mathcal{T}'}$. Keeping in mind this fact we see that the variables associated to the nodes of $\mathcal{G}'$ define a simplex $\Delta_{\mathcal{G}'}$, too. We have

$$\sum_{a\in\mathcal{G}'} \mathbf{X}_{(a)} = \epsilon_G - \epsilon_{\mathcal{T}} + \sum_{b \text{ adjacent to } \mathcal{T}} \epsilon_{\mathcal{T}\cup(b)} - \epsilon_{\mathcal{T}} > 0,$$

where we used both (C.5) and (C.6). The original truncation of $\Delta_{\mathcal{G}}$ descends to truncations of the simplices $\Delta_{\mathcal{T}}$ and $\Delta_{\mathcal{G}'}$ in agreement with the connectivity of the corresponding graphs. This is trivial to see for $\mathcal{T}$ and

for any tube $\mathcal{T}'$ of $\mathcal{G}'$ not adjacent to $\mathcal{T}$ as a tube on $\mathcal{G}$. On the other hand, if $\mathcal{T}'$ is adjacent to $\mathcal{T}$ then we have

$$\begin{aligned}
\mathbf{X}_{\mathcal{T}'} &= \sum_{(a)\text{ not adjacent to }\mathcal{T}} X_{(a)} + \sum_{(b)\text{ adjacent to }\mathcal{T}} X_{(b)} + \sum_{i\in\mathcal{T}} X_{(i)} - \epsilon_{\mathcal{T}\cup\mathcal{T}'} \\
&= \sum_{(a)\text{ not adjacent to }\mathcal{T}} X_{(a)} + \sum_{(b)\text{ adjacent to }\mathcal{T}} X_{(b)} + \epsilon_{\mathcal{T}} - \epsilon_{\mathcal{T}\cup\mathcal{T}'} \\
&= \sum_{(a)\text{ not adjacent to }\mathcal{T}} \mathbf{X}_{(a)} + \sum_{(b)\text{ adjacent to }\mathcal{T}} \left(\mathbf{X}_{(b)} + \epsilon_{\mathcal{T}\cup(b)} - \epsilon_{\mathcal{T}}\right) + \epsilon_{\mathcal{T}} - \epsilon_{\mathcal{T}\cup\mathcal{T}'} \\
&= \sum_{(a)\in\mathcal{T}'} \mathbf{X}_{(a)} - \epsilon'_{\mathcal{T}'},
\end{aligned}$$

and it is not difficult to see that the total constant $\epsilon'_{\mathcal{T}'}$ is negative, by using the conditions i) and ii).

Before concluding this section we wish to establish a connection between the ABHY realisation of $\mathcal{A}_{n-3}$ and the one provided by the graph Associahedron $\mathcal{A}_{\mathcal{G}}$ in the case when $\mathcal{G}$ is a path with $n-2$ nodes. The two combinatorical languages of tubings and planar variables are related to each other by the simple rule depicted in Fig. C.3, so that tubes of equal

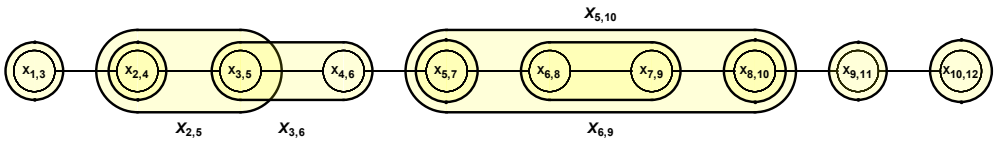

Figure C.3: Correspondence between tubes and planar variables, note that the single-node tubes correspond to variables $X_{i,i+2}$

length are mapped to equal-time points in the right triangle of the standard ABHY realisation. Furthermore, using the light rays shown in Fig. C.4 it is easy to express every variable $X_{a,b}$ in term of the one associated to single-node tubes obtaining

$$X_{a,b} = \sum_{i=a}^{b-1} X_{a,a+1} - \epsilon_{a,b}, \tag{C.7}$$

where $\epsilon_{a,b}$ is the total charge contained in the future light-cone of the point (a,b). By comparison of (C.7) with (C.3) we see that the two convex realisation of $\mathcal{A}_{n-3}$ are actually the same. In particular, we see that the conditions i) and ii) which must be satisfied by the constants $\epsilon_{\mathcal{T}}$ are automatically satisfied by the identification of $\epsilon_{\mathcal{T}}$ with a total charge, see Fig. C.4.

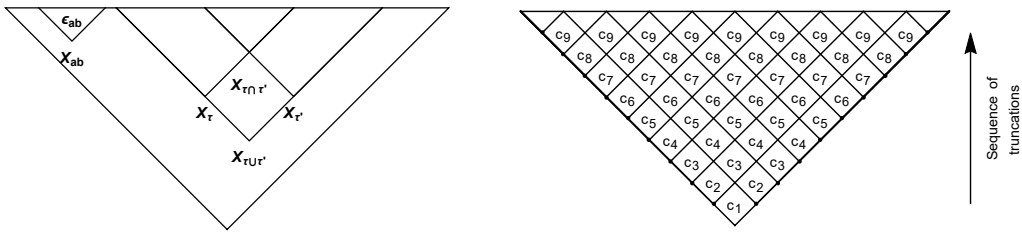

Figure C.4: Left: Any planar variable $X_{a,b}$ can be expressed in term of the variables $X_{a,a+1}$ and the total charge $\epsilon_{a,b}$ in its future light-cone. Conditions i) and ii) easily follows considering four-tuples of variables arranged on a diamond. Right: starting with all constants but c_1 set to zero one obtains a simplex. Progressively switching on the constants c_i according to the index i reproduces the sequence of truncations in order of increasing dimension of the faces.

Upon this identification, i) and ii) are trivialized to the positivity of the mesh constants $c_{i,j} > 0$. It is interesting to see how the series of truncations of the simplex are described in the mesh picture. Let us temporarily adopt the convention of Fig. C.4 in order to label the mesh constants, and suppose that all the mesh constants c_i with $i > 1$ are vanishing. Upon telescopically summing over all mesh relations we obtain

$$\sum_{a=1}^{n-2} X_{a,a+2} = c_1,$$

which we recognise as the condition for the variables $X_{a,a+1}$ to define a simplex. Now suppose that the mesh constants c_2 are turned on, then we also obtain

$$X_{1,n-1} = \sum_{a=1}^{n-2} X_{a,a+1} - c_2 \qquad \text{and} \qquad X_{2,n} = \sum_{a=2}^{n-1} X_{a,a+1} - c_2,$$

which mean that we now truncate two vertices of the original simplex. Similarly, by turning on the remaining mesh constants we recognize the sequence of truncations in increasing order of dimension that defines graph associahedra.

Finally, let us remark that graph associahedra and ABHY polytopes are only partly overlapping: choosing different regions for the wave equation, such as the arrow-tail or the square region, give rise to realisation of $\mathcal{A}_{n-3}$ which are not equivalent to graph associahedra. Conversely, if the graph $\mathcal{G}$ is a cycle with n nodes one obtains a cyclically symmetric realisation of a cyclohedron $\mathcal{B}_{n-1}$. On the other hand, the ABHY realisations for

these polytopes break the cyclical symmetry and is therefore not the same as the graph associahedral one.

C.2 Graph Cubeahedra

We now turn to graph cubeahedra which are described in terms of *design tubings* on a graph $\mathcal{G}$, and realized by truncation of a cube. We begin with the definition of a design tubing, on $\mathcal{G}$ we now allow the ordinary round tubes introduced in the previous section and new *square* tubes, a square tube is a single-node tube which we draw as in Fig. (C.5) to distinguish it from single-node round tubes. We now also allow the round tube covering the entire graph. We extend the notion of compatibility of tubes by declaring any pair of square tubes compatible, a square tube $\mathcal{S}$ and a round tube $\mathcal{T}$ are compatible if $\mathcal{S}$ is not contained in $\mathcal{T}$. A design tubing is a collection of pairwise compatible square and round tubes, the poset of design tubings is defined by the usual set theoretical inclusion $\subset$. The graph cubeahedron associated to $\mathcal{G}$ is combinatorially defined as the poset of design tubings on $\mathcal{G}$, we denote it by $\mathcal{C}_{\mathcal{G}}$

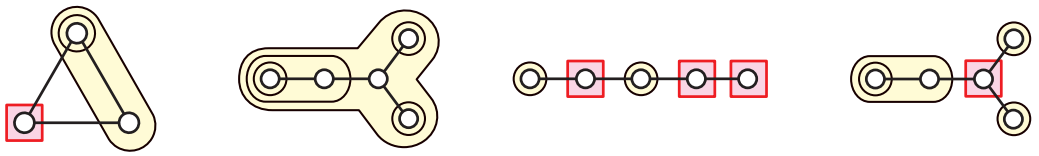

Figure C.5: Example of ordinary and design tubings. The picture is a courtesy of Prof. Satyan Devadoss and it is taken from [29].

The boundary structure of a graph cubeahedron is a straightforward generalization of the one familiar from graph associahedra, in addition to the factorization (C.1) we have boundaries corresponding to square tubes which are the graph cubeahedra associated to the graph obtained by removing the square tube. In other words, if $\mathcal{S} = [v]$ is a square tube at the node v and $\mathcal{G}' = \mathcal{G} \setminus v$ then we have

$$\partial_{[v]}\mathcal{C}_{\mathcal{G}} = \mathcal{C}_{\mathcal{G}'}.$$

It is not difficult to see that when $\mathcal{G}$ is a path with m nodes the corresponding graph cubeahedron $\mathcal{C}_{\mathcal{G}}$ is an Associahedron $\mathcal{A}_m$. When $\mathcal{G}$ is a cycle with m nodes instead $\mathcal{C}_{\mathcal{G}}$ is an m-dimensional Halohedron.

The convex realisation of a graph cubeahedra is obtained from the truncation of a cube rather than a simplex: to any graph $\mathcal{G}$ we associated a cube where pair of opposite facets are given by pair of square and

round tubes centered at the same nodes, in such a way that all square tube facets meet at a common vertex of the cube. Then one truncates the cube at the intersections of the round tubes in the same way already discussed for graph associahedra, see Fig. C.6.

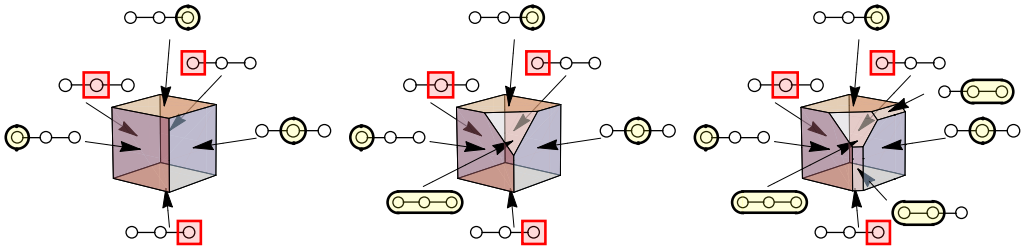

Figure C.6: Sequence of truncations producing $\mathcal{A}_3$ from truncations of a cube. From the leftmost to the central figure a single vertex is truncated, from the central to the rightmost two edges.

It is natural to ask whether graph cubeahedra $\mathcal{C}_\mathcal{G}$, in the case when $\mathcal{G}$ is a path with m nodes, are related to ABHY associahedra $\mathcal{A}_m$ for some choice of region for the wave equation. However it is easy to see that this is not possible by checking the pairs of parallel facets appearing in each construction.

Bibliography

[1] G. Salvatori, arXiv:1806.01842 [hep-th].

[2] G. Salvatori and S. L. Cacciatori, arXiv:1803.05809 [hep-th].

[3] N. Arkani-Hamed, "Talk at Amplitudes 2019, Dublin"

[4] N. Arkani-Hamed, Y. T. Huang and S. H. Shao, JHEP **1906**, 124 (2019) doi:10.1007/JHEP06(2019)124 [arXiv:1812.07739 [hep-th]].

[5] N. Arkani-Hamed, P. Benincasa and A. Postnikov, arXiv:1709.02813 [hep-th].

[6] N. Arkani-Hamed and P. Benincasa, arXiv:1811.01125 [hep-th].

[7] N. Arkani-Hamed, J. L. Bourjaily, F. Cachazo, A. B. Goncharov, A. Postnikov and J. Trnka, "Grassmannian Geometry of Scattering Amplitudes," Cambridge University Press. doi:10.1017/CBO9781316091548, 2016.
N. Arkani-Hamed, T. C. Huang and Y. t. Huang, "Scattering Amplitudes For All Masses and Spins," arXiv:1709.04891 [hep-th].

[8] N. Arkani-Hamed, Y. Bai, S. He and G. Yan, "Scattering Forms and the Positive Geometry of Kinematics, Color and the Worldsheet," arXiv:1711.09102 [hep-th].

[9] N. Arkani-Hamed and J. Trnka, JHEP **1410** (2014) 030 doi:10.1007/JHEP10(2014)030 [arXiv:1312.2007 [hep-th]].

[10] N. Arkani-Hamed, Y. Bai and T. Lam, "Positive Geometries and Canonical Forms," JHEP **1711** (2017) 039 doi:10.1007/JHEP11(2017)039

[11] N. Arkani-Hamed and J. Trnka, "The Amplituhedron," JHEP **1410** (2014) 030 doi:10.1007/JHEP10(2014)030

[12] S. Mizera, "Combinatorics and Topology of Kawai-Lewellen-Tye Relations," JHEP **1708** (2017) 097 doi:10.1007/JHEP08(2017)097

[13] S. Mizera, arXiv:1711.00469 [hep-th].

[14] F. Cachazo, S. He and E. Y. Yuan, "Scattering in Three Dimensions from Rational Maps," JHEP **1310** (2013) 141 doi:10.1007/JHEP10(2013)141 [arXiv:1306.2962 [hep-th]].

[15] F. Cachazo, S. He and E. Y. Yuan, "Scattering equations and Kawai-Lewellen-Tye orthogonality," Phys. Rev. D **90** (2014) no.6, 065001 doi:10.1103/PhysRevD.90.065001

[16] F. Cachazo, S. He and E. Y. Yuan, "Scattering of Massless Particles in Arbitrary Dimensions," Phys. Rev. Lett. **113** (2014) no.17, 171601 doi:10.1103/PhysRevLett.113.171601

[17] F. Cachazo, S. He and E. Y. Yuan, "Scattering of Massless Particles: Scalars, Gluons and Gravitons," JHEP **1407** (2014) 033 doi:10.1007/JHEP07(2014)033

[18] F. Cachazo, S. Mizera and G. Zhang, "Scattering Equations: Real Solutions and Particles on a Line," JHEP **1703** (2017) 151 doi:10.1007/JHEP03(2017)151

[19] Z. Li and C. Zhang, JHEP **1905** (2019) 029 doi:10.1007/JHEP05(2019)029 [arXiv:1812.10727 [hep-th]].

[20] S. He, "Talk at Strings 2019"

[21] X. Gao, S. He and Y. Zhang, JHEP **1711** (2017) 144 doi:10.1007/JHEP11(2017)144 [arXiv:1708.08701 [hep-th]].

[22] S. He and Q. Yang, JHEP **1905** (2019) 040 doi:10.1007/JHEP05(2019)040 [arXiv:1810.08508 [hep-th]].

[23] S. He and E. Y. Yuan, "One-loop Scattering Equations and Amplitudes from Forward Limit," Phys. Rev. D **92** (2015) no.10, 105004 doi:10.1103/PhysRevD.92.105004

[24] S. He, G. Yan, C. Zhang and Y. Zhang, "Scattering Forms, Worldsheet Forms and Amplitudes from Subspaces," arXiv:1803.11302 [hep-th].

[25] Y. Geyer, L. Mason, R. Monteiro and P. Tourkine, "One-loop amplitudes on the Riemann sphere," JHEP **1603** (2016) 114 doi:10.1007/JHEP03(2016)114

[26] E. Witten, Commun. Math. Phys. **252** (2004) 189 doi:10.1007/s00220-004-1187-3 [hep-th/0312171].

[27] S. Fomin and D. Thurston, Cluster algebras and triangulated surfaces, Part II: Lambda lengths [arXiv:1210.5569 math-th]

[28] R. C. Penner, The decorated Teichmüller space of punctured surfaces, Comm. Math. Phys. 113 (1987), no. 2, 299–339 https://projecteuclid.org/euclid.cmp/1104160216

[29] S. L Devadoss, T. Heath and C. Vipismakul, Deformations of bordered Riemann surfaces and associahedral polytopes Notices of the American Mathematical Society. 58. (2011).

[30] S. L Devadoss, A Realization of Graph-Associahedra, Notices of the American Mathematical Society. 58. (2011). [arXiv:math/0612530 [math.AG]]

[31] William Abikoff: The Real Analytic Theory of Teichmüller Space. AMS, Lecture note in mathematics, Springer-Verlag, 1980

[32] Teichmüller Theory and Applications to Geometry, Topology, and Dynamics: Volume 1: Teichmüller Theory, Matrix Editions Ithaca, NY 14850 MatrixEditions.com, 2006

[33] A. Hatcher, W. Thurston - "A presentation for the mapping class group of a closed orientable surface," doi:10.1016/0040-9383(80)90009-9

[34] V. Bazier-Matte,G. Douville, K. Mousavand, H. Thomas and E. Yıldırım, "ABHY Associahedra and Newton polytopes of F-polynomials for finite type cluster algebras", [arXiv:1808.09986]

[35] A. Papadopoulos, L. Liu, D. Alessandrini, W. Su, "The behaviour of Fenchel-Nielsen distance under a change of pants decomposition", [arXiv:1105.0202 [math.GT]]

[36] P. Banerjee, A. Laddha and P. Raman, arXiv:1811.05904 [hep-th].

[37] P. Raman, arXiv:1906.02985 [hep-th].

[38] M. Jagadale, N. Kalyanapuram and A. P. Balakrishnan, arXiv:1906.12148 [hep-th].